Fault Current Management in Power Systems using Inverter Based Distributed Generators

by

Nazila Rajaei

A thesis
presented to the University of Waterloo
in fulfillment of the
thesis requirement for the degree of
Doctor of Philosophy
in
Electrical and Computer Engineering

Waterloo, Ontario, Canada, 2015

I hereby declare that I am the sole author of this thesis. This is a true copy of the thesis, including any required final revisions, as accepted by my examiners.

I understand that my thesis may be made electronically available to the public.

Abstract

Distributed generator (DG) connection to power systems has attained special attention in recent years because it provides a number of operational and economic benefits for both utilities and customers. On the downside, the connection of many deregulated power generation units introduces new challenges to utility sectors. One of the most critical drawbacks of DG installations in power systems can be observed during a fault, when the additional DG fault current violates the original settings of protection systems. Protective devices installed in the system are designed based on the fault current analysis performed for the original system without DGs. When DGs are added, the current seen by protective devices will be different from the values originally specified. The change in the level of fault currents may alter the operation time of protective devices and disturb the coordination between primary and secondary protective devices. Consequently, serious protection problems may occur in the presence of DGs. On the other hand, many types of DGs that produce a dc voltage or a variable ac voltage require power electronic (PE) interfaces in order to connect to the power system. While these PE interfaces are used to control the active and reactive power injected to the system during normal operation, they are usually left idle during fault condition. The novel idea of this work is to employ the idle PE interface of inverter based distributed generators (IBDG) to manage the fault current flows through the power system. The scheme is based on utilizing the available current and voltage phasor information from smart meters and applying the necessary control actions to operate the IBDGs as fault current management (FCM) units. This FCM operation eases the distribution and protection system constraints on new DGs connections. From short circuit point of view, DGs with larger capacity can be connected to any location in the system without affecting the fault current magnitude. This operation also eliminates the need to disconnect DGs during each temporary fault. Moreover, the need to upgrade protective devices is reduced.

From the two controllable parameters of IBDGs current, the current magnitude and current phase angle, the current phase angle is employed to manage the contribution of DGs to the total fault current without deactivating them. Three zones of FCM operation are defined for IBDGs by changing their current phase angle: zones A, B, and C. The reference current phase angle that enables the FCM operation is calculated for zone B operation when only IBDGs exist in the system. The FCM operation and the reference current phase angle are then extended for zone C operation in order to manage the contribution of other types of DGs, such as synchronous DGs, to the fault current.

In another part of this work, two power flow based fault analysis techniques are developed to explore the behavior of IBDGs during fault conditions. In both, the buses

with IBDGs are modeled either as PQ buses or constant current (I) buses, based on their contribution to the fault current. The backward-forward sweep algorithm is used to solve the load flow problem for radial systems during fault conditions. On the other hand, the Newton-Raphson (NR) power flow algorithm is modified for fault analysis of loop systems with IBDGs. In the modified NR algorithm, current formulations rather than conventional power formulations are developed for nodes with constant current IBDGs, thus permitting mismatches in the real and imaginary components of the current to be obtained in addition to the conventional active and reactive power mismatches

The last part of this work introduces an algorithm for constructing protection zones with FCM capability in loop systems. The algorithm is developed in three steps, and deals with both synchronous DGs and IBDGs in the system. The method used for calculating the reference phase angle that enables the FCM operation is modified for the case of system buses with multiple lines connected to them. Further phasor calculations and illustrations are developed to show how the FCM can be applied for loop systems.

Different test systems, including the IEEE 33-bus system and IEEE 30-bus system, are used to validate the proposed FCM operation and the models for fault analysis. The simulations are performed with PSCAD software, OpenDSS, and MATLAB. The results show the effectiveness of the novel FCM technique in managing the fault current seen by protective devices in power systems, and the capability of the proposed power flow based methods to analyze the behavior of IBDGs during fault conditions.

Acknowledgements

I would like to thank my supervisor, Professor Magdy Salama, for his continuous encouragement, support and guidance. His advice and outlook guided my research towards the right direction, and his expertise, understanding, and patience added considerably to my graduate experience.

I would like to thank my examining committee: Professor Mehrdad Kazerani, Professor David Fuller, Professor Walid Ibrahim, Professor Rajiv Varma, and Professor Amirnaser Yazdani for their time and effort in reading my Ph.D. thesis and for their valuable comments.

I would like to thank Dr. Mohamed Ahmed for providing valuable advice, information and support in different aspect of my project.

I would like to express my deep gratitude to my dear husband, my father and my sisters for their endurance, support, and encouragements. Moreover, I would like to express my great appreciation to my in-laws for their love and prayers.

Dedication

In the memory of my mother,

to my father, Mohammadreza, who has devoted his life to me, and for his unstoppable love and support,

to my sisters, Niloufar and Samira, my brothers-in-law, Ali and Ali, and to my niece, Yasemin, for their love and encouragement,

and to my dearest, Iman, who has walked by my side through this journey, and helped me in all difficult moments.

Table of Contents

List of Tables

List of Figures

Nomenclature

APF	Active Power Filter
CB	Current Breaker
CC-VSI	Current Controlled Voltage Source Inverter
CLR	Current Limiting Reactor
CSI	Current Source Inverter
CT	Current Transformer
CTI	Coordination Time Interval
DG	Distributed Generator
FC	Fuel Cell
FCM	Fault Current Management
FL	Fuzzy Logic
GTO	Gate-Turn-Off
HIF	High Impedance Fault
IBDG	Inverter Based Distributed Generators
IMPR	Interface Microgrid Protection relay
ISFCL	Inductive Superconducting Fault Current Limiter
ITA	Inverse Time Admittance
MCPU	Microgrid Central Protection Unit
MM	Minimum Melting
MPPT	Maximum Power Point Tracker
MPR	Microgrid Protection Relay
NR	Newton-Raphson
OC	Over Current
PCC	Point of Common Coupling
PE	Power Electronics
PF	Power Factor
PFCLs	Passice Fault Current Limiter

PI	Proportional Integral
PMU	Phasor Measurement Unit
PV	Photovoltaic
PWM	Pulse Width Modulation
RSFCL	Resistive Superconducting Fault Current Limiter
SFCL	Superconducting Fault Current Limiter
SPWM	Sinusoidal Pulse Width Modulation
SS-FCL	Solid State Fault Current Limiter
STATCOM	Static Synchronous Compensator
T & D	Transmission and Distribution
TC	Total Clearing
UPFC	Unified Power Flow Controller
VC-VSI	Voltage Controlled Voltage Source Inverter
VSI	Voltage Source Inverter
WT	Wind Turbine
WTG	Wind Turbine Generator

Chapter 1

Introduction

1.1 General Overview

The presence of distributed generators (DGs) has changed the traditional centralized structure of power systems into deregulated sectors with more focus on the customer side. As a flexible source of power generation, DGs are at the center of attention from both the utility sector and individual customers. Despite the extensive presence of these generation units in power systems, no universally accepted definition has yet been presented for them [1]-[4]. However, there are certain common aspects such as power rating, location and technology that should be taken into account when investigating their operation [2], [4].

The rapidly growing number of DGs in power systems is mainly due to their capability to provide operational benefits for the power system and to enhance power quality. Some of the main advantages of DGs are [1], [4]-[7]:

- Environmental benefits
- Reduction in transmission and distribution (T&D) network expansion
- Voltage profile improvement
- Power loss improvement
- Peak load shaving
- Reliability

On the downside, the presence of DGs increases the complexity of power systems. Although DGs have the potential to improve the voltage profile in distribution systems, their misplacement can cause a voltage drop or an over-voltage in some points of the system [5],[7]. Moreover, many forms of DGs produce a *dc* voltage or a variable frequency *ac* voltage. Therefore, power electronic (PE) interfaces are required to convert the produced voltages to the desired *ac* voltage. The presence of these conversion units may introduce additional harmonics to the system [8]. However, the most critical drawback of DG installation in power systems is seen during faults when the additional fault current contribution of DGs violates the original settings of protection systems. This thesis introduces a novel method for controlling the contribution of DGs in fault currents so as to manage the total fault current in the system and thereby restore the original protection scheme.

1.2 Research Motivation

Protective devices installed in the system are designed based on fault current analysis performed for the original system with no DGs. When DGs are added to the system, they will contribute to the fault current. Hence, the fault current flowing through protective devices alters from the values they were originally designed to accommodate. Depending on the type, rating, and location of DGs, they may affect the amount of fault current going through the protective devices. In today's power systems, with their high number of installed DGs, the contribution of these extra generation units to fault currents is capable of increasing or decreasing the total fault current and the fault current within protective devices beyond the values originally specified. The change in the level of fault current may alter the operation time of protective devices and disturb the coordination between primary and secondary protective devices. Moreover, connection of DG units to power systems causes the bidirectional flow of fault currents in the systems. Protective devices not originally designed to deal with fault currents in both directions may trip mistakenly and reduce the reliability of the protection system.

From the above discussion, the necessity of a reliable solution to protection problems caused in the presence of DGs is evident. The main focus of the solution should be on maintaining the fault current seen by protective devices at a level close to the original value they were originally designed for. More flexible operation is obtained when it is possible to manage the fault current through the power system in a wider range below and above the original fault current. Accomplishing this task solves a major part of protection problems associated with DGs.

Many studies have been carried out to address the protection problems associated with

DGs. The main protection problem discussed in the literature is the increase of fault current going through protective devices in the presence of DGs. Some researchers have proposed to replacing the existing protective devices with new ones designed for the new configuration of power system with DGs. Another set of solutions, which forms the basis of this research, tries to minimize the contribution of DGs in fault currents. These solutions are usually based on the ability of fault current limiters (FCL) in reducing the fault current. It is shown in the literature that solid state FCLs (SS-FCL), which benefit from the fast operation of semiconductor switches, are able to effectively control the current passing through them [9], [10]. Fast and effective operation of solid state switches can be employed in order to control the fault current through the power system in the presence of DGs.

Distributed generation technologies such as wind turbines (WT) produce a variable frequency *ac* voltage, whereas direct energy conversion sources such as fuel cells (FC) or photovoltaic (PV) sources produce *dc* voltage at their output terminal. Hence, PE interfaces are required to connect these generation units to the utility grid [11]. The building block of these PE interfaces are semiconductor switches that can be utilized during fault conditions for the purpose of fault current control.

According to IEEE std 1547 [12], all DGs should be disconnected during fault conditions. Even if DGs are allowed to be kept connected to the system, in many cases they are turned off by their protection system when the contribution of the DGs exceeds the safe operation limit of solid state switches. Hence, many of the PE interfaces of DGs are left unused during fault periods. These idle PE interfaces are capable of controlling the current passing through them, based on the operation of their solid state switches. Hence, it is expected that by properly controlling PE interface of DGs during fault conditions, the fault current contribution of DGs and consequently the fault current flowing through the power system will be manageable. The need for an effective fault current management (FCM) operation during fault conditions, and the potential of PE interfaces of DGs to manage fault currents, are the main motivations of this research work.

Moreover, in current solutions, either a FCL should be placed at the connection point of each DG, or the original protective devices should be replaced with newly designed ones. However, PE interfaces of inverted based distributed generators (IBDG) are already installed in systems to control the contribution of IBDGs to the power system during normal operation. Hence, by adding an extra control operation for fault conditions, the same interface can be used to manage fault currents in power systems. Therefore, it is expected that applying the proposed methodology will provide a more efficient fault current control operation for power systems with installed DGs.

Another point that makes the proposed FCM operation superior to currently available

solutions is its potential to manage fault currents in remote locations. The proposed FCM technique manages fault currents through the power system instead of locally reducing the fault current magnitude. This fault current control can also be achieved on neighboring feeders to the FCM unit. To the best of the author's knowledge, this is a unique characteristic of the proposed FCM technique, which has not been addressed in any related literature. Moreover, many types of DGs do not require power electronic interfaces to connect to the system. Synchronous DGs are one common type of DGs that are directly connected to the system. Hence, IBDGs are the only controllable type of DGs existing in the system. Consequently, the IBDGs operating as FCM units are responsible for managing excessive fault currents that they themselves have not necessarily generated.

1.3 Research Objectives

The main objective behind this thesis is to mitigate the protection problems caused by the increased level of fault current flows through protective devices in the presence of DGs. In order to accomplish this goal, IBDGs, the assets of power systems which are normally left idle during fault condition, are utilized as FCM units to manage the fault current in local and remote locations. Accordingly, the objectives of this research can be summarized as follows:

Objective 1

The primary objective of this research is to develop an FCM technique to utilize the PE interface of IBDGs for the purpose of fault current control in power systems. As they employ semiconductor switches in their structure, and are equipped with flexible control units, IBDG are expected to have the capability of managing the fault current through the system.

Objective 2

The challenging part of FCM operation is to manage the fault current through the system without disconnecting or reducing the current magnitude of IBDGs. Hence, when operating IBDGs as FCM units during a fault, they should be kept connected to the system while their contribution to the fault current and consequently the fault current seen by the protective devices in the system are managed.

Objective 3

Another important objective is to utilize IBDGs to manage the contribution of directly connected DGs in fault currents. As mentioned earlier, only some types of DG technologies require PE interfaces at their connection point to the grid. Other types of DGs, such as synchronous DGs, are directly connected to power systems and as a result there is no control for their operation during faults. If IBDGs are properly controlled, they should be able to manage the fault current contribution of directly connected DGs in addition to their own fault current.

Objective 4

This thesis also aims to develop comprehensive fault analysis techniques to model the behavior of IBDGs during fault condition. Operating IBDGs as FCM units and not reducing their current magnitudes allows the modeling of IBDGs as constant current sources during fault condition. The model of IBDGs operating as FCM units can then be incorporated in conventional fault analysis methods.

Objective 5

One final goals is to construct protection zones with FCM capability for large loop systems. In large power systems, it might not be necessary to operate all IBDGs as FCM units. The technique can be justified by the self-healing characteristic of smart grids so that only the IBDGs that disturb the short circuit capacity condition of the system are responsible for mitigating the problem they have caused. Detailed analyses should be performed in order to assign the most beneficial operation to PE based DGs.

1.4 Thesis Outline

The remainder of this thesis is organized as follows:

Chapter 2 presents a detailed study on protection problems associated with DGs. A comprehensive literature review explore the performance of different types of DGs during fault condition, and the effect of DG type and location on the fault current seen by the protective devices.

Chapter 3 presents the novel concept of FCM operation during fault conditions. The phasor relations and formulations for FCM operation are developed in the presence of one IBDG and extended to the case of multiple IBDGs in a system. The reference current phase angle required for FCM operation is calculated through phasor relations of fault current elements and validated mathematically. Simulation results are preformed to validate the proposed FCM operation in radial systems and in the presence of IBDGs.

Chapter 4 introduces a novel technique that uses IBDGs as FCM units for directly connected DGs such as synchronous DGs. Three zones of operation are defined for IBDGs by changing their current phase angle. The FCM operation proposed in Chapter 3 is extended to the case when synchronous DGs exist in the system. Three factors affecting the FCM operation of synchronous DGs are explained in detail. PSCAD simulations are used to show the capability of IBDGs in managing their own fault current as well as the fault current contribution of synchronous DGs.

Chapter 5 presents two power-flow-based fault analysis algorithms to investigate the behavior of IBDGs during fault conditions. A backward-forward based algorithm is used for the fault analysis of radial systems in the presence of IBDGs. The Newton-Raphson power flow algorithm is also modified to accommodate the constant current model of IBDGs during fault conditions. Both algorithms are developed in MATLAB and the results are validated.

Chapter 6 introduces a novel algorithm for constructing protection zones with FCM capability in loop systems. The algorithm is developed in two steps, and deals with both synchronous DGs and IBDGs in the system. The method used for calculating the reference phase angle that enables the FCM operation is modified for the case of system buses with multiple lines connected to them. Further calculations and illustrations are developed to show how the FCM operation can be applied for loop systems. The algorithm is developed in MATLAB and the results are presented.

Chapter 7 presents the thesis conclusions, contributions, and directions for future work.

Chapter 2

Background and Literature Review

2.1 Introduction

Distributed generators are currently in the center of attention from both utility sector and individual customers as a more flexible source of power generation. Despite their undeniable benefits, the increasing presence of DGs in power system has introduced new challenges which should be carefully addressed in order to gain the benefits of DGs to its full extent. One of the most critical drawbacks can be observed during a fault, when the additional DG fault current violates the original settings of protection systems. Protective devices are designed based on the fault current analysis of the original system without DGs. When DGs are added to the system, they contribute to the fault current in addition to the grid current so that the fault current detected by the protective devices is different from the original fault current fed by the the main source. As a result, the operation of protective devices installed in the system may be disturbed and the reliability of protection system is reduced.

Overcoming these protection problems clearly requires a reliable solution. A variety of methods have been proposed for diminishing the effects of DGs on fault current magnitude and for providing reliable protection in the presence of DGs. According to [12] all DGs should be disconnected from the power system at the moment of fault detection. As a result, the system returns to its fundamental structure when a fault happens and the protection devices will be able to clear the fault effectively. However, disconnection of DGs for every temporary fault reduces system reliability and increases possibility of synchronization problems during reconnection of these units. Hence, a new series of solutions have been proposed which do not necessarily require the DG units to be disconnected. Gen-

erally, these solutions can be categorized into two main groups. The first set of solutions try to solve the protection problems associated with DGs without changing the existing structure of the protection system. Fault current limiters are used during faults so that the DG contribution is limited and the conventional protection system can clear the fault. The second group of solutions are proposed by the researchers who believe that the conventional protection systems are not able to provide a safe operation in the presence of DGs and new protection schemes are necessary for distribution systems with DGs. Some of the solutions proposed by this group of researchers are to modify the relay coordination curves, use microprocessor based reclosers, or equip the system with communication based devices.

Another important factor about DGs is their operation and modeling during fault condition. Distributed generators can be divided into three main groups: synchronous generators, induction generators and PE based DGs. Depending on the type of DG, its response in fault condition varies. While there is no control on the operation of synchronous and induction generators during fault condition, PE based DGs can be controlled to operate in the desired manner. Based on the operational mode of the DG, different control methods can be used for power electronic based DGs. However, each method has its own advantages and disadvantages which should be considered when designing controllers.

In this thesis, the PE interfaces of IBDGs are employed to manage the fault current contribution of DGs in the system. The method relies on the capability of semiconductor switches to respond quickly to sudden changes [13], a feature already demonstrated in SS-FCL applications. Consequently, a part of this literature review presents a detailed study on the effects of DGs on protection systems. The current solutions, including the use of FCLs, are investigated to compare the performance of the proposed method with the current practices. Moreover, since the method is based on the operation of PE based DGs, the characteristics of this type of DGs, and its control operation during normal and fault condition are investigated.

The rest of this chapter is organized as follows. Section 2.2 presents a detailed study on protection problems associated with DGs. Section 2.3 and Section 2.4 describe comprehensive literature reviews on the techniques available for the protection of power systems in presence of DGs. Section 2.5 explores the performance of different types of DGs during fault condition, and the effect of DG type and location on the fault current seen by the protective devices. Different types of current control techniques used for voltage source inverters are discussed in Section 2.8. A summary of the chapter is given in section 2.9.

2.2 Protection Problems in Presence of DGs

Presence of DGs in power system affects the conventional protection system. In the following subsections, protection problems associated with DGs are explored in details:

2.2.1 Impact on short circuit level

When DGs are added to the system, they contribute to the fault current in addition to the grid current. As a result, the fault current detected by the protective devices is greater than the original fault current from the main source. In this case, if the fault current contributed by the main source is close to the rating of switch gears, addition of DG currents increases the fault current beyond the rating of protective devices, which can cause serious protection problems [14]. Even if the increase in fault current does not exceed the rating of installed devices, coordination of the primary and secondary protective devices may be disturbed due to excessive DG fault currents [15].

2.2.2 Loss of coordination

Presence of DGs may affect the coordination of protective devices installed in the system. This impact of DGs is discussed in more details for three types of coordination:

Fuse-Fuse coordination

Connection of DGs may affect the coordination between fuses installed in the system. Each fuse curve has two characteristics: minimum melting (MM) and total clearing (TC). In order for two fuses installed in a radial system to coordinate, the TC characteristic of the primary fuse should be below the MM characteristic of the secondary fuse with an acceptable time margin.

Consider the system shown in Figure 2.1. For a fault in section DE, F_2 and F_3 should coordinate accordingly. Due to presence of the DG in the system, fault current seen by F_2 would be more than the fault current seen by F_3. On the other hand, when a fault happens in section BC, the fault current going through F_3 would be more than the fault current seen by F_2. Coordination curves for these two fuses are shown in Figure 2.2. For the downstream fault in section DE, the coordination holds if the fault current does not increase beyond the fuse curve. For the upstream fault in section BC, however, a margin

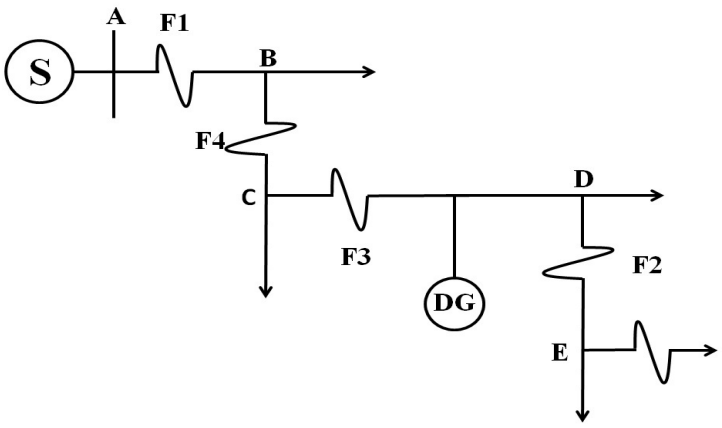

Figure 2.1: Part of a radial system [16]

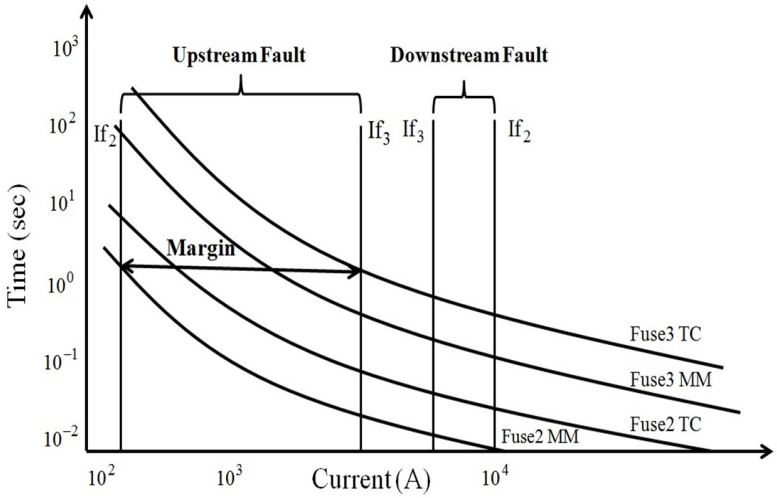

Figure 2.2: Coordination curves for two fuses installed in a distribution system [16]

exists. If the fault current seen by $F3$ is increased beyond this margin, F_3 operates before F_2 and coordination holds. On the other hand, if the fault current difference between F_3 and F_2 is less than the margin, F_2 operates first and the coordination is lost [16].

Fuse-Recloser coordination

Presence of DGs may disturb the fuse-recloser coordination in power systems. Figure 2.3 shows part of a system where the Recloser and Fuse should coordinate for any fault on the Feeder [15], [16]. Recloser has two operation characteristics: slow and fast. For the fuse-recloser coordination, first, recloser should operate twice in its fast operation mode and de-energize the system. If the fault persists after the second operation, fault is permanent, and fuse should clear it. Recloser provides backup for the fuse with its slow operation mode.

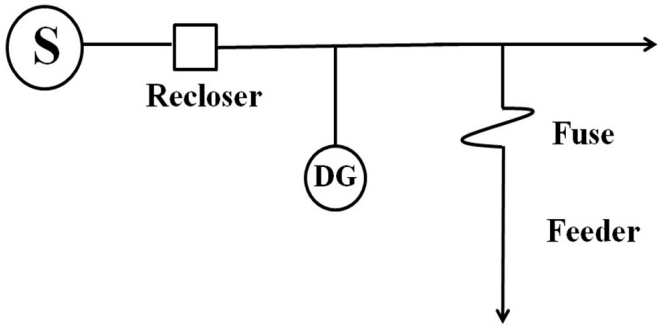

Figure 2.3: Part of a distribution system protected by a fuse and recloser [15],[16]

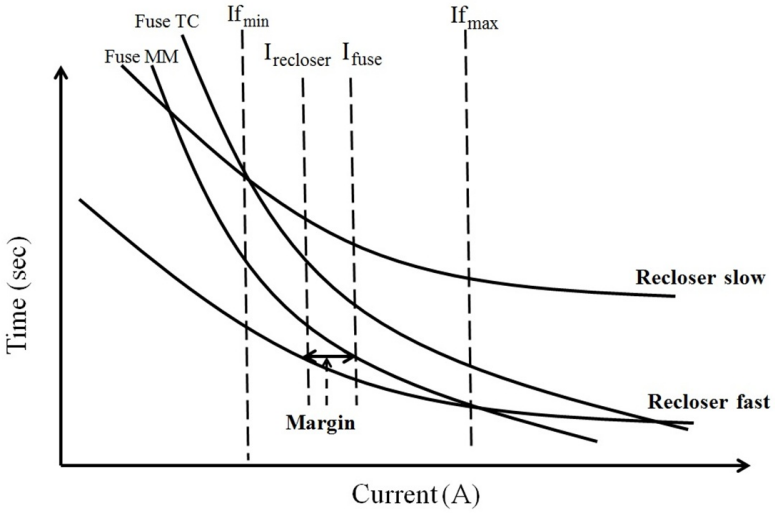

Figure 2.4: Coordination curve for fuse and recloser [16]

Figure 2.4 shows coordination curve for the Fuse-Recloser combination shown in Figure 2.3. When there is no DG installed in the system the fault currents seen by the two devices are the same. Hence, in order for the fuse and recloser to coordinate, fault current should vary between $I_{f_{min}}$ and $I_{f_{max}}$. When the DG is installed, the fault current seen by the fuse would be more than the fault current seen by the recloser. Therefore, there would be a current margin for these two protective devices to operate properly. If the fault current difference between the fuse and recloser goes beyond this margin, fuse operates first and the coordination is lost [16].

Relay-Relay Coordination

Similar to the previous two cases, the presence of DGs in power systems, and their contribution to fault currents, can affect the coordination between the protective relays installed in the system. Consider the system shown in Figure 2.5. With no DG installed in the system, fault current is fed only by the grid. As a result, the fault current going through all the three relays would be the same. The three protective relays are designed to coordinate for any fault in the system. For example, for a fault on $Line_3$, R_3 should operate first followed by R_2 and R_1. On the other hand, for a fault on $line_1$, only R_1 will see the fault current and no fault current goes through R_2 and R_3. When DGs are added, these new sources will also contribute to the fault current. Hence, the fault current seen by the relays would not be the same. For a fault in $line_3$, R_3 will see the maximum fault current followed by R_2 and R_1. In this case if the fault current seen by the relays exceeds the relay curves, then coordination is lost. For the case that fault current remains inside the allowable range, coordination holds as long as the coordination time interval (CTI) between the relay curves is not disturbed. In order to have the desired coordination for a fault in $Line_1$, R_2 should operate before R_3. In this case, since R_2 sees more fault current than R_3, there would be a coordination margin. This margin is shown in Figure 2.6 [16]. If the disparity in fault currents seen by the two relays exceeds the margin, coordination holds and R_2 operates before R_3; otherwise, the coordination is lost.

2.2.3 Bi-directionality issue

Distributed generators may cause bi-directionality issues in protection systems, and consequently disrupt a healthy part of the system [15]. This issue is more common in distribution systems where two feeders are fed from one common source. Consider the system shown in Figure 2.7 where two parallel feeders are connected to the grid. When DG is not connected to the system, any fault that happens on either of the two feeders is fed only from the grid.

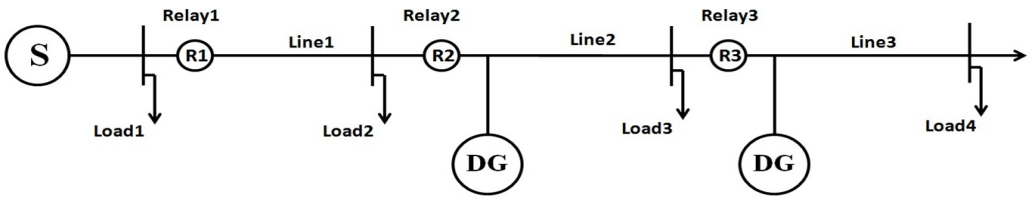

Figure 2.5: Part of a distribution system protected with three inverse time over current relays [16]

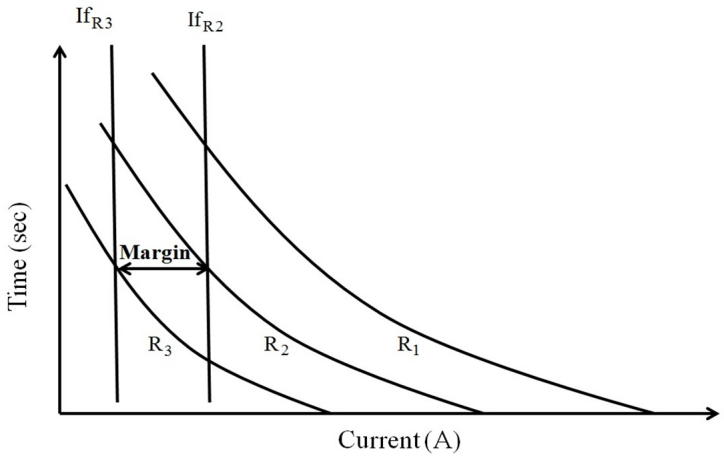

Figure 2.6: Coordination curves for three inverse time over current relays [16]

As a result only the protective devices on the faulty feeder will see the fault current. When the DG unit is connected on Feeder$_2$, for a fault on Feeder$_1$, both grid and DG contribute to the fault current. As a result, R_2 will also see the fault current coming from the DG unit. In this case, if R_2 has a faster response time than R_1, a healthy part of the system will be disconnected unnecessarily.

2.2.4 Loss of sensitivity

Presence of DGs in the system may affect the ability of protective relays to see the fault [15],[17]. This effect is illustrated in Figure 2.8. When DG is not installed in the system, the fault current is fed only by the grid. The substation relay is designed to see the minimum fault current coming from the grid. When DG is connected to the system, both DG and the grid feed the fault. Contribution of DG to the fault current depends on its size, type

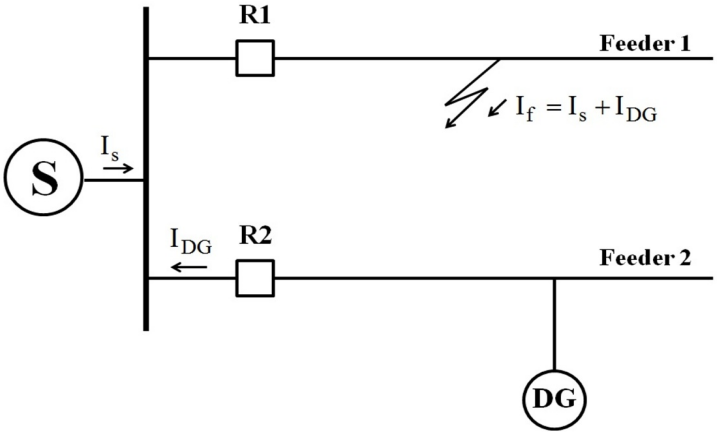

Figure 2.7: Bi-directionality issue in distribution system with DG [15]

and the fault-to-source impedance. As a result, existence of DG in the system may reduce the fault current drawn from the grid which affects the reach of the main feeder relay. Hence, it is possible that a fault on the feeder goes undetected until it damages a larger area of the system [15].

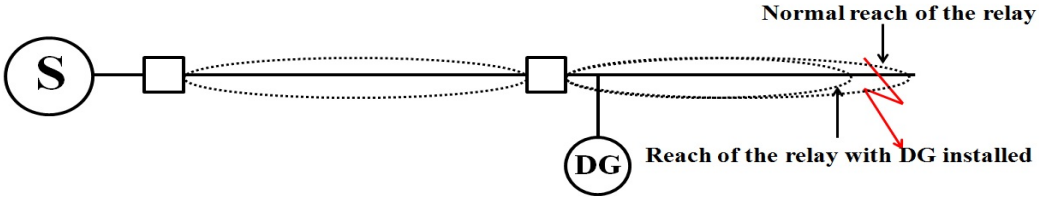

Figure 2.8: Loss of sensitivity in distribution system with DG [17]

2.3 Application of Fault Current Limiters

Fault current limiters, which are connected in series with the power line, limit the current during a fault while showing no effect in normal operation of the system. Depending on the technology used, FCLs are divided into two main categories [18]:

- Passive FCLs (PFCLs)
- Solid State FCLs

Current limiting reactors (CLR) and supperconducting fault current limiters (SFCL) are the most common types of passive FCLs [19],[20]. Although simple and cheap to use, current limiting reactors cause voltage drop during normal operation of the system [18]. On the other hand, SFCLs are capable of introducing a large impedance in faulty condition while showing no effect in normal operation of the system. Supperconducting FCLs operation can be divided into three modes [19]: In normal operation of the system when the current density and temperature of the device is less than the superconductor critical value, the SFCL stays in superconducting mode and shows resistance of zero. When a fault happens in the system, the current density exceeds the superconductor critical current density and its resistance increases rapidly. Fault current is limited as a result of this sudden increase. The third mode of operation is the recovery process. Superconducting FCLs heat up during the limiting mode of operation. Since they are connected in series to the line, it is necessary to cool them down instantly to the temperature where they would work as superconductor with negligible resistance [20]. This recovery time can be considered as the main concern for SFCLs use. Noe et. al. [19] states that the recovery time depends on the size and material of the superconductor and varies from 1 second to few seconds for thin films and remains below 1 minute for big superconductors. Depending on their structure, SFCLs can be further divided into resistive-SFCL (RSFCL) [19] and inductive-SFCLs (ISFCL) [19], [21]. However, due to its simplicity, the resistive type SFCL is the preferred type of SFCL [21].

Solid state FCLs use the advanced switching technology to limit the fault current. This type of FCLs can be further divided into two groups: resonance based FCLs [22], [23] and impedance switch in FCLs [24]-[26]. Resonance based FCLs limit the fault current by using thyristor switches and introducing a parallel resonant LC circuit into the system. There are different possible switching arrangements for this type of FCLs. However, the basic operation of all configurations is similar. In all cases, the LC circuit of the resonance based FCL is tuned to the power frequency and show minimum impedance in line. When a fault happens, the switches separate (add) a capacitor or inductor from (to) the system. As a result, the new LC circuit is no more tuned to the power frequency, and a large impedance is introduced to the system.

Impedance switch in FCL operates by introducing a large impedance in series with the power line when a fault happens. In normal operation, the current goes through a set of Gate-Turn-Off (GTO) thyristor switches which are connected in parallel to the limiting impedance. At the moment of fault detection, the GTO switches are blocked which forces the current to go through the high impedance. Disadvantage of this type of FCLs is its switching losses during normal operation. In order to overcome this problem a more advance SS-FCL is introduced in [18],[26]. This type of FCL can be a better choice to limit

the fault current contribution of DGs. Since it uses mechanical switches, there would be no losses during normal operation of the system [18].

2.3.1 Application of Solid-State Fault Current Limiters

In the recent years, FCLs have been widely used by researchers as a potential device to attenuate the effects of DGs during fault condition. Tang. et. al [18] suggested to use a hybrid SS-FCL [26] in series with DGs to minimize their contribution in fault current. The DGs connected to the system are synchronous generator which have high contribution in fault current. It is shown through three sets of simulations that the connection of FCLs at DG buses can minimize the contribution of DGs in fault current, improve the stability of synchronous machines, and reduce the effects of DGs on coordination of over current (OC) relays. Same type of FCL is used in [27]. However, in this paper transient fault currents are used to coordinate the relays in a distribution system with installed DGs. Transient currents of synchronous generators are considered, and it is shown through simulations that the hybrid SS-FCL is capable of limiting the steady state fault current. However, due to fault detection delay and operation time of FCLs, OC relays see the fault current for the first few cycles. Hence, it is possible that the coordination between OC relays is disrupted if transient currents are considered instead of steady state currents. In order to investigate the performance of relays for transient currents, the detection time delay and switching effects of FCL are considered for relay settings. Moreover, the dynamic model of inverse time overcurrent relays which is explained in [28] is used. Simulation results show that when transient currents are applied to OC relays designed based on steady state currents, the coordination between some of the primary and back up relays are lost. On the other hand, when the relays are designed based on transient currents, all of the relay pairs coordinate properly during transient time.

In [29] different misscoordination problems caused in presence of distributed generators are reviewed. The effectiveness of a SS-FCL to restore the original protection scheme of power systems is investigated. It is discussed that the SS-FCLs installed at the connection point of DGs, are capable of restoring the original protection scheme. Same type of SS-FCL is used in [30],[31] to diminish the contribution of DGs to the fault current. In these two studies genetic algorithm is used to obtain the optimal location, number and size of the SS-FCLs in order to minimize the number of protective devices that should be replaced. Hence, a fitness function is defined and minimized to obtain these optimal variables. This function includes number and cost of protective devices that should be replaced as well as the number of SS-FCLs which are necessary to restore the original protection scheme. Performance of the algorithm is examined for different numbers of SS-FCLs. Comparing

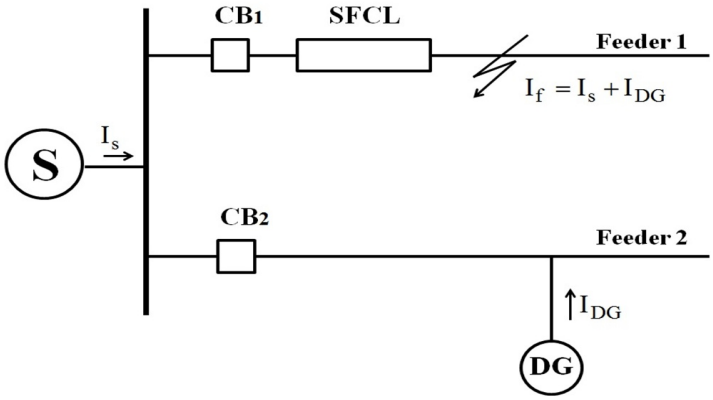

Figure 2.9: Distribution system with installed SFCL [32]

the results, it is concluded that optimal location and number of SS-FCLs highly depend on their price. As the price of SS-FCLs decreases the optimal numbers calculated for these units increases.
Although SS-FCL has shown promising performances in minimizing the fault current contribution of DGs, they have the main drawback of high cost which is hardly mentioned in the related literature. In a system with high number of DGs, in order to restore the original protection coordination, it is required to install one FCL for each DG which is not considered as a cost effective solution and may diminish the economical advantages of DGs.

2.3.2 Application of Superconducting Fault Current Limiters

In order to complete the study on the effects of FCLs on limiting the fault current contribution of DGs, performance of SFCLs is also investigated in the presence of DGs. Compared to SS-FCLs, SFCLs are more commonly suggested in the literature for the application of DGs. In [32] a SFCL is used to limit the contribution of a DG to the fault current, and to improve the instantaneous voltage sag resulting from the excessive fault current. In this paper the SFCL is not installed at the connection point of the DG. As shown in Figure 2.9 the output terminal of the faulty distribution subsystems is chosen as the installation point. The FCL is able to limit the fault current contribution of the DG effectively, and improve the voltage sag. However, in the presence of FCL, the total fault current is reduced to a level below the original fault current. This is expected since the SFCL is installed at a location where it would limit the fault current contribution from both the grid and DG. As a result of this limitation, the operation time of the circuit breaker on the faulty line is

increased to a value twice its original tripping time. Moreover, since the SFCL is installed on the faulty feeder, the circuit breaker on the healthy feeder still sees the fault current coming from the DG. This may cause bi-directionality issue if this circuit breaker has a faster response characteristics. From the result of this paper it can be concluded that the location of FCLs should be chosen properly so that the original operation of the system is not affected. The best location is at the connection point of DGs to the grid, so that only the contribution of DGs into the fault current is limited.

Effects of SFCLs are also investigated for the purpose of excessive fault current management in a distribution system with connected wind farms [33]. For this study, a SFCL is installed at the connection point of a wind farm to a distribution system. It is shown that the SFCL is capable of limiting the steady state current as well as the peak value of fault current. A short circuit reduction ratio of 70% is obtained in the first half a cycle. In [34] the effects of FCLs is studied from a different point of view. It is shown that FCLs can affect the optimal sizing of wind-turbine generators. A resistive SFCL consists of n series connected SFCL is used for this study. Figure 2.10 shows how the presence of resistive

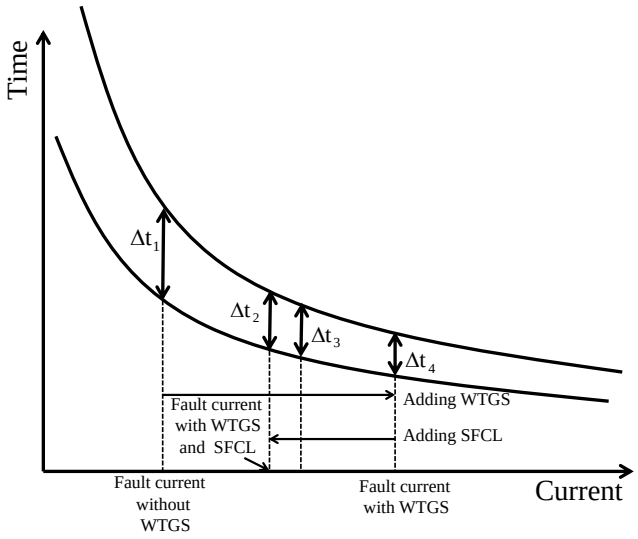

Figure 2.10: Effect of WTG system and SFCL on CTI [34]

SFCL can enhance the CTI between two overcurrent relays connected to the system, and increase the optimal size of wind turbine generators (WTG). When a wind turbine generator is installed to the test system, the CTI is reduced from Δt_1 to Δt_4 which is smaller than the desired CTI, Δt_3. This means that the initial size of WTG should be reduced in order to keep the CTI within the desired range. However, when the SFCL is installed

between the WTG and the distribution feeder, the CTI is increased from Δt_4 to Δt_2 which is more than Δt_3. Hence, with the SFCL installed in the system, there is no need to reduce the size of the WTG in order to meet the original coordination requirements.

Same type of FCL is used in [35] to evaluate the effects of FCLs on fault current magnitude, rotor speed, terminal voltage and output active power of a WTG. With no FCL in the system, when a fault happens, the rotor speed of WTGs increases, and it takes a long time until the original value is restored after the fault clearance. Moreover, there is a significant voltage drop at the WTG terminal and large oscillations happen in the active output power. On the contrary, when a FCL is installed in the system, the rotor speed remains stable and the voltage drop improves significantly. Furthermore, no large oscillations appear at the output active power of the WTG. The FCL can also reduce the fault current fed by the WTG, and helps with restoring the original OC relay coordination scheme.

In [36], it is shown through simulations that the presence of DGs disrupts the coordination between some of the primary and secondary OC relays installed in a looped power delivery system. This means that the coordination time interval between the primary and secondary OC relays goes below the required CTI, or in a worse case the backup relay operates before the primary one. In exploring the performance of two types of FCLs, inductive SFCL and resistive SFCL, installed in series with the DG units, it is argued that the minimum impedance of FCL depends on the capacity, number, and location of DGs as well as the fault location. The minimum impedance of FCL provides an acceptable CTI between the primary and secondary relay, and hence an iterative approach is adopted to calculate the minimum FCL impedance. During this process the impedance of FCL is increased till CTI for all sets of primary and backup relays meet the minimum CTI value. Simulation results show that when the FCL impedance increases, the coordination time interval between the primary and backup relays increases. Moreover the results show that the resistive FCLs are able to restore the original protection scheme with a much smaller impedance value compared to inductive FCLs. In another work [37], the location and size of FCLs are considered as two important factors affecting their performance. Different locations for FCLs are examined, and the authors concluded that in order to obtain the most proper coordination between the relays, FCLs should be installed close to the newly installed DGs.

The reliability of a SFCL is examined in [38]. It is shown that SFCLs are capable of tolerating high load currents without transitions to the limiting mode. Moreover, it is explored through simulations that while the SFCLs limit the current effectively during a fault, they maintain as superconductors for inrush currents. In [39] a novel dual FCL is proposed to limit the fault current contribution of DGs, depending on the fault location.

The fault current limiter is connected at the connection point of DG and consists of two limiters, FCL_{DG} and FCL_{Grid}. FCL_{DG} is responsible to operate for faults at the local bus while FCL_{Grid} limits the fault current contribution of DG for a fault on the grid side. Fault locations are categorized depending on the fault current direction seen by the two current sensors connected with each FCL. If sensors see the fault current in different directions, fault is detected at the local bus otherwise it is categorized as a grid side fault. Each FCL consists of a superconducting element in parallel with a power switch. When a fault is detected, first both FCLs operate in limiting mode due the excessive fault current seen by the superconducting elements. Then, depending on the fault location, a signal is sent to the appropriate power switch to close and bypass its superconducting element. As a result of this operation, the fault current contribution of the DG unit is only limited for a fault on the local bus. On the other hand, for a fault on the grid side, DG is able to feed the local load.

A new idea is proposed in [40] to protect looped distribution systems in both grid connected and islanded mode operation using FCLs. In this work, unlike all other papers presented so far, FCLs are installed in series with the utilities to limit their fault current contribution when the system operates in grid connected mode. In fact, the relays are designed to coordinate in islanded mode of operation. In grid connected mode, the FCLs connected in series with the grids limit their contribution to the fault current. As a result, same relay settings can be used in both modes of operation. Optimization algorithms are used to obtain the optimal relay settings as well as the FCL impedance which gives satisfactory performance in both modes of operation. It is shown through simulations that using the optimal settings for the relays and FCLs, relays can successfully operate in both modes of operation.

From the presented surveys it can be concluded that SFCLs are able to limit the fault current contribution of DGs. However, this type of FCL has the main drawback of long recovery time. As mentioned earlier, SFCLs should be cooled down instantaneously in order to avoid any resulted voltage drop in the power line where they are connected. This process takes time and requires special equipments. Moreover, SFCLs are not direction sensitive and limit the fault current in both direction which is not the desired operation in all cases [18]. For an effective and safe operation of protection system, it is required to install at least one SFCL for each DG. This might not be an economical solution especially in large systems with high number of connected DGs.

2.4 Application of Other Protection Schemes

Some authors have proposed to replace the conventional protection devices with more advanced ones in order to provide safe protection operation in the presence of DGs. One of the primary works in this area is proposed by the authors of [41]. In this work, the fuse-recloser coordination problem is investigated in presence of DGs. The authors suggest to replace the installed reclosers with microprocessor based reclosers which have the ability to store multiple curves, and allow the suitable curves to be chosen for each operation. It is shown that for the system under study, the fault current seen by the fuse would be more than the fault current going through the recloser if DGs are connected to the system. Hence, a ratio of fuse current to the recloser current is used to modify the recloser curve. This modification shifts the recloser curve to coordinate with the fuse in a new current range. However, the DGs should be disconnected after the first operation of recloser. So, it is necessary to modify the curves according to the new structure of the system. A similar idea is proposed in [42]. The only difference is the use of a non-adaptive method. In order to have one common scheme for all conditions of DGs, it is suggested to choose the minimum and maximum fault currents so that the curves coordinate in a wider range. As a result, the minimum fault current is calculated when the DG is disconnected from the system, and the maximum fault current is calculated when it is connected. The fuse and recloser curves are coordinated in the obtained range. Presence of the DG increases the fuse current above the recloser current. Hence, the recloser fast curve is revised using the fuse to recloser ratio (FRR), and the new revised curve is programmed in the microprocessor based recloser. This revised curve is used for coordination purposes even when the DG is disconnected after the first operation of recloser.

A new inverse time admittance (ITA) relay is proposed in [43]-[45]. The inverse time overcurrent tripping characteristic is used for the relay tripping time. However, instead of the multiple of pickup current used in the tripping formula, a new factor called normalized admittance is used. This factor is defined as the ratio of measured admittance by the relay to the zone pickup admittance. The measured admittance is calculated using the current and voltage seen at relay location while the relay pickup current and its corresponding voltage are used to calculate the pickup admittance. Since the proposed admittance relay uses multiples of relay pickup current and voltage, its performance does not depend on fault current seen by the relay. The test results for this relay shows an acceptable performance in clearing the fault in both radial and meshed distribution systems. However, performance of the relay depends on the normalized admittance which is a function of measured admittance. In order to have an effective relay with correct tripping time, it is necessary to measure voltage and current at relay point correctly.

An adaptive protection scheme is proposed in [46]. The solution is proposed to minimize the effects of DGs on reducing the reach of the substation OC relays. It is discussed that the presence of DGs in distribution system can reduce the capability of feeder's relay to see the fault. As a result, time operation of substation relay which is usually an inverse time overcurrent relay increases. In order to solve this problem, it is proposed to modify the pickup current of the relay depending on the DG contribution. This means the pickup current of the substation relay should decrease when fault current contribution of DGs increases. For this purpose, the DG is modeled, and the fault current seen by the substation relay is estimated in the presence of the DG. Therefore, pickup current of the substation relays is modified accordingly. The authors also note that if the DG is disconnected during the fault period, the proposed approach can still work. It is argued that when the DG is disconnected from the system, the fault current drawn from the grid and as a result the current seen by the substation relay increase. Hence, it takes less time for the relay to trip.

Another approach is proposed in [47] for protection of two radial feeders connected in parallel. It is discussed that DG units should stay connected in order to achieve the full benefits of distributed generation. As a result, it is proposed to keep IBDGs connected during a fault. Considering the maximum output current of the inverter, the output voltage yielding this current is obtained. In order to limit the output current below its maximum value, a safety margin is deducted from the calculated voltage. A voltage based detection method is used to sense the current direction. Fault detection modules are installed in the system to detect the direction of fault current and enable the selective protection scheme. Depending on the detected fault zone, the fault detection modules operates after a time delay. As a result of this coordination, the minimum faulty section of the system is disconnected for in zone faults. For out zone faults, time delays are set so that the maximum part of the healthy system continue to operate in islanded mode.

In [48] it is proposed to use microprocessor-based relays to protect a low voltage microgrid in both grid connected and islanded mode of operation. The proposed protection scheme is not a communication based method but it relies on capabilities of microprocessor-based relays to choose between different functional modules. Since it is not economical to replace all the available protective devices with new circuit breakers/relays only some of the fuses would be changed. This would include fuses installed at the beginning of secondary mains (SM), and the fuse connected at the interface point of microgrid to the utility grid are replaced by microprocessor based relays. All other network fuses are kept without any modification. The proposed microgrid protection relays (MPR) and interface microgrid protection relays (IMPR) consist of three main protection modules: grid-connected mode block, islanded mode block and high impedance fault (HIF) protection block. In islanded mode, a definite time grading method in combination with fault detection and directional

elements are used for protection purposes. In order to avoid false tripping in case of a fault on neighbor feeder, directional elements should be incorporated in the MPRs. For grid connected mode of operation, the method proposed in [41] and [42] is used to make the protective devices coordinate in the new ranges of fault current. Moreover, for HIFs detection, the method suggested in [49] is adopted and incorporated in the MPRs. The proposed method shows that in islanded mode of operation, the MPRs are the primary relays which reacts to a fault. Since the fault current level is low in this mode of operation, it takes a long time for fuses to operate. In this situation, the MPRs installed on healthy feeders operate after a time delay as the backup protection for the main MPR. In grid connected mode of operation, it is shown that appropriate fuse trips first and the respective MPR operates as the backup. Also, the IMPR operates with a longer time delay as the second backup followed by other MPRs installed at the healthy feeders.

Protective relaying approaches which are based on communication between the elements of power system have gained more attention as a solution for protection problems associated with DGs. Brahma and Girgis [50] tackled the problem from this point of view. It is discussed in the paper that it is not reliable to disconnect all DGs in the system for each temporary fault. As a result it is proposed to divide the system into zones of operation where each zone has a balance between the number of DGs and connected loads. Since in this approach the zones may operate in islanding mode during fault condition, at least one DG in each zone should have load frequency control capability. Zones are separated using breakers. These breakers should be capable of disconnecting and reconnecting the zone upon receiving signal from the main relay. The main relay is located at the substation and is responsible to detect the fault, identify the type of fault and faulted zone. When the faulted zone is identified, the relay sends a tripping signal to appropriate breakers to disconnect the zone and the DGs connected to the zone. The main challenge in this approach is to distinguish the faulty zone. For this purpose data related to load flow and short circuit analysis of the system is required. Also, the fault current contribution from all available sources in the system for different types of fault happening at each system bus should be available. It is discussed in the paper that the fault current contribution from a source to a fault happening on a line would lie between the fault current contribution from the same source to the same type of fault happening at buses connected to the line. In order to check the persistence of the fault, the main relay sends a reclosing signal to one of the zone forming breaker specified for reclosing operation. The current contribution from all generation units are monitored continuously, so if the fault persists after the reclosing operation, it would be detected quickly and the signal is sent to the zone forming breaker to disconnect the zone. On the other hand, if the fault disappears, closing signal is sent to zone forming breakers one by one to connect the zone to the system. As discussed in the

paper the accuracy of the method depends on the number of DGs connected to the system and their level of penetration. The essential part of this approach is to spot the faulty zone. When a low number DGs are installed in the system the possibility of incorrect detection increases and as a result the accuracy of the approach lessens.

In [51] it is suggested to use the IEC 61850 standard to provide appropriate communication between the relays and generation units. The proposed method is based on communication between a microgrid central protection unit (MCPU), the relays and generation units. The operating currents of relays and fault current direction are the information obtained by continuous monitoring of relays. The fault current seen by each relay is obtained as follows:

$$I_{relay} = (I_{faultGRID} * Operating\,Mode) + \sum_{i=1}^{m}(K_i * I_{faultDG_i} * Status_{DGi}) \qquad (2.1)$$

where $I_{faultGRID}$ presents the fault current contribution from the grid. $I_{faultDG}$ is the fault current contribution from each DG which depends on the type of DG. "$Operating\,Mode$" and "$Status_{DGi}$" show the status of microgrid and DGs respectively. K_i is the impact factor of ith DG on a relay. This value varies between 0 to 1 depending on the closeness of the DG to a relay. In order to guarantee the coordinated operation of relays a selective level is associated to each relay. As a result of this selective level each relay operates after a time delay. When current flowing through a relay exceeds the relay operating current, a fault detected signal is sent to the MCPU. If the fault is not cleared by other relays in the time delay, a signal is sent to the relay to open and clear the fault. In a similar work [52], authors propose to use inverters with FCL ability as the interface of DGs to the power system. Hence, when a fault happens, the output current of inverter based DGs are limited to a predetermined value, $I_{faultDG}$. In this case since the output current of DGs are known, they can be stored in CPU and there is no need for communication lines between the DG units and the CPU. In [53], the authors proposed a control strategy to reduce the output current of IBDGs during fault condition based on the severity of voltage sag experienced by each IBDG. However, in these methods, in order to decrease the contribution of IBDGs to zero, the inverter current magnitude should be so small that it would be equivalent to deactivating the inverter. In [54] performance of a solid-state switch-based field discharge circuit in controlling the output current of synchronous DGs is investigated. The method is able to reduce the contribution of synchronous DG in fault current, however, it requires modification of the internal circuit of installed synchronous DGs which might not be a feasible solution in all situations.

An adaptive agent based protection scheme is discussed in [55]. The approach is based on communication between the protective relays, DGs and other equipments of power system such as circuit breakers (CB) and current transformers (CT). The proposed multiagent protection scheme consists of three main groups of agents: DG agents, relay agents and equipment agents. A communication protocol allows the agents which are allocated in different locations of power system to communicate with each other. The CB and CT agents provide local information for relay agents and operate the local equipments. Relay agents receive necessary information from DG and equipment agents to protect the system. Moreover, the coordination strategies suitable for different system configuration are set in the relay agents. The relays have the updated information from other agents in the system, so they adapt themselves with the new configuration and choose the proper coordination scheme to clear a fault.

Microprocessor-based directional relays are used in [56] to provide an adaptive protection scheme in presence of DGs. Use of relays with different tripping characteristics can be planned depending on the system structure. In addition to the grid connected and islanded mode of operation, the case when fault current changes due to disconnection of one DG is also considered. The forward relays have two tripping characteristic, one for grid connected mode and one for islanded mode of operation. On the other hand, the reverse relays have also two characteristic, one for the case all DGs are in place and one for the situation that one of the DG units is disconnected. The status of the grid is detected using an islanding detection method.

The authors of [57] also believe that the traditional protection equipments are not able to properly deal with the protection problems that occurs in presence of DGs. Consequently, the concept of agent based protection system is introduced. The wavelet components of load current and voltage are analyzed using the wavelet transform. The fault current is detected by feeding the obtained spectral components into a neural network. The fuzzy cluster analysis is used to classify all relays in a line which is protected by a relay agent into two groups depending on their energy spectral. The fault location is identified by comparing these group structures. Information are transferred between the relay agents and other equipments and fault is cleared by proper relays.

Digital relays are used in [58] to protect the microgrid with the help of a phasor measurement unit (PMU). It is proposed to use the differential protection scheme to detect the faults. The relays connected on the sides of a transmission line should communicate to clear a fault. For relays installed on short lines the communication between the relays takes a short time, so there is no need for a synchronization unit. However, for long distance transmission lines a PMU is required to have time synchronized measurements. If the primary relays fail to operate, a tripping signal is sent to the adjacent relays to operate

as backup for primary relays. Moreover, in case of relay or communication link failure, an alert is sent to the relays indicating that the differential protection scheme is lost and the relays should operate based on the comparative voltage protection scheme.

An agent based approach is discussed in [59] where the distribution system is divided into separate sections. The proposed protection system is a communication based method where the installed agent relay should communicate with each other based on the received signal from the CTs. The CBs are responsible to open the faulted section upon receiving signal from the agent relays. Agent relays use the fault current direction to categorize the faults as either internal or external faults. When a fault happens in the system, first it is categorized by the relays as either an internal or external fault. In case of an internal fault, the agent relay at the busbar is capable to detect the fault without communicating with other relays. For external faults, the relay communicate with its neighbor relays and the relays connected to the faulted section will clear the fault.

Many of the proposed solutions in this area are able to provide a reliable protection operation in presence of DGs. However, these solutions either require replacement of all the protective devices with new ones or changing the entire protection system. Either way, the solutions are not appropriate for the existing power system with high number of protective devices. Modifying the current distribution systems using the new designed protection schemes would be too costly and may diminish the economical benefits of distributed generation. Hence, more economical solutions are necessary to provide the safe operation of protection systems in presence of DGs.

2.5 Modeling and Control of DGs

The behavior of DGs during fault condition and their contribution in the fault vary depending on the type of DG. In general, DGs can be divided into three main categories: synchronous machine DGs, induction machine DGs and PE based DGs. Synchronous generators are conventional DGs which are used to employ the traditional energy resources such as diesel and gas engines or hydro units [15]. Induction generator are commonly used with WT. On the other hand, PE based DGs are used to connect the nontraditional energy resources such as PV, FCs or WTs to the power system. These renewable resources produce a *dc* voltage or a variable frequency *ac* voltage and require PE interface to connect to the *ac* power system [15], [60].

Table 2.1 shows the fault current contribution of different DG technologies [5], [61]. Synchronous DGs provide a greater contribution to a fault current than do IBDGs. While

Table 2.1: Fault current contribution from DGs with different technologies [5],[61]

Types of DG	Fault current contribution(as a percentage of rated current)
Inverter Based DG	100-400%(duration depends on inverter control strategy)
Synchronous Generators	500-1000% (first few cycles) and thenreduce to 200-400%
Induction Generators	500-1000% (first few cycles) and then reduce to 0

an IBDG fault current is limited to two to three times its rated current, synchronous DGs can contribute about four to five times their rated current. It should be noted that IBDGs feed the fault as long as the fault current remains below the maximum current limit of their inverters. This is the case for remote faults where fault current level is not very high [62]. If the fault current contribution of IBDGs exceed their current threshold, the inverter interfaces are disconnected to avoid any damages to the transistor switches [15],[62],[63]. Hence, in order to avoid damage to the PE interfaces of IBDGs, the fault current contribution of these units should be kept below the tripping threshold of inverter interfaces.

In the following sections, a brief description is given on the operation of two common types of DGs during fault condition.

2.5.1 Synchronous Generators

Synchronous generators are used to generate electrical energy from high power turbines such as gas, steam and hydro. Using these generators the mechanical energy of high power resources are converted to electrical voltages at power frequency [13]. These generators can be modeled as a voltage source in series with an equivalent impedance [15],[64]. When a fault happens, the internal voltage of generator decays in time while the internal impedance remains constant representing the machine physical characteristic. However, in order to simplify the operation of synchronous generator in fault situation, same results can be obtained if it is assumed that the generator voltage remains constant and the internal impedance increases by time [65].

Figure 2.11 shows the fault current contribution of a synchronous generator for a fault at its terminal [15]. As can be seen, the current consists of both *ac* and *dc* components in the first few cycles. Presence of *dc* component in fault current prevents the sudden change of current in the inductive circuits. When a fault happens, the *ac* current increases rapidly. However due to the presence of inductive element in the circuit, the total current cannot vary instantaneously. As a result, the *dc* component of the fault current is produced to

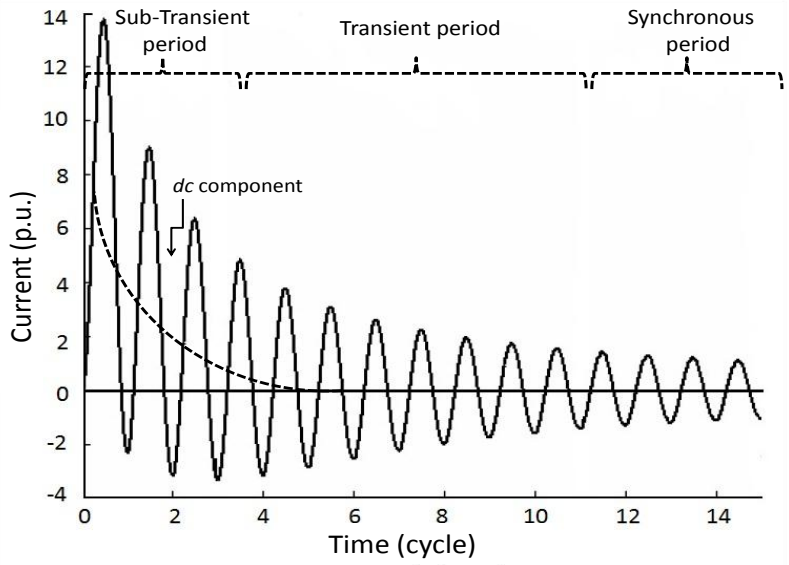

Figure 2.11: Fault current contribution of synchronous generators [15]

compensate for this rapid increase of *ac* current. The *dc* component of fault current is at its maximum level in the first cycle and decay to zero depending on the resistance and inductance of the circuit. As a result, the current becomes symmetrical around zero when the *dc* component disappears [65].

The symmetrical *ac* component of fault current varies as time passes. In the first few cycles, the symmetrical fault current is at its maximum value and decreases rapidly. This period is called sub-transient period. After this period, the fault current continues to decrease in the transient period with a much lower rate till it reaches a steady state value. After this moment, the fault current remains constant implying steady state condition [64]. The symmetrical component of fault current can be obtained as follow [64]:

$$I(t) = (I^{''} - I^{'})e^{\frac{-t}{T^{''}}} + (I^{'} - I_{ss})e^{\frac{-t}{T^{'}}} + I_{ss} \tag{2.2}$$

where:

$$I_{ss} = \frac{V}{X_s} \tag{2.3}$$

In (2.2) $I^{''}$, $I^{'}$ and I_{ss} are the sub-transient, transient and steady state currents. $T^{''}$ and $T^{'}$ represent the sub-transient and transient time constants. Also, V is the per-phase internal generated voltage of the generator and X_s is the synchronous reactance.

2.5.2 Power Electronic Based Distributed Generators

Many types of renewable energy resources such as FCs, PV systems and WTs require power electronics as an interface to power system [13],[15]. Depending on the type of generated power, *dc* or *ac*, the interface can consist of an inverter or a rectifier and an inverter [13]. In order to simplify the analysis, here it is assumed that a constant *dc* voltage is provided at the input of the inverter and the rest of the analysis is focused on the grid-side converter [66],[67].

There are two types of inverters: current source inverters (CSI) and voltage source inverters (VSI). Since distributed generation resources can be simulated as voltage sources, VSI are commonly used as their interface to the grid [15]. Voltage source inverters can be further divided into two categories: voltage controlled VSI (VC-VSI) and current controlled VSI (CC-VSI) [15],[68].

Voltage controlled VSI

In VC-VSIs, the output voltage of the inverter is the control variable. Mimicking the operation of synchronous generators, the output active and reactive power of VC-VSIs can be controlled by manipulating the magnitude and phase angle of the output voltage [15],[69]. Voltage controlled VSIs are able to provide voltage support to the load. In this mode of operation where the voltage magnitude of the inverter is kept constant, the only controllable parameter is the power angle. Hence, unity power factor is obtained only at a specific grid voltage and power flow condition depends on the maximum limit of power angle, size of coupling inductor and the load. Another disadvantage of VC-VSI is that decoupled active and reactive power control is not possible [68]. Moreover, the quality of power in VC-VSI highly depends on the grid voltage quality [15],[69].

VC-VSI can be modeled as a voltage source in series with the coupling impedance. Peak value of the fundamental phase voltage of VC-VSI, $\hat{V_1}$, can be obtained as follows [15],[70]:

$$\hat{V_1} = \frac{m.V_{dc}}{2} \tag{2.4}$$

where m is modulation index of pulse width modulation (PWM) inverter and V_{dc} is the *dc* side voltage.

Current Controlled VSI

In current-controlled VSI, the output power of the inverter is controlled by manipulating the current injected to the grid [15]. Current controlled VSI can be modeled as a current source in parallel with an equivalent impedance [68],[15]. This modeling is possible since the current controllers in CC-VSI are usually designed with a high bandwidth. Therefore, in a control frequency range which is much less than the controller bandwidth, current controller has a gain close to unity and the CC-VSI can be modeled as a current source within its bandwidth.

Compared to VC-VSIs, a higher quality of power can be obtained in current control mode of operation since the current is less affected by the grid voltage [15]. Moreover, in CC-VSI the active and reactive output powers are decoupled since the output current of the inverter is controlled independently from the grid voltage [68]. Due to these advantages, CC-VSIs are considered in this work as the interface of DGs.

2.6 Modeling of Inverter Based DGs for Fault Analysis

As discussed in Section 2.4, advanced solutions have been proposed in recent years to keep DGs connected to the system while limit their contribution in fault currents. In properly employing these methods, there is an inevitable need to model the behavior of DGs under fault conditions. The behavior of synchronous DGs under fault conditions is well known [65]. However, the behavior of IBDGs during fault conditions is mainly dominated by their control units. When a fault happens in a power system, in order to avoid any damages to the semiconductor devices, the VSIs are automatically disconnected when their fault current exceeds 100%-400% of the rated current [5],[61]. In order keep IBDGs connected to the system, the current contribution of these units should be limited to a value below the tripping threshold of their inverter interfaces. Hence, with the increasing number of IBDGs in power systems, it is necessary to investigate the behavior of this type of DGs for fault analysis. A number of methods have been proposed in recent years to facilitate the fault analysis in systems with high penetration of IBDGs. It is shown in [60] that the fault current contribution from synchronous based DGs is noticeably higher than the fault current contribution of IBDGs. A dynamic simulation technique based on state space representation of the system is used to analyze the effects of IBDGs; however, no detailed discussion on the modeling and control procedure of IBDGs is presented. In [62], the authors proposed a step-by-step method to include IBDGs in conventional fault analysis

techniques. Although the method is capable of estimating the IBDG current, it cannot be easily generalized for all system configurations, requires high computational calculations, and depends on many system assumptions. A reduced converter model based on switching function concept is proposed in [71]. Although, the results point out a limited current contribution from IBDGs during the fault condition, neither the operation of the controller for generating this contribution, nor the type of modelings are mentioned. In [72], a double loop current controller is presented to control the output current of IBDGs that feed the fault with a rated current. However, the method is examined on a single IBDG, and the criteria for defining the output current of the inverter are not defined. References [73]-[75] are based on the idea of modeling IBDGs as constant current sources during fault condition. While [75] proposes a model for islanded IBDGs under fault condition, [73] and [74] focus on the behavior of IBDGs in grid connected fault conditions. In [73], the effect of a single IBDG during fault condition is investigated, and the unit is modeled as a constant current source in this situation. In [74] a system with multiple IBDGs is considered and a load flow based technique is used to find the contribution of each DG to fault current. In this case, IBDGs are modeled either as PQ generators or as constant current sources, based on their contributions in fault currents. Although this method is conceptually correct, the authors used Gauss-Seidel load flow solution, which is not a recommended load flow technique for weak meshed radial systems.

2.7 Effect of DG Location on the Fault Current Seen by Protective Devices

As discussed in subsection 2.5.1 and subsection 2.5.2, the fault current contribution of DGs varies based on the type of DG. Additionally, the location of DGs affects the fault current seen by the protective devices installed in the system.

2.7.1 Effect of IBDGs Location

The effect of DG location has been analyzed in depth in [53] for the case of IBDGs. Consider the system shown in Figure 2.12. For a fault at F_1, when no IBDG is connected to the system, the fault currents flowing through the two relays, R_1 and R_2, are equal to the fault current fed by the grid:

$$I_{R_1} = I_{R_2} = I_s = \frac{E}{Z_{net} + Z_1 + Z_2 + R_{flt}} \tag{2.5}$$

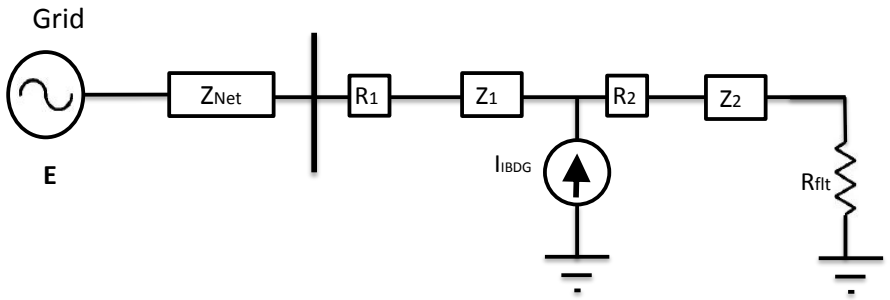

Figure 2.12: Equivalent model of a distribution system with an IBDG for a downstream fault [53]

where Z_1 and Z_2 are the equivalent impedance of the lines from the substation to the point of common coupling (PCC) and from the PCC to the fault respectively. The voltage source is E, and Z_{net} presents the equivalent model of the network upstream the substation. The fault impedance is represented by R_{flt}.

When the IBDG is connected to the system, it affects the fault current seen by R_1 and R_2. The IBDG is modeled as a constant current source during fault conditions. Depending on the location of DG in respect of the fault location and substation, from the total fault current contribution of IBDG, I_{IBDG}, a part goes towards the fault, I_{IBDG_2}, and a part flows in the other part of the system, I_{IBDG_1}. I_{IBDG_1} and I_{IBDG_2} are calculated as in [53]:

$$\begin{aligned} I_{IBDG_1} &= I_{IBDG}.\frac{Z_2 + Z_{flt}}{Z_{net} + Z_1 + Z_2 + Z_{flt}} = I_{IBDG}.Z_{Eq_1} \\ I_{IBDG_2} &= I_{IBDG}.\frac{Z_1 + Z_{net}}{Z_{net} + Z_1 + Z_2 + Z_{flt}} = I_{IBDG}.Z_{Eq_2} = I_{IBDG}.(1 - Z_{Eq_1}) \end{aligned} \tag{2.6}$$

Consequently, the fault current seen by R_1 and R_2 can be calculated as in [53]:

$$I_{R_1} = I_s - I_{IBDG_1} = \frac{E}{Z_{net} + Z_1 + Z_2 + R_{flt}} - I_{IBDG}.\frac{Z_2 + Z_{flt}}{Z_{net} + Z_1 + Z_2 + Z_{flt}} \tag{2.7}$$

$$I_{R_2} = I_s + I_{IBDG_2} = \frac{E}{Z_{net} + Z_1 + Z_2 + R_{flt}} + I_{IBDG}.\frac{Z_1 + Z_{net}}{Z_{net} + Z_1 + Z_2 + Z_{flt}} \tag{2.8}$$

The increase in the fault current seen by R_2 and the decrease in the fault current seen by R_1 depends on Z_{net}, Z_1, Z_2 and Z_{flt}. For the faults happening close to the IBDG when $(Z_2+R_{flt}) \ll (Z_1+R_{net})$, Z_{Eq_1} will be a small value and I_{IBDG_1} can be ignored. In this case the fault currents seen by R_1 and R_2 are obtained as [53]:

$$I_{R_1} \approx I_s = \frac{E}{Z_{net} + Z_1 + Z_2 + R_{flt}} \tag{2.9}$$

$$I_{R_2} \approx I_s + I_{IBDG} = \frac{E}{Z_{net} + Z_1 + Z_2 + R_{flt}} + I_{IBDG} \tag{2.10}$$

On the other hand, in large networks when the IBDG is located farther from the fault location, the equivalent line impedance from the fault location to the IBDG is considerable ($(Z_1+R_{net}) \ll (Z_2+R_{flt})$). As a result, the fault current seen by R_1 and R_2 are obtained as [53]:

$$I_{R_1} \approx I_s - I_{IBDG} = \frac{E}{Z_{net} + Z_1 + Z_2 + R_{flt}} - I_{IBDG} \tag{2.11}$$

$$I_{R_2} \approx I_s = \frac{E}{Z_{net} + Z_1 + Z_2 + R_{flt}} \tag{2.12}$$

Placement of IBDGs anywhere between Z_1 and Z_2 results in fault currents with values between those of the above mentioned extreme cases.

2.7.2 Effect of Synchronous DGs

The same type of calculation is possible for the case of synchronous DGs. Consider the system shown in Figure 2.13 where a synchronous DG with the inductance of X' is connected in place of the IBDG. For the same fault F_1, the fault currents contributed by the grid and synchronous DG are respectively calculated as:

$$\begin{aligned} I_{s_{DG}} &= \frac{E}{Z'} \\ I_{Synch} &= \frac{E_{Synch}}{Z''} \end{aligned} \tag{2.13}$$

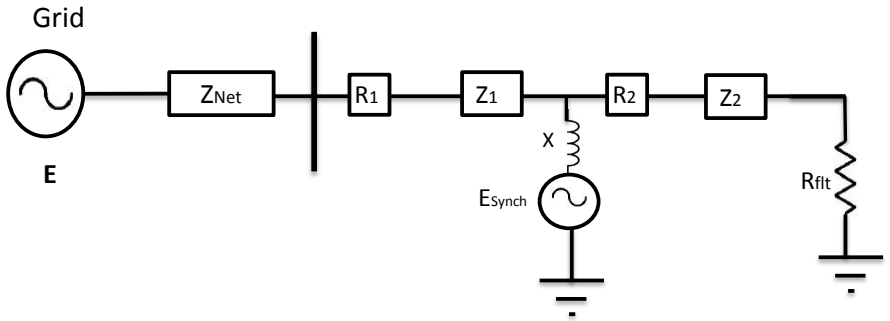

Figure 2.13: Equivalent model of a distribution system with a synchronous DG for a downstream fault

where:

$$\begin{aligned} Z' &= \frac{X' \times (Z_2 + R_f)}{X' + Z_2 + R_f} + Z_1 + Z_{Net} \\ Z'' &= \frac{(Z_1 + Z_{Net}) \times (Z_2 + R_f)}{Z_1 + Z_{Net} + Z_2 + R_f} + X' \end{aligned} \tag{2.14}$$

Comparing the equivalent impedance of the line seen by the grid when no synchronous DG is connected to the system, with the one calculated in the presence of synchronous DG, shows that:

$$\frac{X' \times (Z_2 + R_{flt})}{X' + Z_2 + R_{flt}} + Z_1 + Z_{Net} < Z_2 + R_{flt} + Z_1 + Z_{net} \tag{2.15}$$

Hence, the fault current contributed by the grid is increased when the synchronous DG is connected to the system:

$$I_{s_{DG}} > I_s \tag{2.16}$$

On the other hand, the portions of synchronous DG fault current flows in each part of the system are calculated as:

$$\begin{aligned} I_{Synch_1} &= I_{Synch} . \frac{Z_2 + Z_{flt}}{Z_{net} + Z_1 + Z_2 + Z_{flt}} = I_{Synch} . Z_{Eq_1} \\ I_{Synch_2} &= I_{Synch} . \frac{Z_1 + Z_{net}}{Z_{net} + Z_1 + Z_2 + Z_{flt}} = I_{Synch} . Z_{Eq_2} = I_{Synch} . (1 - Z_{Eq_1}) \end{aligned} \tag{2.17}$$

where I_{Synch_1} and I_{Synch_2} are the portions of I_{Synch} that flow towards the network and the grid respectively.

Consequently, the fault currents seen by R_1 and R_2 are calculated as:

$$I_{R_1} = I_{s_{DG}} - I_{Synch_1} \tag{2.18}$$

$$I_{R_2} = I_{s_{DG}} + I_{Synch_2} \tag{2.19}$$

As a result, compared to the case without the synchronous DG, the fault current seen by R_2 is increased when the synchronous DG is added to the system. On the other hand, the fault current seen by R_1 depends on the fault current contributed by the grid and the portion of DG fault current which flows towards the grid, I_{Synch_1}. If the increase in the fault current contributed by the grid is more than I_{Synch_1}, the fault current seen by R_2 will increase, otherwise, it will decrease.

2.8 Current Control Methods

Sinusoidal pulse width modulation (SPWM) is a common modulation technique used for voltage source inverters. In this type of modulation technique the switching commands of the inverter are produced by comparing a high frequency triangle waveform with a sinusoidal control signal. The frequency of the control signal is set to the desired fundamental frequency while its amplitude is used to modulate the switching duty ratio [70]. Sinusoidal pulse width modulated voltage source inverters (PWM-VSI) are used in conjunction with different types of linear and nonlinear controllers [76]. Although nonlinear controllers such as fuzzy logic (FL) based types show promising performance for application of VSIs, their implementation is more complex than the linear controllers. As a result, linear controllers are used in this work for both normal and fault condition.

Proportional integral (PI) regulators implemented in *abc* frame have been used as the traditional current regulators for PWM-VSIs. Although this type of controller has a long history of use for this application, its performance is degraded by steady state current magnitude errors and phase shift [77]-[79]. The steady state error is due to the fact that in *abs* frame, the controller operates on *ac* quantities and the PI regulator is not capable of introducing an infinite gain on non-zero frequencies [79],[80]. In contrast to natural frame regulators, synchronously rotating frame PI regulators are able to regulate the output current of PWM-VSIs with zero steady state error [78],[79]. For Synchronous frame

computation, the *ac* quantities in natural frame are converted to *dc* quantities using the following transformation [81]:

$$\begin{bmatrix} i_d \\ i_q \end{bmatrix} = \frac{2}{3}. \begin{bmatrix} cos(\theta) & cos(\theta - \frac{2.\pi}{3}) & cos(\theta + \frac{2.\pi}{3}) \\ sin(\theta) & sin(\theta - \frac{2.\pi}{3}) & sin(\theta + \frac{2.\pi}{3}) \end{bmatrix} . \begin{bmatrix} i_a \\ i_b \\ i_c \end{bmatrix} \tag{2.20}$$

As a result, the PI controller is able to introduce an infinite gain on the obtained *dc* quantities [79],[82].

The main drawback of the synchronous frame PI regulator is the need for a complex transformation between the natural and synchronous frame. To implement the synchronous frame PI regulators in rotating coordinate, the output currents of VSIs, which are *ac* quantities in natural frame, are converted to d-q synchronous frame quantities. On the other hand, after manipulation of *dc* quantities, the output current of PI regulators is transferred back to *ac* quantities in natural frame [76],[77]. This high amount of mathematical computation can be considered as the main drawback of synchronous PI regulators working in rotating frame. Another drawback is that single phase analysis and control is not possible using this controller. Even the *abc* frame representation of the rotating frame PI regulator introduced in [67] is not suitable for independent control of phases, due to the presence of off-diagonal terms in the controller matrix. Due to such off-diagonal terms, the phase quantities are functions of both corresponding and non corresponding phase errors [67].

In order to overcome this problem, a new controller, called P+Resonance controller, is proposed in [80]. This controller, (2.21), makes it possible to control the phase currents of VSIs independent of each other while zero steady state error is achieved in each phase.

$$\begin{bmatrix} V_a \\ V_b \\ V_c \end{bmatrix} = \begin{bmatrix} K_P + \frac{K_I s}{s^2+\omega_0^2} & 0 & 0 \\ 0 & K_P + \frac{K_I s}{s^2+\omega_0^2} & 0 \\ 0 & 0 & K_P + \frac{K_I s}{s^2+\omega_0^2} \end{bmatrix} . \begin{bmatrix} E_a \\ E_b \\ E_c \end{bmatrix} \tag{2.21}$$

where V_{abc} indicates the three phase voltage commands of the inverter, E_{abc} shows the error fed to the controller, and ω_0 is the operating frequency. As can be seen, the P+Resonance controller is able to achieve zero steady state error for *ac* quantities due to its infinite gain at ω_0. Also, the off-diagonal terms of zero show the independency between the phase signals.

2.9 Summary

This chapter has presented a comprehensive study on the background related to this research. A detailed study is performed on the protection problems observed in the presence of DGs. Operation of conventional protection systems in the presence of DGs is studied, and their performance deficiencies are explained. Different solutions that have been offered to overcome the protection problem associated with DGs are outlined. It is explained that all solutions require either the addition of extra elements to the system or changes to the structure of protection systems. In fact, based on current solutions, fundamental modifications are necessary for protection systems, which sometimes diminish the economical benefits of DGs. The performance of DGs during fault conditions is investigated, and the effects of DG type and location on the fault current seen by the protective devices are discussed. Since the research presented in this thesis is based on the operation of IBDGs during fault condition, this type of DG is studied in more detail, and different methods used to control these units are investigated.

Chapter 3

Fault Current Management in Radial Systems with Inverter Based Distributed Generators

3.1 Introduction

Inverter based distributed generators have been used for various power applications such as unified power flow controller (UPFC), active power filter (APF) and static synchronous compensator (STATCOM). However, to the author's best knowledge, no work has been reported in the literature to use IBDGs for FCM in power systems. In this chapter the novel idea of FCM operation is presented for radial systems with IBDGs. The idea is to employ IBDGs, the assets which are normally left idle during fault conditions, to manage the total fault current magnitude. The scheme is based on utilizing the available current and voltage phasor information from smart meters and applying the necessary control actions to operate the IBDGs in the FCM mode.

As discussed in the previous chapter, at the point of connection to a power system, many DGs require PE interfaces. During normal operation of power system, these PE interfaces have the potential to control the injected active and reactive power to the system, feed a local load, regulate the voltage or eliminate the current harmonics. On the other hand, in order for the original protection system to operate accurately during fault conditions, the IEEE std 1547 requires all DG units to be disconnected from the power system. This condition forces the DGs to be disconnected from the power system for every temporary fault. Such a response decreases the reliability of the system.

It should be noted that the response of IBDGs to a fault depends on the amount of fault current going through the PE interface. The current contribution of IBDGs in a fault varies based on the severity of the fault and its closeness to the unit. For less severe faults or for faults at farther locations, IBDGs can be kept connected to the system as long as their current contribution does not exceed the current rating of their interface inverter. In case of a severe fault close to the IBDG, the protection system of the PE interface trips the DG due to the excessive level of fault current.

The novel idea is to employ the IBDGs, which are normally left idle during fault conditions, to manage the total fault current magnitude by controlling their current contribution in the fault. For this purpose the IBDGs are kept connected to the system during a fault and their current magnitude is limited to a value below the tripping level of the connected inverters. To fulfil the FCM operation, the other controllable parameter of IBDGs, current phase angle, is chosen as the means of managing the total fault current magnitude. The reference phase angle which enables the FCM operation is calculated based on the relation between the fault current elements and their phase angles. The calculated reference phase angle is then extended for radial systems with multiple IBDGs.

By accomplishing this task, not only IBDGs are kept connected to the system, but the total fault current magnitude is also managed in the system. Moreover, there would be a minimum need to upgrade the protective devices which were designed for normal operation of the power system without IBDGs. Another advantage of the proposed protection methodology is the capability of PE interfaces to respond quickly to sudden changes in the system [13]. This capability of PE interfaces makes them a suitable choice for FCM. Furthermore, the proposed FCM methodology does not limit the contribution of DGs, but manages the total fault current by controlling the contribution of IBDGs. Hence, the method gives more flexibility on the amount of fault current reduction by IBDGs.

The rest of this chapter is organized as follows. Section 3.2 provides a basic introduction to the modeling and control of IBDG PE interfaces during normal and fault operation. Section 3.3 explains the concept of FCM using IBDGs and presents a method for calculating the reference current phase angle required for FCM operation. The phasor relations among the fault current elements are mathematically solved, and the results are used to validate the proposed phase angle calculation method in the following section. Section 3.4 provides the validation of the phase angle calculation method for a system with one IBDG. The effectiveness of FCM operation is also examined based on the IEEE 33-bus system for multiple IBDGs. A summary is provided in Section 3.5.

3.2 Control and Modeling of IBDG PE Interfaces

In order to simplify the operation of IBDGs during normal and faulty conditions, it is assumed that a constant *dc* voltage is provided on *dc* side of the inverter irrespective of the type of connected distributed energy system [67]. Hence, only grid side of DG power electronic interface is considered for the study. The inverter interface is modeled as a typical CC-VSI [83] with an L-filter connected on its *ac* side. The filter is used to attenuate high order current harmonics caused by high switching frequency of inverters while low frequency current harmonics are eliminated through a sinusoidal PWM scheme. Since the IBDG PE interfaces are modeled as CC-VSIs in both normal and fault conditions, the modulation parameters of the PWM modulator are set using a current control loop based on the inverter current references. During normal operation of the system, current references are updated continuously in order to control output power of the inverter. When a fault happens in the system, the control system is triggered with a signal from the fault detection unit. In this situation, the IBDGs change their operation to FCM units and manage the fault current based on the new references calculated for the fault condition.

Moreover, choice of controller plays an important role in regulating the output current of VSIs. In this work synchronous PI regulators are chosen for normal operation to regulate the PWM-VSI output current with a zero steady state error. Same type of controller can be used for balanced fault situations. However, it is suggested to use a P+Resonance controller [80] for unbalance fault situations if the control operation is intended to perform for each phase in *abc* frame. This controller makes it possible to control three phases of output current independently while zero steady state error is achieved in each phase. In case of poor transient response of P+Resonance regulator, next controller choice will be a PCI regulator as proposed in [82].

As mentioned in Section 2.8, for synchronous frame computation, the *ac* quantities in a natural frame are converted to dc quantities using the following transformation [81]:

$$\begin{bmatrix} i_d \\ i_q \end{bmatrix} = \frac{2}{3}. \begin{bmatrix} cos(\theta) & cos(\theta - \frac{2.\pi}{3}) & cos(\theta + \frac{2.\pi}{3}) \\ sin(\theta) & sin(\theta - \frac{2.\pi}{3}) & sin(\theta + \frac{2.\pi}{3}) \end{bmatrix} \cdot \begin{bmatrix} i_a \\ i_b \\ i_c \end{bmatrix} \tag{3.1}$$

As a result, the PI controller can introduce an infinite gain for the *dc* quantities obtained.

Since the IBDG PE interfaces are modeled as CC-VSIs in both normal and fault conditions, the modulation parameters of the PWM modulator are set using a current control loop based on the inverter current references. For this purpose, the d-axis and q-axis components of the inverter output current are compared with the corresponding current

references, and the difference is fed into a simple PI regulator. With consideration of the voltage drop across the inverter output filter, the inverter voltage components are obtained in d-q frame that rotates synchronously with the angular speed of the grid ω, as follows:

$$v_q = Ri_q + L\frac{di_q}{dt} + L\omega i_d + v_{pcc_q} \tag{3.2}$$

$$v_d = Ri_d + L\frac{di_d}{dt} - L\omega i_q + v_{pcc_d} \tag{3.3}$$

where v_d, v_q, i_d, and i_q are the d-axis and q-axis components of the inverter output voltage and current, respectively; v_{pcc_d} and v_{pcc_q} are the d-axis and q-axis components of voltage at the point where the inverter is connected to the grid; and R and L are the output filter components.

As shown in Figure 3.1, the d-axis and q-axis current components of inverter output current are compared with the corresponding current references and the difference is fed to a simple PI regulator. The steady state d-axis and q-axis components of the inverter

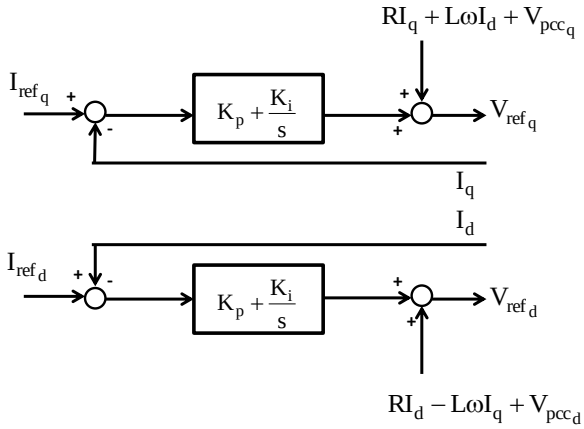

Figure 3.1: Current controller block diagram [84]

control voltage can be obtained in frequency domain as follow [84], [85]:

$$V_{ref-q} = RI_q + L\omega I_d + V_{pcc_q} + K_p(I_{ref-q} - I_q) + K_i(\frac{I_{ref-q} - I_q}{s}) \tag{3.4}$$

$$V_{ref-d} = RI_d - L\omega I_q + V_{pcc_d} + K_p(I_{ref-d} - I_d) + K_i(\frac{I_{ref-d} - I_d}{s}) \tag{3.5}$$

where K_p and K_i are the proportional and integral gains of PI controller.

3.2.1 Normal Operation

During normal operation, the IBDGs can be controlled to operate either as a PQ or PV generator. The PQ mode at unity power factor is chosen in this work since based on IEEE std. 1547, DGs are expected to operate at unity power factor and are not allowed to regulate the voltage at their point of common coupling [86]. However, the mode of operation of the IBDG during normal condition is independent of its FCM operation during fault condition. To operate the IBDG as PQ generators during normal operation, the active and reactive power injection of these units are controlled using the CC-VSI interface. The d-axis and q-axis components of the IBDG output current are separately controlled to follow their reference values, i_{ref_d} and i_{ref_q}. These two components of the IBDG current are responsible to provide the desired active and reactive power injected by the unit.

Active and reactive components of power can be represented in terms of d-axis and q-axis components of voltage at the PCC and injected currents [83]:

$$p = \frac{3}{2}(v_{pcc_d} i_d + v_{pcc_q} i_q) \tag{3.6}$$

$$q = \frac{3}{2}(v_{pcc_q} i_d - v_{pcc_d} i_q) \tag{3.7}$$

Choosing the d-axis component of voltage aligned with the grid voltage angular position, d-axis and q-axis voltage components are obtained as: $v_{pcc_d} = V_{pcc}$ and $v_{pcc_q} = 0$.

To provide the desired operation at unity power factor, the d-axis and q-axis components of the current references are obtained:

$$i_{ref_d} = \frac{2}{3}\frac{P_{ref}}{v_{pcc_d}} \tag{3.8}$$

$$i_{ref_q} = 0 \tag{3.9}$$

where P_{ref} is the active power reference which is considered as a constant value for a period of operation, during normal and fault condition [87]. This reference power can be either provided by the utilities, in case of energy storages, or determined by the control unit of dc-dc converter of connected PE interfaces to track the maximum power point of renewable resources. It should be noted that, in the later case, in order to guarantee the system stability, the speed at which P_{ref} is provided by the maximum power point tracker (MPPT) should be much lower than the speed of current control loop [87].

3.2.2 Operation during Fault Condition

When a fault is detected, IBDG operation is modified in order to manage the total system fault current. The idea is to keep IBDGs connected to the system during a fault and employ them to manage the excessive fault current contribution of DGs. Similar control strategies are employed for IBDGs during both normal and fault conditions. The only discrepancies are the current references of the CC-VSIs applied to the system. When a fault is detected in the system, current and voltage information available from the smart meters is used to calculate the magnitude and phase angle of the IBDG reference current, which enables the desired FCM operation. The d-axis and q-axis components of the reference current during the fault condition can therefore be obtained as follows:

$$i_{ref_d} = \hat{I} sin(\phi) \tag{3.10}$$

$$i_{ref_q} = \hat{I} cos(\phi) \tag{3.11}$$

where $\hat{I}$ is the magnitude of the IBDG reference current that is normally kept below the current threshold of the PE switches, and ϕ is the reference current phase angle, which is the main IBDG control parameter for the FCM operation.

It should be noted that in order to avoid damage to the PE interfaces the magnitude of current references is limited to the rating of semiconductor switches. Given by inverter manufacturer, the current rating of semiconductor switches vary from 1 to 4 times the rated current [5], [88] with the most common values are reported as 2-3 times the rated current [89], [90]. With a constant current magnitude, the current phase angle is the controllable parameter that determines the IBDG contribution.

3.3 Fault Current Management in Radial Systems

For the purposes of FCM using IBDGs, it is assumed that IBDGs are kept connected to the system during a fault and that their contribution in fault current is limited to a value below the tripping level of the connected VSIs. The total fault current then consists of the grid contribution plus the contribution from all IBDGs. Since the only controllable sources of fault current are IBDGs, the operation of these units is modified at the moment of fault detection. To this end, current references that result in a manageable fault current should be obtained.

The output current of inverter has two controllable parameters: current magnitude and current phase angle. Decreasing the current magnitude of the inverter output reduces the

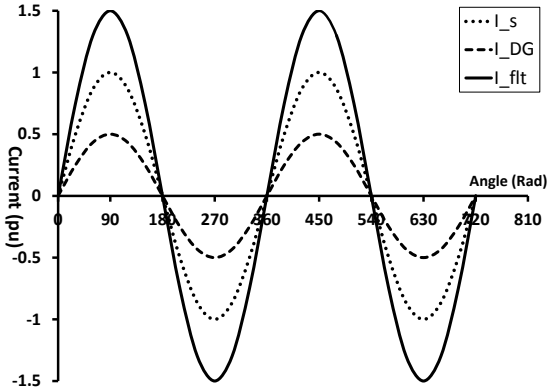

Figure 3.2: Fault current waveforms for $\theta_{DG} = 0°$

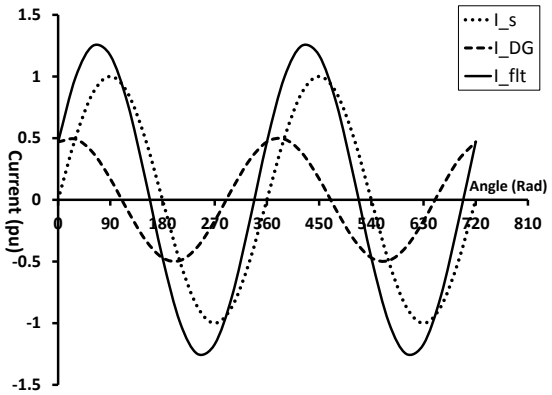

Figure 3.3: Fault current waveforms for $\theta_{DG} = 70°$

contribution of IBDG in total fault current. However, in order to decrease this contribution to zero, the inverter current magnitude should be reduced to a very small value that it is equivalent to deactivating the inverter. Moreover, in best case scenario when the inverter current magnitude is reduced to a value close to zero, the contribution of IBDG in total fault current is eliminated. However, it is not possible to reduce fault current below the grid current or eliminate the effects of synchronous DGs by controlling inverter current magnitude. The other controllable parameter of the IBDG current, current phase angle, must therefore be employed in order to manage its contribution to the total fault current without deactivating the PE interface.

Assuming a constant magnitude for IBDG current, its effect on the total fault current depends on the current phase angle. The worst case scenario happens when the IBDG

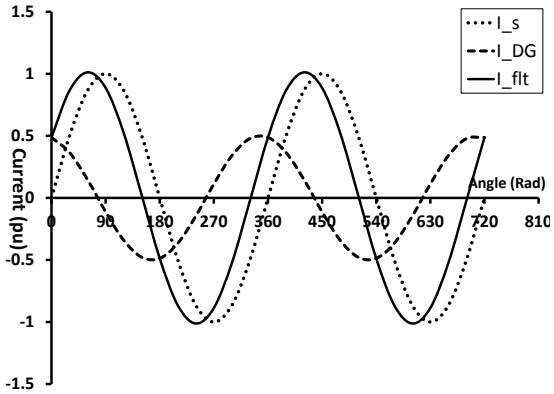

Figure 3.4: Fault current waveforms for $\theta_{DG} = 103°$

generates a current with the same phase angle as the grid current. Figure 3.2 illustrates this situation when the peak moments of the grid current and IBDG current happen simultaneously and as a result the maximum peak for the fault current is created. The effects of IBDG current on total fault current reduces when the peak moments of the contributing currents diverges. This scenario is shown in Figure 3.3. As can be seen, by changing the IBDG current phase angle to 70°, the peak values of the grid current and IBDG current are diverged. As a result, the total fault current is reduced. Based on the same idea, it is expected that there would be a current phase angle for the IBDG that, in contribution with the grid current would result in a fault current peak value equal to the grid current peak value. Figure 3.4 illustrates this scenario in which by using a proper phase angle for IBDG current, its contribution to the total fault current is effectively neutralized. It should be noted that the FCM operation is possible when the IBDG contributes to the fault current in addition to the grid current. In other words, it is required to have at least one current added to the IBDG current in order to be able to control the total fault current in the system. In situations where the DG current is the only element of fault current, modifying the current phase angle does not have any effect on fault current magnitude, given that reducing the current magnitude is required. However, an IBDG by itself should not cause a protection problem as the fault current contribution of this unit is limited.

Figure 3.5 depicts the current phasor diagram for a fault condition during which an IBDG contributes to the fault current in addition to the grid current. It is clear from the phasor diagram that the contribution of IBDG current shifts the total fault current away from its original value i.e., the grid current. As discussed, by manipulating the phase angle of the IBDG current it is possible to control the total fault current to be very close to the grid current. It is expected that an IBDG operating as a FCM unit would be able

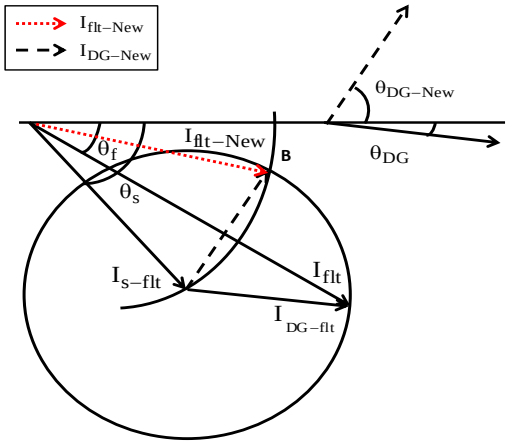

Figure 3.5: Phasor illustration of fault current elements with and without FCM

to control the fault current in three zones of operation. These three fault current control zones of IBDGs can be expressed as follows:

- Zone A: $I_{flt-New} < I_{flt}$ & $I_{flt-New} > I_{s-flt}$
- Zone B: $I_{flt-New} < I_{flt}$ & $I_{flt-New} = I_{s-flt}$
- Zone C: $I_{flt-New} < I_{flt}$ & $I_{flt-New} < I_{s-flt}$

Zone B gives the boundary condition which separates the other two regions. When only IBDGs are connected to the system, working in zone B results in a fault current that has the same magnitude as the grid current, I_{s-flt}. As indicated in Figure 3.5, when a fault occurs, if the inverter output current is equal to the vector shown at location B, the fault current (I_{flt}) and the contribution from the grid (I_{s-flt}) would be equal in magnitude because they are radiuses of a circle. Consequently, with no reduction in the IBDG current magnitude, a current phase angle would exist that results in a minimum IBDG contribution to the total fault current. The primary task thus becomes the determination of the IBDG current phase angle that results in $I_{flt-New}$ and I_{s-flt} being radii of a circle. If the phase angle of IBDG current is set to follow a value less than the boundary condition, the total fault current would be more than the fault current contribution from the grid meaning an operation in region A. On the other hand, when the reference phase angle is larger than the boundary condition, the system operates in zone C, which results in a fault current that is less than the grid current. This operation zone is the desirable one for systems with both synchronous DGs and IBDGs and will be discussed in Chapter 4.

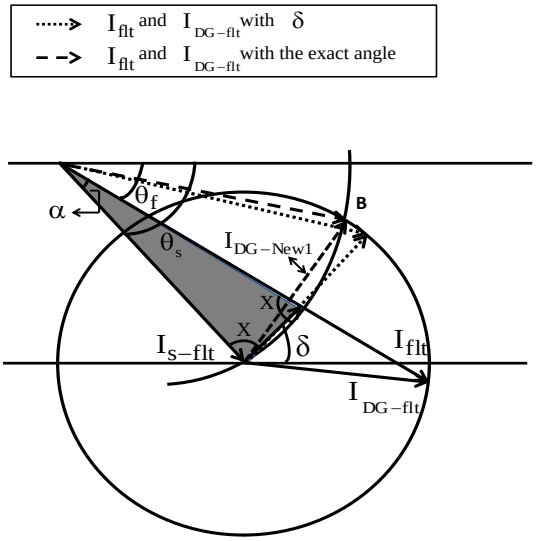

Figure 3.6: Phasor illustration of the IBDG current for FCM operation

3.3.1 Phase Angle Calculation Method

Successful management of the fault current requires determination of the reference current phase angle that enables the desired operation. The reference current phase angle which enables the FCM operation is calculated for a fault during which an IBDG contributes to the fault current in addition to the grid current. The FCM operation is then extended for the case where multiple IBDGs are installed in the radial system and the case where synchronous DGs exist in the system.

Consider the gray isosceles triangle shown in Figure 3.6. The smallest side of triangle makes the angle δ_B with the horizontal line. As can be seen, this angle is the desired phase angle for IBDG operation in zone B if its current magnitude is reduced to $I_{DG-New1}$. It can be shown that if this angle is set as the reference phase angle for the current injected by IBDG, the total fault current magnitude is reduced to a value close to the magnitude of grid current.

Angle δ_B can be calculated using sets of equations that are true for isosceles triangles. Consider the isosceles triangle as shown in Figure 3.7. The two equal angles of the isosceles triangle, X, can be calculated as functions of θ_{flt} and θ_s:

$$\alpha + 2X = 180 \Longrightarrow X = \frac{180 - \alpha}{2} \Longrightarrow X = \frac{180 - |\theta_s - \theta_{flt}|}{2} \tag{3.12}$$

where α is the angle between θ_{flt} and θ_s.

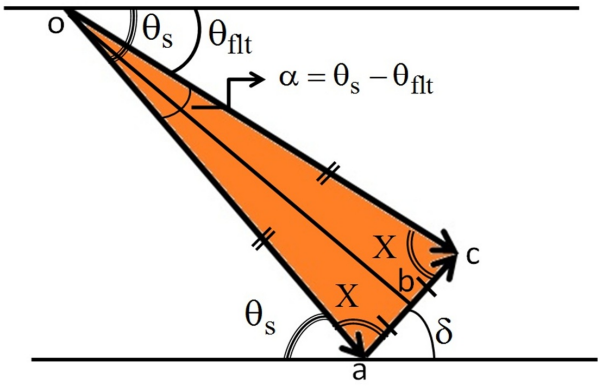

Figure 3.7: Isosceles triangle

Thus, δ_B can be found, as follows:

$$\delta_B + X + \theta_s = 180 \Longrightarrow \delta_B = 180 - X - \theta_s \Longrightarrow \delta_B = 180 - \frac{180 - |\theta_s - \theta_{flt}|}{2} - |\theta_s| \quad (3.13)$$

Moreover, the inverter current magnitude corresponding to the calculated δ_B can be obtained based on the fact that in isosceles triangles the height of triangle divides the base side in half.

$$cos(X) = \frac{\bar{ab}}{\bar{oa}} \Longrightarrow \bar{ab} = \bar{oa}.cos(X) \Rightarrow \hat{I}_{IBDG} = 2.\hat{I}_s.cos(X) \quad (3.14)$$

where ab is half the base of the isosceles triangle, and oa is one of the equal sides.

With the reduced current magnitude, the total fault current is limited to the exact value of the grid current. However, it is shown in this work that without reducing the inverter current magnitude and only by manipulating the current phase angle, the total fault current would be reduced to a value very close to that of the grid current magnitude.

3.3.2 Validation of the Proposed Phase Angle Calculation Method

To validate the proposed method, the phasor relation between the fault current elements can be solved mathematically. With one IBDG, the total fault current consists of the grid contribution plus that of the IBDG. The phasor relation between the elements of the fault current can generally be written as:

$$\vec{I}_{flt} = \vec{I}_s + \vec{I}_{IBDG} \quad (3.15)$$

or in complex exponential form of:

$$\hat{I}_{flt}.e^{j\theta_{flt}} = \hat{I}_s.e^{j\theta_s} + \hat{I}_{IBDG}.e^{j\theta_{IBDG}} \tag{3.16}$$

where $\hat{I}_{flt}$, $\hat{I}_s$, $\hat{I}_{IBDG}$ are the fault current, grid current and IBDG current magnitudes respectively; θ_{flt}, θ_s and θ_{IBDG} are the respective phase angles associated with the fault current, grid current and IBDG current elements.

When the total fault current has the same magnitude as the grid current, then $\hat{I}_{flt} = \hat{I}_s$ and Eq. 3.16 can be written as:

$$\begin{aligned} \hat{I}_s.cos(\theta_{flt}) &= \hat{I}_s.cos(\theta_s) + \hat{I}_{IBDG}.cos(\theta_{IBDG}) \\ \hat{I}_s.sin(\theta_{flt}) &= \hat{I}_s.sin(\theta_s) + \hat{I}_{IBDG}.sin(\theta_{IBDG}) \end{aligned} \tag{3.17}$$

Solving the above equations for two unknown variables, θ_{IBDG} and θ_{flt}, the desired phase angle for FCM operation of the IBDG is obtained as:

$$\theta_{IBDG} = \theta_s + cos^{-1}(\frac{-I_{DG}}{2.I_s}) \tag{3.18}$$

In a similar fashion, when multiple IBDGs are added to the system, Eq. 3.17 can be written as:

$$\begin{aligned} \hat{I}_s.cos(\theta_{flt}) &= \hat{I}_s.cos(\theta_s) + \sum_{i=1}^{n} \hat{I}_{DG_i}.cos(\theta_{DG_i}) \\ \hat{I}_s.sin(\theta_{flt}) &= \hat{I}_s.sin(\theta_s) + \sum_{i=1}^{n} \hat{I}_{DG_i}.sin(\theta_{DG_i}) \end{aligned} \tag{3.19}$$

where n indicates the number of IBDGs installed in the system.

As can be seen, when more than one IBDG is installed in the system, the phasor relation between the fault current elements becomes increasingly complex and the desired IBDGs current phase angles cannot be easily calculated. Moreover, calculating the reference phase angle using the above equation is not an easy task due to the presence of the cos^{-1} term which is hard to calculate in practice.

3.3.3 Current References for Multiple IBDGs

When multiple IBDGs are installed the contribution of each unit in fault current depends on its proximity to the fault. In this case, the effects of multiple IBDGs are automatically

considered in the FCM formulations as both the fault current magnitude and phase angle are changed by the contribution of these units. In this situation, fault current contributions of all IBDGs are summed to a single vector which is added to the grid current. The calculated δ_B value can be used as the reference current phase angle for all IBDGs. Another point is that it might not be necessary to operate all IBDGs as FCM units. Hence, among all the IBDGs installed in the system, the ones chosen to operate as FCM units should be controlled according to the reference current phase angle. As a result of this operation, it is expected that the total fault current will be reduced to a value much less than the fault current level obtained without FCM operation.

Another technique which can be applied for the case of multiple IBDGs is to control each unit to manage the fault current locally at its own bus. In general, for this operation each IBDG manages the fault current at its own bus so that the fault current magnitude would be equal before and after the bus. In this case, fault current phase angle, θ_{flt}, in (3.13) is substituted with the phase angle of the current going out of the bus with IBDG, and the grid current phase angle, θ_s, is replaced with the phase angle of the current injected to the bus.

Since in radial systems there is one grid point only and a large portion of the fault current is fed by the grid, the IBDGs which are connected to feeders other than the faulty feeder affect the fault current phase angle less than the ones connected to the faulty feeder. Hence, it is expected that using (3.13) with θ_{flt} and θ_s would solve the problem in radial systems, and there is no need to modify the formulation. However, the second technique should be used for loop systems where there are multiple grid points and there are buses with more than two lines connected to them. This operation for loop systems will be discussed in more detail in Chapter 6.

3.3.4 Phase Angle Measurement in Smart Grids

As shown in (3.13), the reference current phase angle, δ, is calculated as a function of the phase difference between the grid current and fault current. Since the FCM operation is defined for smart grids, the scheme utilizes the smart grid communication and metering infrastructure to manage the fault current. Transition of the existing centrally controlled electric power systems to smart grids enables the continuous monitoring and control of power system elements. Owing to the advanced metering and communication infrastructure of smart grids, realtime current and voltage information, including the magnitudes and phase angles from all system buses, are available to control different assets of the power system. Smart grids hence have a self-healing feature where the available information from

different points of the grid makes it possible to detect the abnormal conditions and take the necessary control actions. In this regard, the current and voltage phasor information communicated between the smart meters and the control units enables the FCM operation during fault condition. Based on the received data, the fault location is detected, the reference current phase angle for FCM operation is calculated, and the signals are sent to the IBDGs which are assigned to operate as FCM units.

However, the scheme can also be used for systems which do not have the necessary monitoring equipment. Synchronous PMUs offer a practical means of obtaining the real-time current phase angles required in (3.13). Using a synchronization signal received from the GPS satellite, PMUs installed at different locations of the power system are able to provide simultaneous phasor measurement of current and voltage waveforms [91]. Providing the system phasor information, presence of PMUs in power systems is beneficial for many other power applications such as protection, control and power system monitoring [92]. Regardless, it should be noted that placing PMUs at every bus of the power system is not necessary. Hence, the best possible locations which results in minimum number of PMU installations while providing enough current information for FCM operation should be determined in advance.

When current phasors are not available, fault current phase angle can be evaluated for faults at different locations of the system. It is expected that for faults happening in a region, fault current phase angle will vary over a very narrow range. Hence, by conducting an off line study on the system, fault current phase angles can be obtained for use during the FCM operations.

Moreover, performance of the system can be examined for a range of possible fault current phase angles. It can be shown that FCM units can still reduce the total fault current effectively even if a possible range is used instead of the exact fault current phase angle. This is true because variation of fault current phase angle in (3.13) does not directly affect the calculated δ_B. In fact, contribution of fault current phase angle in δ_B is reduced due to presence of the 180° term and the grid current phase angle. By varying the fault current phase angle between 0° to 180°, a possible range for $|\theta_s - \theta_{flt}|$ and consequently for δ_B can be obtained. Variation of the current phase angle around δ will result in different total fault current magnitudes. However, as explained in Section 3.3 for small phase variations around δ_B, total fault current magnitude will vary either in zone A or in zone C which, in both cases, results in a total fault current less than than the original fault current magnitude.

A sensitivity index, as the one shown in (3.20), can be a good measure to observe the

variation of total fault current from its desired value for different values of δ_B.

$$SI_{I_{flt}} = \frac{I_{flt} - I_{flt_{ref}}}{I_{flt_{ref}}}.100\% \tag{3.20}$$

3.4 Simulation Results

In order to investigate the effectiveness of the FCM technique and to evaluate the accuracy of the calculated reference phase angle, the operation is first evaluated on a balanced 3-bus system with one IBDG only. The validation technique explained in Section 3.3.2 is used to evaluate the accuracy of (3.13) in calculating the reference current phase angle for FCM operation. In order to evaluate the reliability of the FCM operation, and to assess the FCM operation for the case the exact value of the fault current phase angle is not known, sensitivity of fault current magnitude is examined for a typical error of 10% in the fault current phase angle. The results confirm the accuracy of the calculation method and the effectiveness of the FCM technique. In the next step, the FCM technique is applied on the IEEE 33-bus system with multiple IBDGs. The results prove the success of the FCM technique in managing the fault current magnitude in radial systems with multiple IBDGs. Investigating the time operation of an inverse time over current relay connected on the faulty feeder of the system, shown the effectiveness of the method in bringing back the normal operation of protective devices. The effect of the FCM technique on the voltage profile at the PCC of IBDGs, and on the power level of these units are shown. Moreover, the effect of communication time delay on the FCM operation of IBDGs is investigated.

3.4.1 Simulation Results for the 3-bus System

Figure 4.1 shows the 3-bus system adopted in this study to evaluate the accuracy of the proposed phase angle calculation method for FCM. This system is a balanced system with an IBDG on its bus 2 which is connected to the grid through a 3-phase CC-VSI and used to feed a local load. R and L represent the resistance and inductance of the *ac*-side filter, respectively; R_l and L_l represent the respective line resistance and inductance; R_s and L_s are the respective gird resistance and inductance; V_{pcc} is the voltage at the connection point of inverter; and V_{dc} is the *dc*-link voltage. The system parameters are shown in Table 3.1. Performance of the system during fault condition is evaluated by applying a 3-Phase balanced fault at load bus.

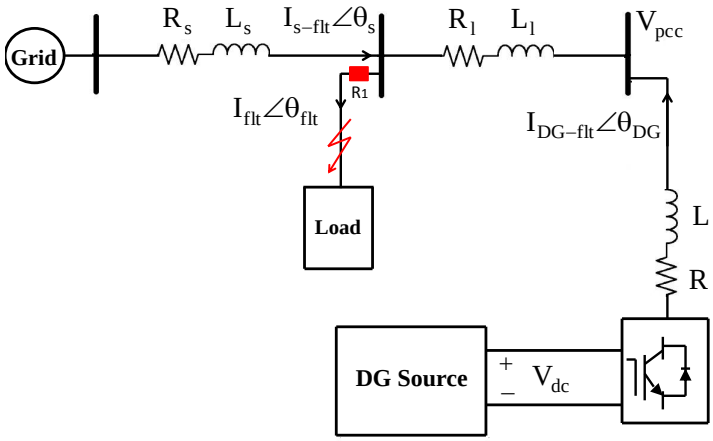

Figure 3.8: System configuration the 3-bus test system

Table 3.1: System Parameters

R_s	1 [ohms]
L_s	0.0025 [H]
R_l	0.02 [ohms]
L_l	0.00001 [H]
R	0.0097 [ohms]
L	0.02 [H]

During normal operation of the system, IBDG operates as a PQ generator at unity power factor. the d-axis and q-axis components of current references are obtained considering unity power factor operation of the IBDG:

$$i_{ref-d} = \frac{2}{3}\frac{P_{ref}}{v_{pcc_d}} \tag{3.21}$$

$$i_{ref-q} = 0 \tag{3.22}$$

where P_{ref} is the active power reference (0.03 MVA) and v_{sd} is the d-axis component of voltage at the PCC.

Fault Response without FCM Operation

Figure 3.9 shows the localized fault current when the IBDG does not operate as an FCM unit. It is evident that the contribution of the IBDG increases the total fault current at

the fault location to more than the normal level when the grid is the only source feeding the fault.

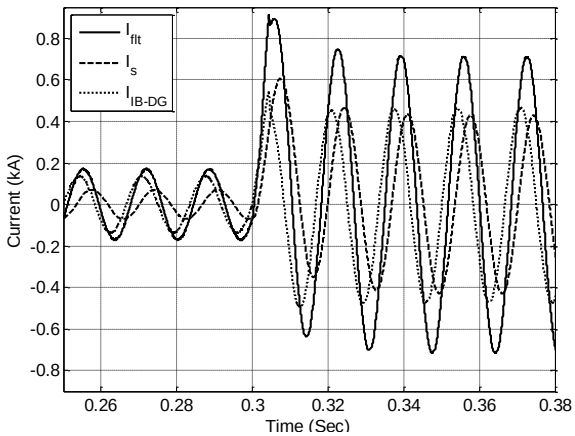

Figure 3.9: Phase a fault current without FCM operation (3-bus system)

In order to protect the switching interface of IBDG its current magnitude is limited to a value below the rating of semiconductor switches. The limit of 3.5 times the rated current is primarily chosen for the reference current in order to show the effectiveness of the proposed FCM operation even for IBDGs with higher than normal fault current contribution capability. In another words, the purpose of choosing this high value is to express the independency of the proposed method on IBDG current magnitude.

As discussed, there would be a phase angle for the IBDG current which in contribution with the grid current would result in a fault current magnitude equal to grid current magnitude. With this phase angle which enables the FCM operation the IBDG will contribute to the fault current, but its contribution does not affect the total fault current magnitude.

Fault Response with FCM Operation

When IBDG operates as a FCM unit, current reference of the CC-VSI is modified at the moment of fault detection. Similar to normal operation, the magnitude of the reference current is limited to a value equal or less than 3.5 times the rated of inverter while current phase angle is modified according to the desired operation region. In this case study since there is one IBDG only, the FCM operation is performed in zone B.

Figure 3.10 shows the calculated reference phase angle obtained from (3.13) and the resulting FCM operation for phase a of the fault current elements. As can be seen, when

the calculated reference phase angle of δ applied, the fault current magnitude is managed so that it equals the grid current magnitude.

To validate the accuracy of the phase angle calculation method, the results were compared with those obtained when (3.18) is used for calculating the reference phase angle. Figure 3.11 shows the phase angle calculated and the resulting FCM operation for this scenario. A comparison of the two calculated phase angles reveals that the reference phase angle obtained from the phase angle calculation method tracks the angle obtained by solving the phasor equations with a negligible error of 0.7%. As a result, a closely similar FCM operation is obtained using either of the two calculated phase angles. It can thus be concluded that the phase angle calculation method accurately determines the phase angle required for efficient FCM. The results also prove the effectiveness of the FCM technique for managing the fault current without reducing the DG current magnitude.

In order to better show the independency of the obtained result on IBDG current magnitude another case study has been presented where the maximum current magnitude of twice the rated current is chosen for IBDG, and the resulted fault current magnitude is compared with the one obtained in the first case study. Figure 3.12 the result for this scenario. It can be seen that the total fault current magnitude is managed to the same value, independent of the IBDG current magnitude.

Operation in Region A

Figure 3.13 shows FCM operation in zone A for two different phase angles. This operation is achieved by deducting two constant phase angles of 10° and 20° from the reference phase angle calculated for operation in Zone B, δ_B. For both cases the total fault current is reduced to a value higher than the grid current but less than the original fault current magnitude, $I_{flt} < I_{flt-New} < I_{s-flt}$. However, the reduction in fault current magnitude is higher when a value of 10° is deducted from the boundary value which means when the phase angle is closer to δ_B.

Operation in Region C

Operation of IBDGs as FCM units in zone C is investigated for two phase angles. In this case, two constant phase angles of 10° and 20° are added to the reference phase angle calculated for zone B operation, δ_B. Figure 3.14 shows the performance of the FCM unit in zone C for these two phase angles. As can be seen for both cases, the total fault current is reduced to a value below the grid current. Moreover, it is evident that a larger phase angle will result in a higher reduction in the total fault current magnitude.

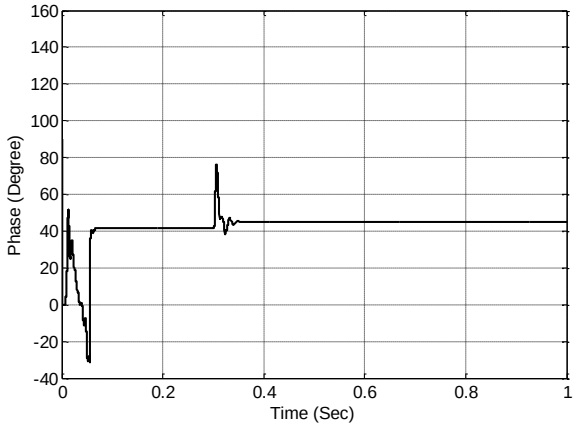

(a)

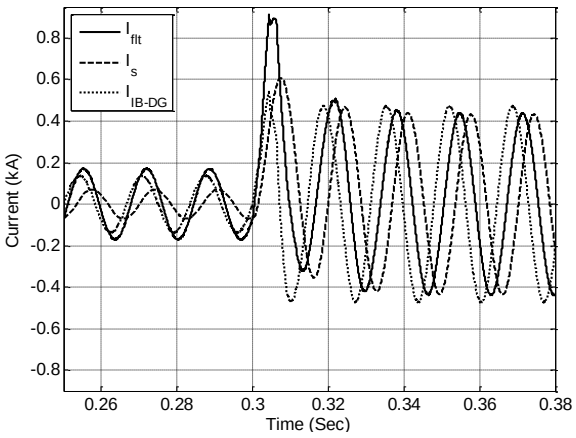

(b)

Figure 3.10: Fault current management using the proposed phase angle calculation method a) Calculated phase angle b) Phase a of I_{flt}, I_s, I_{IBDG}

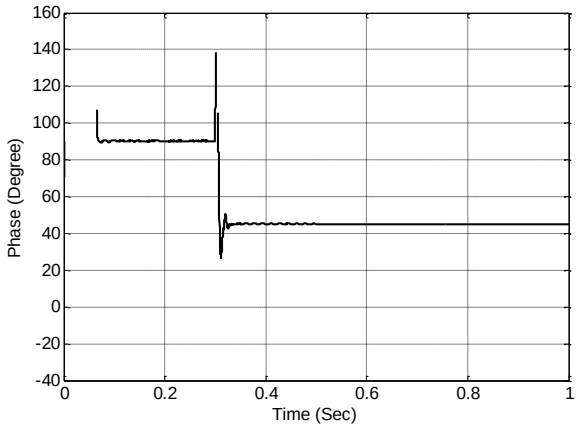

(a)

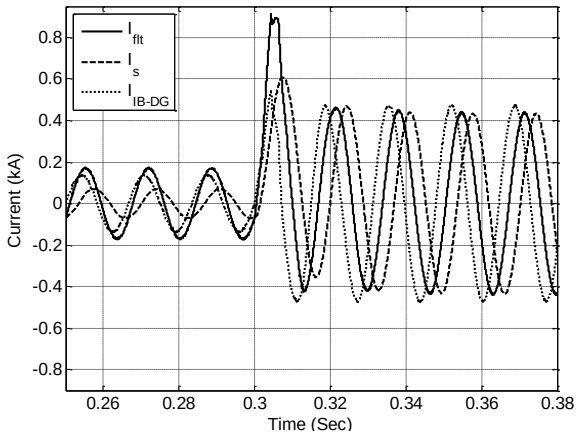

(b)

Figure 3.11: Fault current management using the validation method a) Calculated phase angle b) Phase a of I_{flt}, I_s, I_{IBDG}

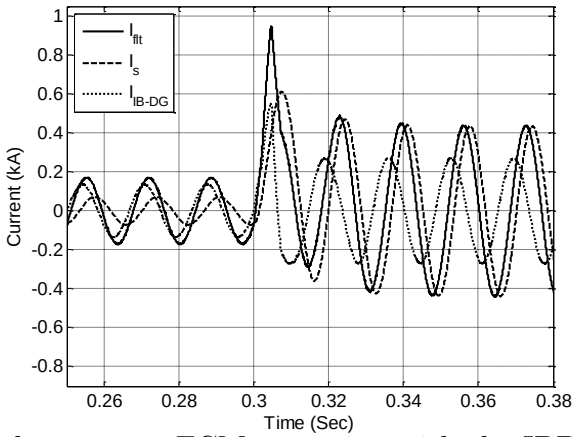

Figure 3.12: Phase a fault current - FCM operation with the IBDG contribution of twice the rated current

Comparison of the FCM Operation in zones A, B and C

Figure 3.15 compares the proposed FCM operation in three zone of A, B and C. In this case, for operation in region A/C, a constant value of 20° is subtracted from/added to δ_B. As can be seen, in all three cases, the fault current magnitude is successfully managed to a value below the fault current seen without FCM operation. The output current of the IBDG is shown in Figure 3.16 for operation in three zones. It is clear that the current magnitude of the IBDG is kept constant in all cases. This proves that the FCM operation obtained in all three cases is a result of phase angle control of IBDG current.

Sensitivity Analysis for FCM Operation

In order to evaluate the reliability of the FCM operation and to examine its performance in case the exact value of fault current is not known, sensitivity of fault current magnitude is examined for a typical error of 10% in the calculated fault current phase angle. Considering (3.13), the reference current phase angle for FCM, δ_B, is a function of θ_s and θ_{flt}. The grid current phase angle, θ_s, is a known quantity and for the 3-bus system shown in Figure 4.1, this phase angle is obtained as $-167°$ during fault condition. Assuming a $\pm 10\%$ error for fault current phase angle, the possible range for δ_B is obtained as:

$$-102° - 10° \leq \theta_{flt} \leq -102° + 10° \Longrightarrow 40° \leq \delta \leq 50° \tag{3.23}$$

It is shown that the calculated δ value is not affected significantly by the measurement errors in fault current phase angle. This is mainly because δ_B is not directly proportional

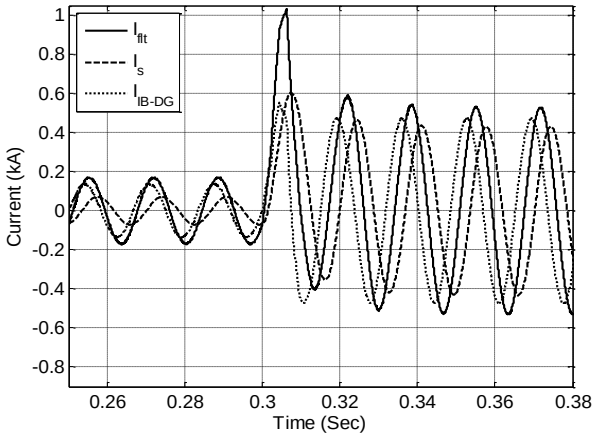

(a)

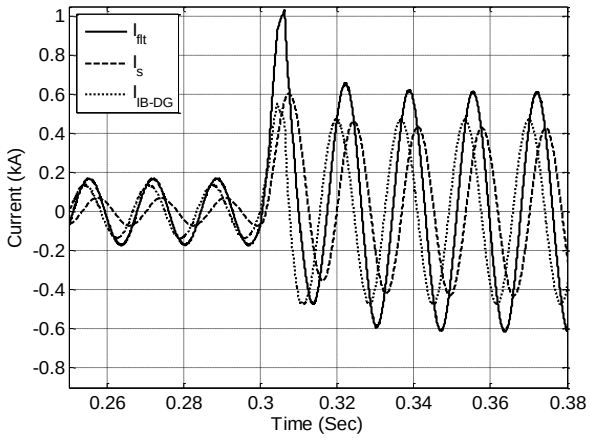

(b)

Figure 3.13: Simulation results for operation in region A a) $\theta_{IBDG} = \delta$-10 b) $\theta_{IBDG} = \delta$-20

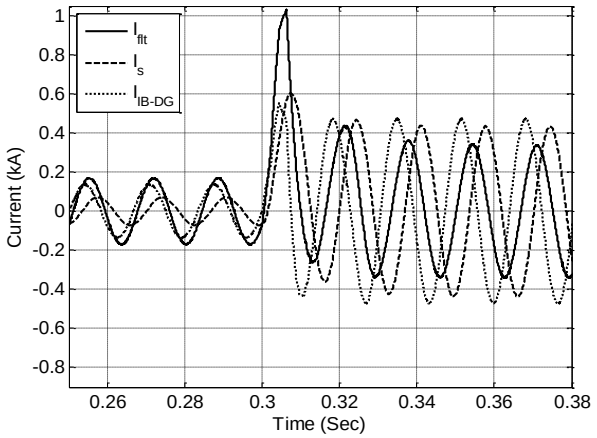

(a)

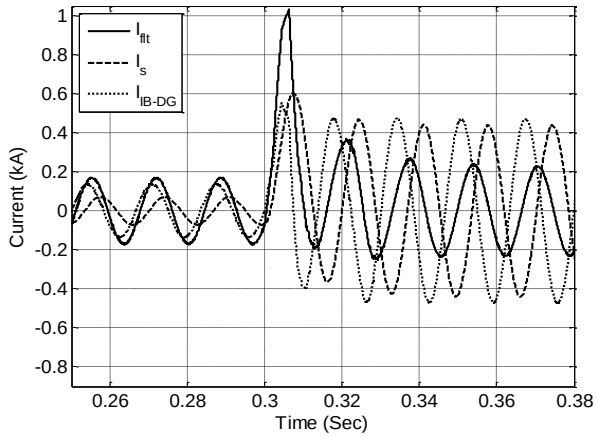

(b)

Figure 3.14: Simulation results for operation in region C a) $\theta_{IBDG} = \delta$+10 b) $\theta_{IBDG} = \delta$+20

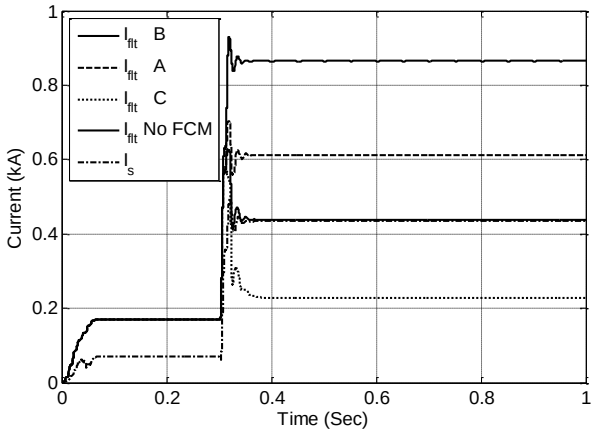

Figure 3.15: Comparison of fault current magnitude for three ranges of FCM operation

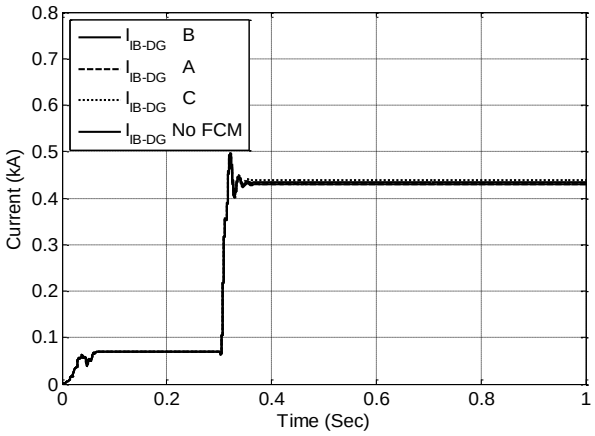

Figure 3.16: Comparison of IBDG current magnitude for three ranges of FCM operation

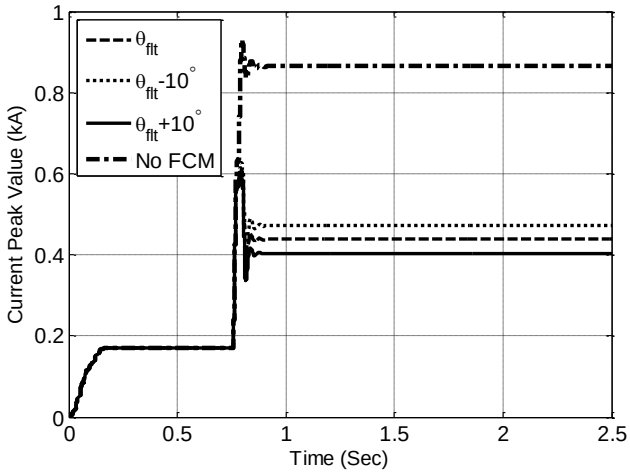

Figure 3.17: Current sensitivity for $\pm 10\%$ error in θ_{flt} (3-bus system)

to θ_{flt}, and the presence of other elements in (3.13) reduces the effects of fault current phase angle errors on δ_B.
Figure 3.17 compares the fault current magnitude for four different scenarios: when there is no FCM operation, with the exact value of θ_{flt}, and with $\theta_{flt} \pm 10\%$ error. As can be seen in this figure, even with an error of 10% in fault current phase angle, FCM unit is able to effectively reduce the total fault current magnitude.

3.4.2 Simulation Results for Multiple IBDGs

The IEEE 33-Bus distribution system was chosen for the investigation of the effectiveness of the proposed FCM operation in a larger system with multiple IBDGs. This network is a 3-phase balanced system at a nominal voltage of 12.66 kV. The load data and distribution line information can be found in [93]. As shown in Figure 3.18, five IBDGs are connected to the system at buses 7, 13, 19, 23, and 26. Distributed generators are represented at 0.408 kV, connected to the distribution system through five 0.408/12.66 kV Δ-Yg transformers. All five IBDGs operate at unity power factor and in total provide 60% of the required power of the system. Current and voltage phasor information from all system buses, including the faulty bus, are used to calculate the phase angle required for FCM operation.

The IBDG FCM operation was verified for a 3-phase fault occurrence on bus 27 at $t = 0.22\ s$. Figure 4.6 shows the total fault current and the contribution from all available generation units when the IBDGs continue normal operation during the applied fault. As

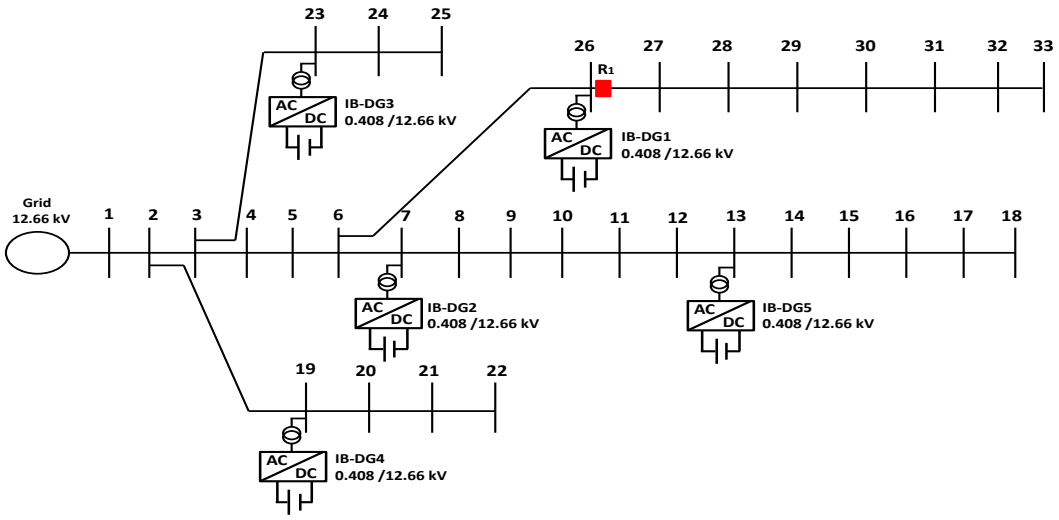

Figure 3.18: IEEE 33-Bus distribution system

can be seen, the IBDGs contribution results in a total fault current greater than the current seen when no IBDG is installed in the system. As in the previous case, performance of the proposed FCM operation is first examined for IBDGs with maximum current contribution of 3.5 the rated current. Next, the maximum current contribution of IBDGs is reduced to twice their rated current, and it is shown that independent of the IBDGs current magnitude, the proposed FCM operation manges the total fault current to the same level.

When IBDGs function as FCM units, their operation is modified following the moment of fault, and the phase angle calculated for FCM operation is therefore fed into the system as the IBDG reference current phase angle. For this case study, the current references for all IBDGs are modified. However, since the IBDGs which are closer to fault location have the highest contribution into fault current, they are the main units which are responsible for managing the fault current. Hence, a subset of IBDGs can also be selected to operate as FCM units.

Figure 3.20 illustrates the fault currents that result when IBDGs operate as FCM units. As can be seen, for a fault at bus 27, the total fault current is limited to a value almost identical to the fault current observed when there is no IBDG installed in the system. The fault current obtained in this case follows the primary fault current with a negligible error of 0.38%. The output currents of the five installed IBDGs are also shown in Figure 3.20. The IBDG current magnitude is clearly kept at the same level as it is without FCM. Hence, the IBDG current phase angle is the only factor that ensures the total fault current equals the grid current.

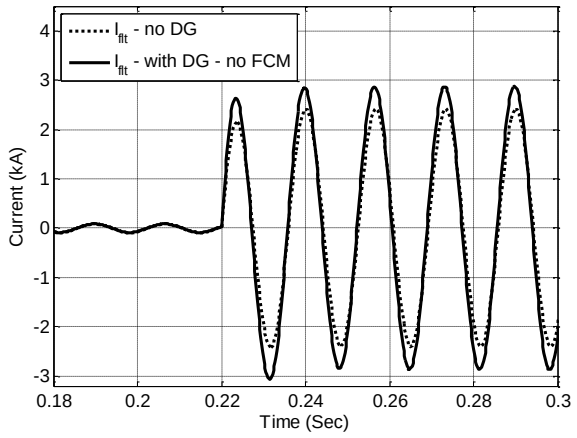

(a)

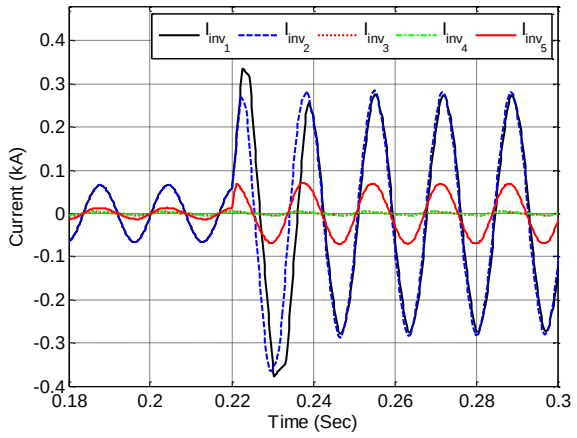

(b)

Figure 3.19: Fault current contribution from generation units - IBDGs contribute 3.5 times their rated current a) I_{flt} and I_s b) I_{inv_1}, I_{inv_2}, I_{inv_3}, I_{inv_4}, I_{inv_5}

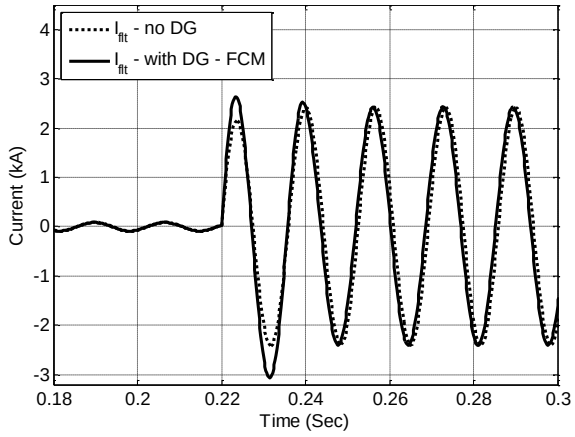

(a)

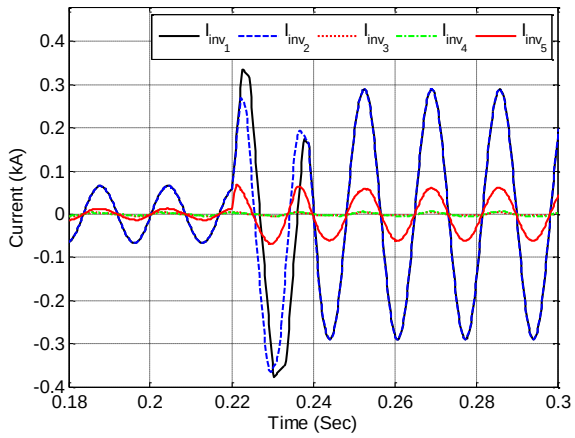

(b)

Figure 3.20: Operation of IBDGs as FCM units - IBDGs contribute 3.5 times their rated current a) I_{flt} and I_s b) I_{inv_1}, I_{inv_2}, I_{inv_3}, I_{inv_4}, I_{inv_5}

In order to better show the independency of the FCM operation on current magnitude of IBDGs, the maximum current contribution of these units is reduced to twice their rated current. Figure 3.21 shows that even though the IBDGs have lower current magnitudes, the total fault current is managed to the same level as before.

Figure 3.22 and Figure 3.23 show snapshots of voltage and power at the point of common coupling of each IBDG for the case they continue their normal operation and when they operate as FCM units. As can be seen, with the applied changes in the current phase angle of IBDGs during fault condition, their output power changes. The voltage at the point of common coupling of IBDGs express the similarity of fault situation for the two scenarios.

Effects of Time Delay on FCM Operation

In the simulation results shown in Figure 3.20 there is a delay of 10 ms for the fault to be detected and the new current references to be updated. The output current of inverter tracks the new current references 10 ms after this time. It should be noted that although the total applied time delay is negligible, any further increase in fault current magnitude does not affect the FCM operation. The reason for this is that by the time new references are set (20 ms after the fault) the first cycle of current is passed, and the fault current is managed in the second cycle after the fault occurrence. Hence, any increase in the applied time delay does not affect the effectiveness of the proposed FCM operation. In order to further investigate the effect of time delay on FCM scheme, another case study has been presented. In this case study, the new current references are applied with a time delay of 150 ms. Figure 3.24 illustrates the resulting fault current magnitude. It can be seen that at the moment when new references are applied, fault current is managed to a value very close to the grid current.

Effects of IBDGs Power Level on FCM Operation

As mentioned before, the four installed DG provide 60% of the required load of the system. All IBDGs operate at unity power factor. IBDG1 and IBDG2 each has the output power of 0.97 MW, IBDG3 and IBDG4 provides 0.045 MW, and IBDG5 generates 0.18 MW. The operation of proposed FCM technique is however independent of the IBDGs output power. Figure 3.25 compares the managed fault current magnitude for two different power level of IBDG1: 0.97 MW and 1.5 MW. It is clear that the fault current magnitude is managed to the same level when IBDGs operate as FCM units independent of the power level of IBDG1.

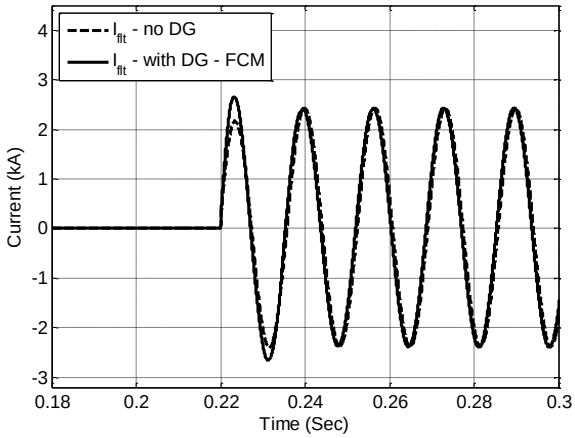

(a)

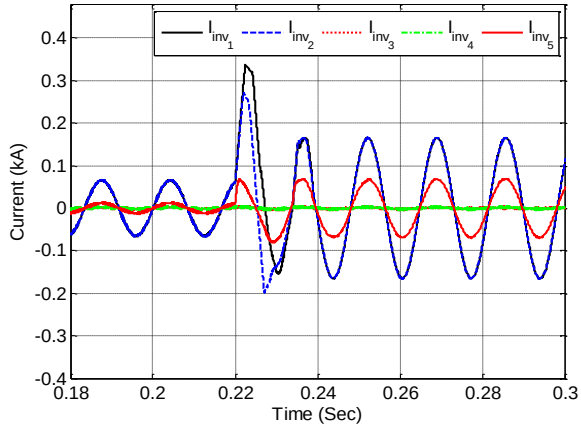

(b)

Figure 3.21: Operation of IBDGs as FCM units - IBDGs contribute twice of their rated current a) I_{flt} and I_s b) I_{inv_1}, I_{inv_2}, I_{inv_3}, I_{inv_4}, I_{inv_5}

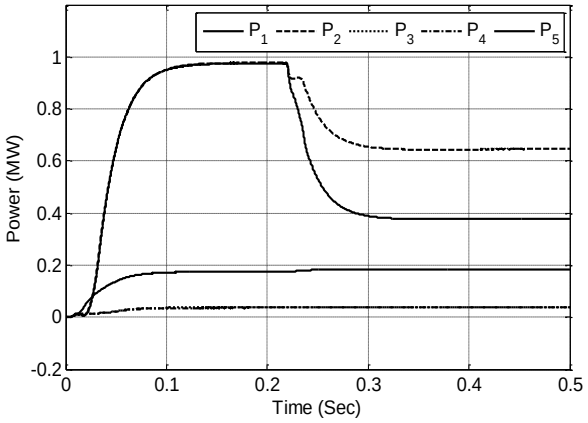

(a)

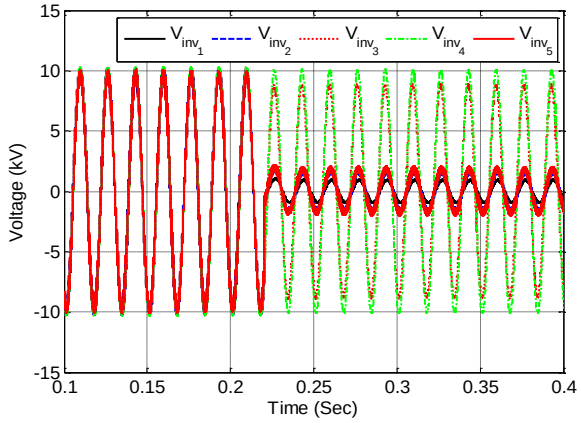

(b)

Figure 3.22: Active power and voltage at PCC - No FCM a) Output power b) V_{pcc}

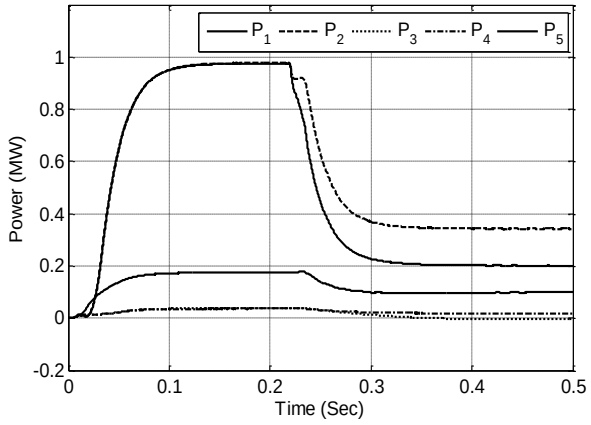

(a)

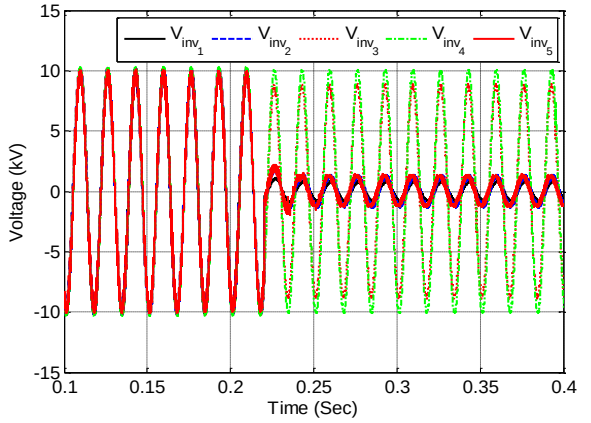

(b)

Figure 3.23: Active power and voltage at PCC - FCM a) Output power b) V_{pcc}

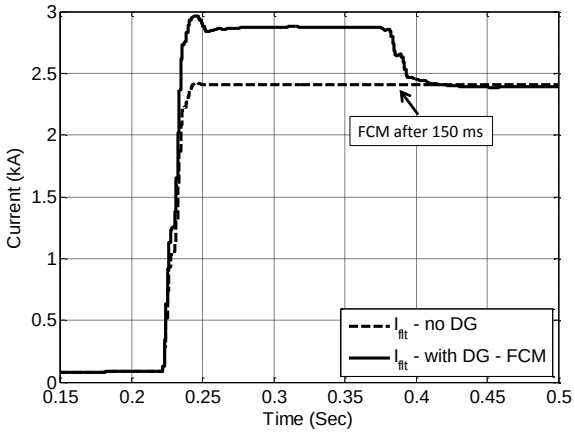

Figure 3.24: Effect of time delay of 150 ms on fault current magnitude

Effects of FCM Technique on Operation of Protective Devices

Presence of IBDGs increases the fault current seen by the protective devices and may violate the time operation of these units. In order to clarify this point, an inverse time overcorrect relay is connected on line 26-27 of the system in Figure 3.18, and the time operation of this relay is examined for three scenarios: When there is no IBDG connected to the system; When 5 IBDGs are connected to the system but none of them operate as FCM unit; When 5 IBDGs are connected to the system and operate as FCM units during the fault. Simulation results demonstrate that when there is no IBDG connected to the system, the relay operates at 0.319 sec. When 5 IBDGs are connected, due to their contribution in fault current, the operation time of relay is decreased to 0.292 sec. On the other hand, when IBDGs operate as FCM units, the time operation of the relay is increased to 0.318 sec which is very close to the operation time of relay when there was no IBDG connected to the system.

FCM for Single Phase Faults

Since three-phase balanced faults are considered in this work, the FCM technique is developed for one phase only. Same formulations can be extended for single phase faults in two ways; First, the fault current in each phase can be managed independently in *abc* coordinate. To implement this method in *abc* coordinate other types of stationary frame controllers such as P-Resonant regulators [80] are required to avoid the steady state error associated with PI regulators. In another approach, the unbalanced phase components

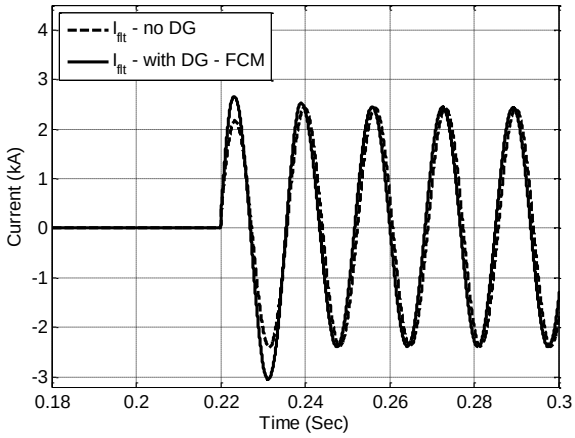

(a)

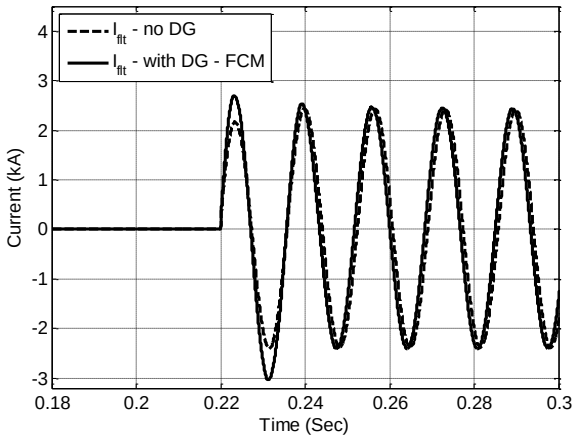

(b)

Figure 3.25: Effects of IBDGs power level on FCM operation a) FCM result when $P_{IBDG_1} = 0.97MW$ b) FCM result when $P_{IBDG_1} = 1.5MW$

of the current can be converted into three balanced positive, negative, and zero sequence components. Hence, the fault current can be managed in *dq* frame for each balanced sequence.

3.5 Summary

This chapter has proposed a novel technique of using IBDGs as FCM units. For this operation, when a fault is detected in the system, the function of the IBDGs is modified from that of PQ generators to that of FCM units by changing the IBDG current phase angle. The reference current phase angle, which enables the FCM operation, is calculated for a system with one IBDG and extended for the case multiple DGs in the system. The phasor illustration of fault current elements, in the presence of one IBDG, is used to calculate the reference phase angle required for FCM operation as a function of grid current and fault current phase angles. The calculated phase angle is validated mathematically. Also explained is how to extend the FCM operation when multiple IBDGs exist in the system. Current and voltage phasor information from all system buses, including the faulty bus, are used to calculate the phase angle required for FCM operation. However, it is also shown that the method is capable of managing the fault current in systems where the phasor information is not available on a regular basis. The proposed operation is examined on two test systems: a 3 bus test system with a single IBDG, and IEEE 33-bus system with 5 IBDGs. The results show that the proposed algorithm is capable of managing the fault current to a value close to the grid current. A negligible error of 0.38% in the case of the IEEE 33 bus system proves the capability of the method in maintaining the currents flowing through protective devices at their original values.

Chapter 4

Fault Current Management in Radial Systems with Inverter Based DGs and Synchronous DGs

4.1 Introduction

The fault current contribution of a DG unit varies depending on the type of DG [40], [60]: synchronous DGs provide a greater contribution to a fault current than do IBDGs. While an IBDG fault current is limited to two to three times the rated current of the unit, synchronous DGs can contribute about four to five times their rated current [5],[88]-[90]. When synchronous DGs are added to systems designed to work without DGs, they are thus considered to be the primary source of protection problems. The zone B FCM operation explained in Chapter 3 is capable of managing fault currents contributed by IBDGs but does not function effectively when synchronous DGs are added.

As explained in Section 3.3.1, the FCM operation in zone C results in a fault current less than the grid current. When both IBDGs and synchronous DGs exists in the system, by operating IBDGs as FCM units in zone C, the current gap generated between the grid current and the total fault current can be used for managing the contribution of the synchronous DGs. In this case, the current and voltage information available from smart meters enables the acquisition of appropriate zone C reference current phase angle for managing the contribution of synchronous DGs, which can then be fed to the IBDGs. Unlike zone B operation, the FCM operation in zone C is dependant on the IBDG current magnitude. However, unlike what is generally expected, the IBDGs with higher current

ratings or the ones which are closer to the fault location have higher contribution in the fault current, and are more effective units in managing the fault current contribution of synchronous DGs connected to the system. Moreover, it is shown in this chapter that more effective FCM operation is obtained in presence of synchronous DGs with higher numbers of IBDGs and with a larger reference current phase angle in zone C.

The operation in zone C would resolve the main protection problem arising from the connection of synchronous DGs, which would enable both synchronous DGs and IBDGs to be kept connected to the system during fault conditions without incurring associated increases in the magnitude of the fault current. Consequently, there would be minimum need to add current limiting devices or change the existing protection system in presence of DGs. Moreover, the protection system constraints associated with connection of new DGs could be relaxed.

The rest of this chapter is organized as follows. Section 4.2 presents the proposed FCM operation for managing the fault current contribution of synchronous DGs. Section 4.3 describes the factors affecting the FCM operation of synchronous DGs in zone C. The effectiveness of the proposed FCM scheme for addressing the contribution of synchronous DGs is examined on the IEEE 33-bus; the simulation results are presented in section 4.4. A summary is provided in section 4.5

4.2 Fault Current Management of Synchronous DGs using IBDGs

In a system with multiple DGs, the total fault current consists of the grid current plus the contribution from all DGs. Of the two common types of DGs, IBDGs and synchronous DGs, IBDGs are the only controllable sources of fault currents. Therefore, the operation of these units can be modified during fault conditions in order to manage the contribution of synchronous DGs. The inverter output current has two controllable parameters: current magnitude and current phase angle. Although decreasing the magnitude of the IBDG current reduces the contribution of these units to the fault current, it does not provide the flexibility required for the management of the synchronous DG contribution. In fact, in the best case scenario, when the magnitude of the inverter current is reduced to a value close to zero, the IBDG contribution to the total fault current is eliminated. However, it is not possible to eliminate the effects of synchronous DGs by controlling the inverter current magnitude. Therefore, a novel concept introduced in this chapter to employ the IBDG current phase angle as a control parameter for managing the synchronous DG contribution,

which makes it possible to manage the total fault current over a wide range.

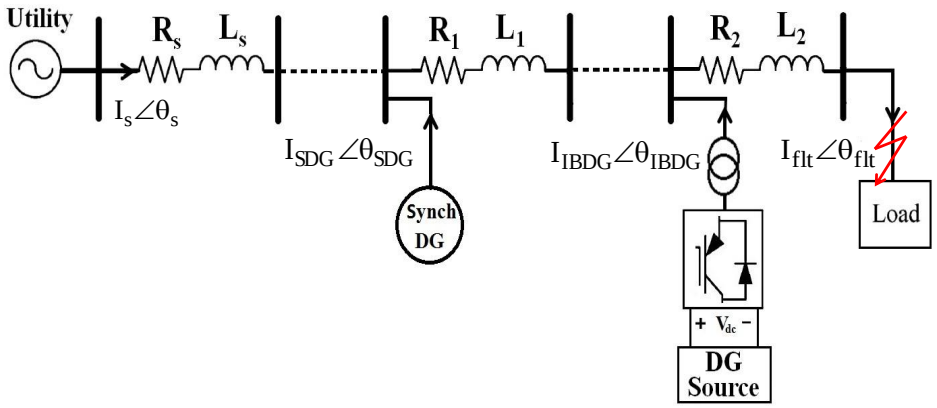

Figure 4.1: Simple radial system with a synchronous DG and an IBDG

Consider the system shown in Figure 4.1. As explained in Chapter 3, for the case the synchronous DG is not connected to the system, the fault current consists of the contribution from the IBDG in addition to the grid current. If the phase angle of the IBDG current is changed, while its magnitude is kept constant, it is possible to manage the total fault current around the grid current. When the synchronous DG is added to the system, it is considered to be the primary source of protection problems by providing more than twice the fault current contribution of IBDGs. As a result the FCM operation in zone B which is explained in Chapter 3 does not function adequately when synchronous DGs are added. Hence zone C FCM operation is proposed for IBDG when synchronous DGs exist in the system.

An examination of the current waveforms illustrated in Figure 4.2 provides further clarification of the three zones of FCM operation. Figure 4.2(a) shows the maximum fault current obtained when the IBDG generates a current that has the same phase angle as the grid current. Separating the peak values of the contributing currents can reduce the magnitude of the total fault current. Hence, Figure 4.2(b), illustrates the zone B phase angle for the IBDG that, in combination with the grid current phase angle, neutralizes the effect of the IBDG on the fault current. Further increases in the phase angle of the IBDG current makes it possible to decrease the total fault current to a value below that of the grid current. This scenario is shown in Figure 4.2(c). In fact, considering only the fault current contribution of the IBDG and the grid, it is shown in Figure 4.3 that there is a range of phase angle for the IBDG that in combination with the grid current decreases the total fault current to a value below that of the grid current. For this zone,

the current gap generated between the grid current and the total fault current can be used for managing the contribution of the synchronous DG while keeping it connected to the system during the fault condition. The three zones of FCM operation and the proposed technique for managing the fault current of synchronous DGs can be further clarified through consideration of the phasor relation between the elements of the fault current for the system shown in Figure 4.1 when synchronous DG is not connected. As can be seen in Figure 4.4, due to the contribution of the IBDG, the total fault current deviates from its original value, which is the grid current. However, manipulating the phase angle of the IBDG current neutralizes the effect of the IBDG, and more importantly, enables the management of the contribution of the synchronous DGs to the total fault current. As shown in Figure 4.4, keeping the magnitude of the IBDG current constant and changing its phase angle permit the introduction of three zones of FCM operation. Working in all three FCM operating control zones results in a fault current that is less than the total fault current, I_{flt}. Zone B represents the boundary condition that separates the other two zones. As shown in Chapter 3 when only IBDGs are connected to the system, working in zone B results in a fault current that has the same magnitude as the grid current, $I_{s\text{-}flt}$. If the phase angle of the IBDG current is set to correspond to a value less than that of the boundary condition, the total fault current would be greater than the grid contribution to the fault current, indicating an operation in zone A. When the reference phase angle is larger than the boundary condition, the system operates in zone C, which results in a fault current that is less than the grid current. Depending on the amount of the reduction in the fault current in zone C, the current gap generated between the reduced fault current and the grid current can be used in order to manage the synchronous DG contribution to the current. This operation zone is the desirable one for systems with both synchronous DGs and IBDGs.

4.2.1 Calculation of the Phase Angle for Zone C Operation

As explained in Section 3.3, to manage the synchronous DG contribution to the fault current, IBDGs should operate as FCM units in zone C. To this end, the phase angle required for zone B operation is first determined from Eq. 3.13, and a positive constant value, Δ, is then added to the phase angle that has been calculated in order to establish region C operation:

$$\phi = \delta_B + \Delta \tag{4.1}$$

Applying the calculated ϕ as the reference IBDG current phase angle enables the management of the contribution of the synchronous DGs to the fault current.

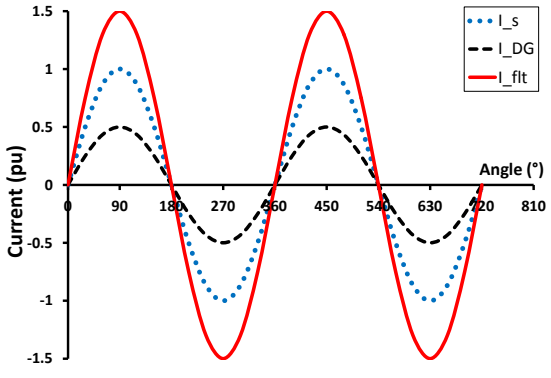

(a)

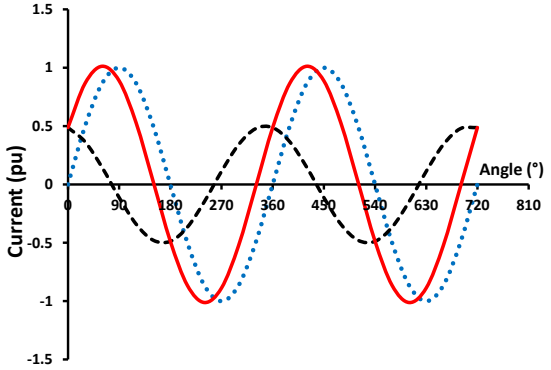

(b)

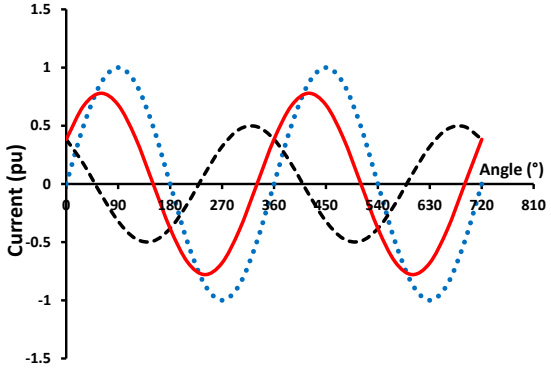

(c)

Figure 4.2: Effect of the IBDG current phase angle on the fault current for (a) $\theta_{\text{IBDG}} = 0°$; (b) $\theta_{\text{IBDG}} = 103°$; (c) $\theta_{\text{IBDG}} = 130°$

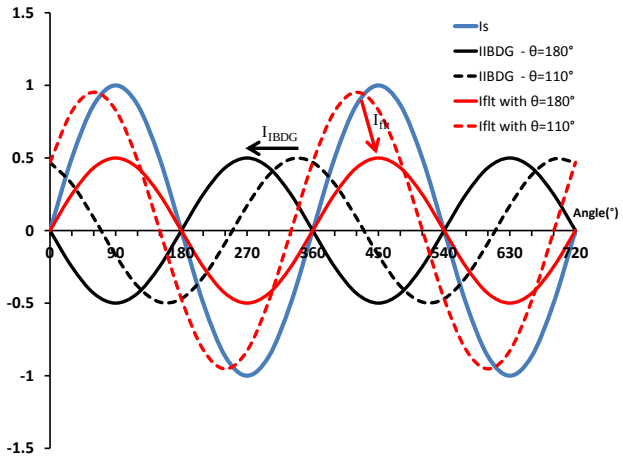

Figure 4.3: Zone of operation for managing the fault current contribution of synchronous DG with $\theta_{\text{IBDG}} = 110°$ to $\theta_{\text{IBDG}} = 180°$

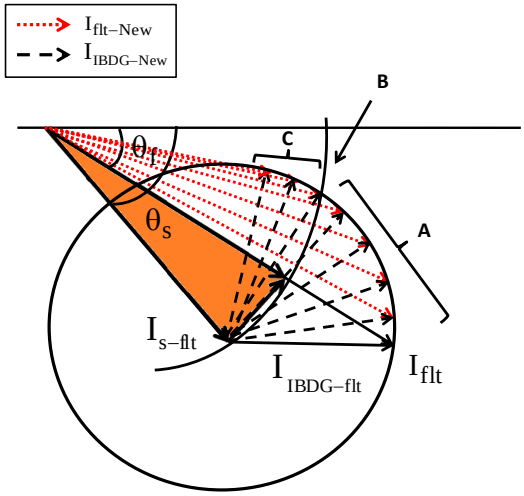

Figure 4.4: Illustration of the fault current control regions

4.3 Three Factors That Affect the FCM of Synchronous DGs in zone C

Fault current management of synchronous DGs is achieved by operating the IBDGs as FCM units in zone C. The proposed operation in region C depends on three factors, which are illustrated in Figure 4.5. First, the amount of the reduction in the total fault current depends on the constant phase angle that is added to the zone B reference phase angle. Figure 4.5(a) reveals that the addition of a larger phase angle, Δ_2, to the zone B reference phase angle, δ_B, reduces the total fault current even further, which means that greater current contributions from synchronous DGs can be compensated if the IBDGs operating in zone C have larger current phase angles. The second important factor is the number of IBDGs that operate as FCM units in zone C. For DGs located at similar positions relative to the fault, the fault current contribution from synchronous DGs is greater than that from IBDGs with similar ratings. The correct number of IBDGs should thus be assigned to each synchronous DG for the successful management of its contribution to the fault current. This point is illustrated in Figure 4.5(b), in which three IBDGs are assigned to operate as FCM units in zone C. As can be seen, the total fault current is reduced to a value less than the one obtained through the operation of two IBDGs as FCM units. An additional factor that affects the current gap generated by the zone C operation of the IBDGs is the magnitude of the current of the IBDGs operating as FCM units. IBDGs that contribute more to the current create a greater reduction in the total fault current. In fact, for zone C operation, the IBDGs with higher current ratings or the ones that are closer to the fault location are more effective in keeping synchronous DGs connected to the system. Figure 4.5(c) illustrates the effect of this factor.

4.4 Simulation Results

The ability of IBDGs to manage the current contribution of synchronous DGs is examined by adding a synchronous DG to bus 6 of the test system used in section 3.4.2. Figure 3.18 shows the test system with the DGs connected: one synchronous DG is connected to bus 6, and five IBDGs are connected to buses 7, 12, 19, 23, and 26 through five 0.48/12.66 kV Δ-Yg transformers. Similar to the previous case, all five IBDGs operate at a unity power factor and, in total, provide 60% of the power required by the system. The synchronous DG provides 1.2 MVA at a 0.9 PF. The effectiveness of the proposed operation was examined for a three-phase fault at bus 27.

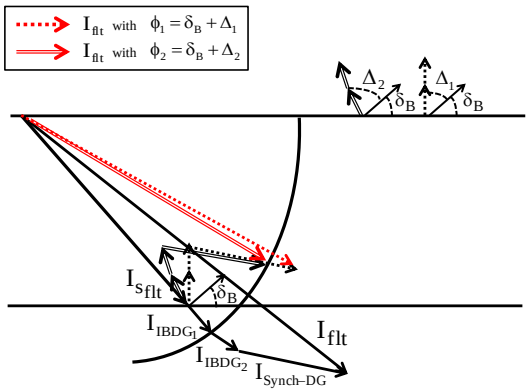

(a)

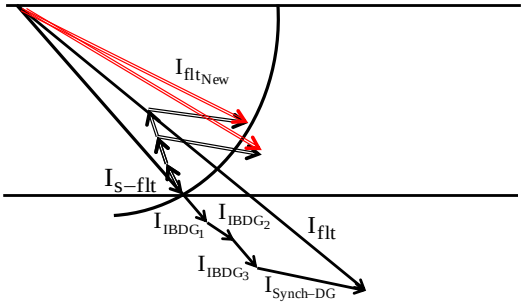

(b)

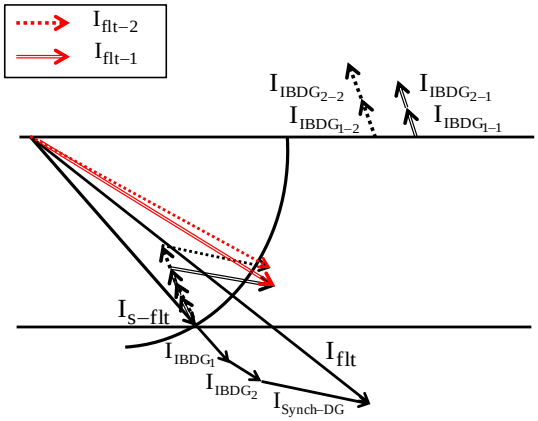

(c)

Figure 4.5: Visual representation of the factors affecting FCM in region C: (a) constant phase angle added to δ_B (b) number of IBDGs operating as FCM units in region C (c) current magnitude of IBDG

To manage the synchronous DG contribution to the fault current, IBDGs are controlled so that they operate in zone C during fault conditions. To achieve this goal, the first step entails the use of current and voltage phasor information from the system buses for the calculation of the phase angle required for zone B operation: δ_B. In the next step, a positive constant value, Δ, is added to the zone B phase angle in order to determine the current phase angle for zone C operation: ϕ. The calculated phase angle, ϕ, is then applied as the reference phase angle of the IBDGs that are responsible for managing the fault current contribution of the synchronous DGs. For all studies the current magnitude of IBDGs is kept at a constant level below the tripping threshold of interface inverters. In order to show the effectiveness of the proposed method for IBDGs with lower ratings, the contribution from the IBDGs is limited to twice of their rated current. With the current magnitude of DGs being constant, the only factor which manages the fault current contribution of synchronous DG is the current phase angles of IBDGs. The effects of the three factors discussed in section 4.3 with respect to the synchronous DG current management are investigated. All tests are performed using the PSCAD software. The results are presented in the following subsections:

4.4.1 Fault Current Management of Synchronous DGs in zone C for $\Delta = 30°$, and $\Delta = 60°$

To verify the effectiveness of the technique proposed for managing the fault current contribution of synchronous DGs, a three-phase fault was applied at bus 27, and the magnitude of the total fault current was compared for two scenarios: with and without the proposed FCM technique. The total fault current and the DG contribution are shown in Figure 4.6 for the case in which the IBDGs continue normal operation during the fault condition. Due to the contribution of the IBDGs and the synchronous DG, the magnitude of the total fault current is clearly much greater than when no DG is connected to the system, with the largest contribution being from the synchronous DG. As can be seen in Figure 4.6(b) the contribution of this unit is more than twice that of IBDG_1 and IBDG_2, which are closest to the fault location. As mentioned before, the fault current contribution of IBDGs is limited to twice their rated current.

To manage the contribution of the synchronous DG, the operation of IBDG_1 and IBDG_2 is modified at the moment of fault detection, and the phase angle calculated for zone C operation is therefore fed into the system as the IBDG reference current phase angle. The effectiveness of the proposed technique for managing the contribution of the synchronous DGs is examined for two different phase angles in region C. In the first case, a phase angle of

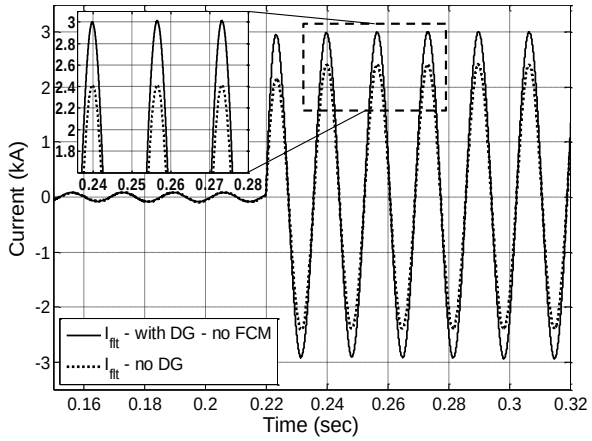

(a)

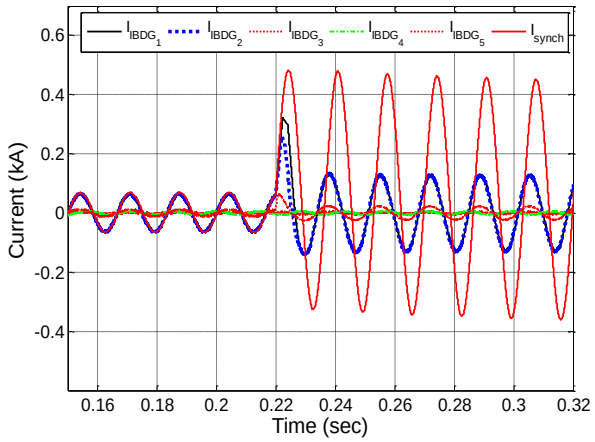

(b)

Figure 4.6: Fault current elements without FCM: (a) fault current (I_{flt}) (b) I_{IBDG_1}, I_{IBDG_2}, I_{IBDG_3}, I_{IBDG_4}, I_{IBDG_5}, I_{synch}

$\Delta = 30°$ is added to the reference phase angle calculated for zone B. Figure 4.7 illustrates the results for this scenario. It is clear that by having $\Delta = 30°$ and operating $IBDG_1$ and $IBDG_2$ in zone C, not only is their contribution to the fault current neutralized, but the contribution of the synchronous DG to the fault current is also significantly reduced. Figure 4.7(b) clearly shows that the magnitude of all DG currents is kept at the level indicated in Figure 4.6(b). Hence, the only parameter managing the contribution of the synchronous DG current is the current phase angle of $IBDG_1$ and $IBDG_2$.
The contribution of the synchronous DG can be further reduced by increasing the IBDG operating phase angle. To examine this scenario, a phase angle of $\Delta = 60°$ is added to the zone B reference phase angle: δ_B. Figure 4.8 shows the total fault current and the contribution to the fault current from all DGs for this case. The contribution of the synchronous DG has been successfully compensated through the application of the new reference current phase angle for the IBDGs: the total fault has been managed so that it is in accord with a value very close to that of the grid current. A comparison of Figure 4.6 and Figure 4.8 clearly reveals that the magnitudes of the DG currents are kept at a level identical to the ones exhibited without the FCM operation. These results demonstrate that changing only the phase angle of the IBDGs current, without reducing the current magnitude of DGs, enables the management of the synchronous DG contribution to fault currents. It should be noted that in both case studies presented in Figure 4.7 and Figure 4.8, a time delay of 20 milliseconds is considered for the current elements to follow the new references for fault condition. As a result of this time delay, the first cycle of fault current is passed and the fault current is managed in the subsequent cycles. However, if the system is equipped with fast fault location detection algorithms, the proposed technique is able to catch the first current peak. The result for this scenario is illustrated in Figure 4.9.

4.4.2 Effects of the Number of IBDGs on FCM Operation of Synchronous DGs in Zone C for $\Delta = 60°$

As mentioned in section 4.3, the number of IBDGs that are operating in zone C affects the fault current management of the synchronous DGs. To test the validity of this statement, the total fault current resulting from the FCM operation of $IBDG_1$ and $IBDG_2$ is compared with that produced when only $IBDG_1$ operates as a zone C FCM unit. The results are shown in Figure 4.10. For both scenarios, the reference phase angle applied to the IBDGs is δ_B+60°. As can be seen, when both $IBDG_1$ and $IBDG_2$ operate as zone C FCM units, the reduction in the total fault current is greater than with only one IBDG. The contribution of synchronous DGs to the fault current can therefore be managed more effectively if a larger number of IBDGs operate as FCM units in zone C.

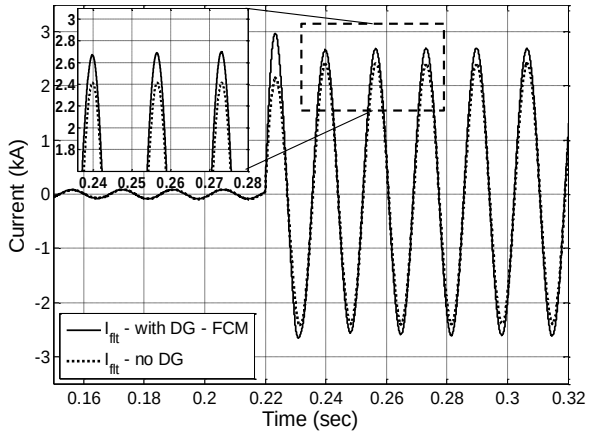

(a)

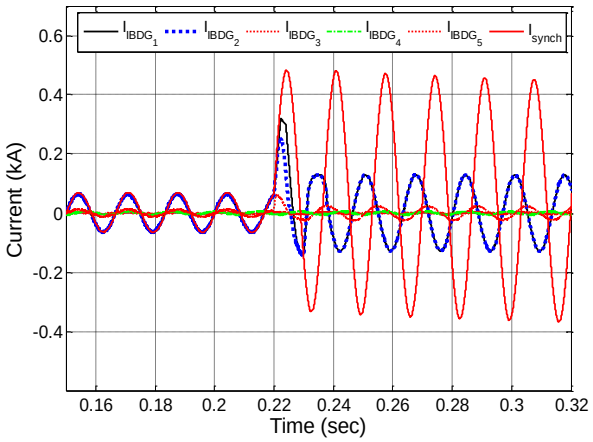

(b)

Figure 4.7: Fault current elements for zone C operation with $\Delta = 30°$: (a) fault current (I_{flt}) (b) I_{IBDG_1}, I_{IBDG_2}, I_{IBDG_3}, I_{IBDG_4}, I_{IBDG_5}, I_{synch}

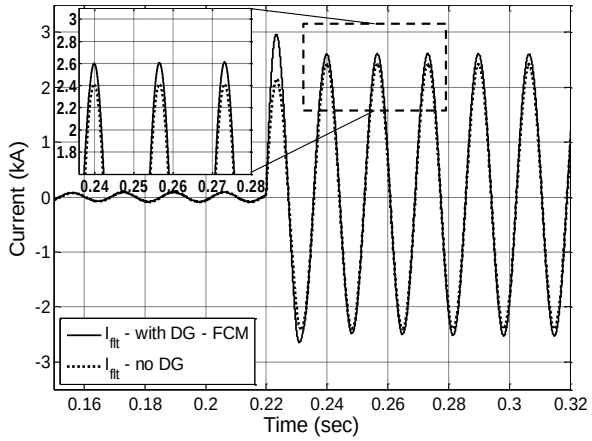

(a)

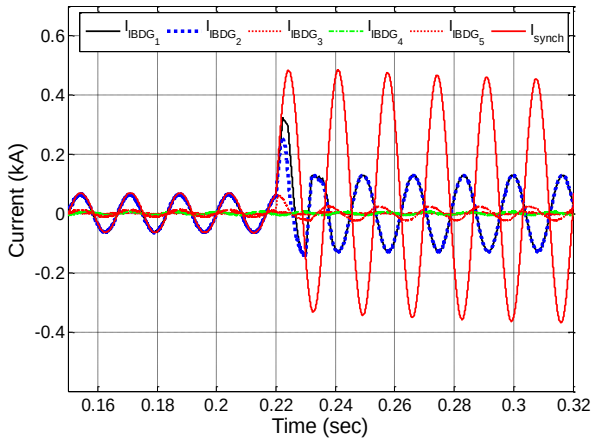

(b)

Figure 4.8: Fault current elements for zone C operation with $\Delta = 60°$: (a) fault current (I_{flt}) (b) I_{IBDG_1}, I_{IBDG_2}, I_{IBDG_3}, I_{IBDG_4}, I_{IBDG_5}, I_{synch}

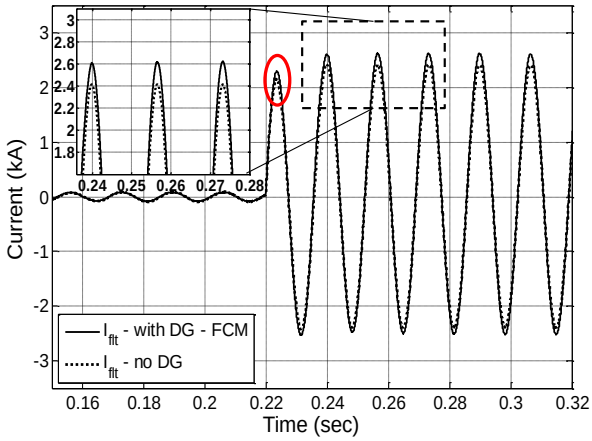

Figure 4.9: Fault current (I_{flt}) for zone C operation with $\Delta = 60°$ without time delay

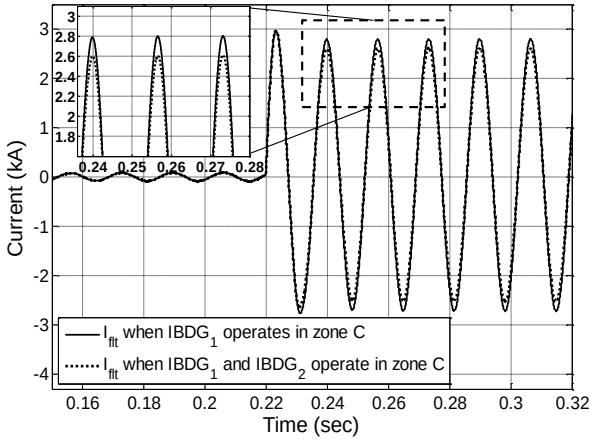

Figure 4.10: Total fault current resulting from the FCM operation of different numbers of IBDGs in zone C with Δ=60°

4.4.3 Effects of the Magnitude of the IBDG Current on FCM Operation of Synchronous DGs in Zone C

In both of the previous case studies, the management of the synchronous DG current is performed solely through the modification of the IBDG reference phase angle. The current magnitude, which is the other controllable parameter of IBDG, was kept below twice the normal IBDG current in order to protect the switching interface. However, as mentioned in section 4.3, when the IBDGs are operating in zone C, in contrast to the usual case, a greater IBDG current magnitude results in a lower total fault current. In other words, IBDGs with higher current capacities are able to manage the contribution from synchronous DGs more effectively. To illustrate the effects of the IBDG current magnitude on the FCM operation of synchronous DGs, two scenarios were compared. For both scenarios, $IBDG_1$ and $IBDG_2$ are controlled so that they operate as FCM units in zone C. In the first case, the magnitude of the IBDG current is limited to 1.5 times the normal IBDG current in order to protect the PE interfaces. The second scenario is based on the assumption that the IBDG inverter interfaces are able to tolerate greater current contributions from DGs, so their current magnitude is limited to three times their rated current.
A comparison of the results obtained from these case studies is shown in Figure 4.11. As can be seen, the total fault current is reduced to a lower value when the magnitude of the IBDG current increases. It can thus be concluded that IBDGs that have higher current capacities are more effective for managing the contribution of synchronous DGs to fault current.

4.5 Summary

This chapter has presented a novel technique for managing the fault current contribution of synchronous DGs using IBDGs already existing in a system. The proposed operation is based on the technique proposed in Chapter 3. It is shown that changing the IBDG current phase angle enables the definition of three IBDG operation zones during the fault condition: zones A, B and C. It was determined that operation in zone C produces the desired fault current management of synchronous DGs. In this zone, the effectiveness of the operation depends on three factors: the IBDG current magnitude, the phase angle of the IBDG current, and the number of IBDGs operating in zone C. Three sets of simulations have explored the effects of these factors on the management of the synchronous DG contribution to the fault current. IBDGs with higher current capacities are shown to effectively manage the contribution of synchronous DGs. Moreover, as the reference current phase angle of

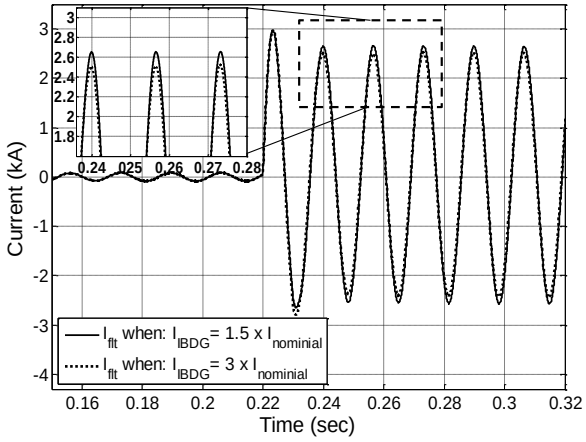

Figure 4.11: Total fault current resulting from the FCM operation of $IBDG_1$ and $IBDG_2$ in zone C with Δ=60° and different current magnitudes: 1.5 times the IBDG rated current and 3 times the IBDG rated current

zone C IBDGs increases, the IBDGs can manage a greater current contribution from the synchronous DGs. It is also shown that an enhanced reduction in the total fault current is obtained if the number of IBDGs assigned to the management of the synchronous DG contribution is increased. The IEEE 33-bus system was chosen as the test system. From the simulation results, it can be concluded that IBDGs are able to manage their own fault current in addition to the fault current contribution of synchronous DGs. As a result, the proposed operating technique makes it possible to keep all DGs connected to the system during fault conditions if existing IBDGs are utilized for the management of the total fault current.

Chapter 5

Short Circuit Analysis for Radial and Loop Systems with Inverter Based Distributed Generators

5.1 Introduction

As explained in Chapters 3 and 4, for the purpose of FCM operation, IBDGs are kept connected to the system during a fault, while their current phase angle is employed to manage the total fault current magnitude. Even if the FCM operation is not performed during fault conditions, the behavior of IBDGs is mainly dominated by their control unit. During fault conditions, if the IBDGs are not severely affected by the fault and their fault current remains below the short circuit capacity of the inverter interfaces, they can continue their normal operation and be modeled as PQ generators in fault analysis. On the other hand, the fault current magnitude of the IBDGs located in close proximity to the fault location and thus are affected severely by the fault is limited to a value below the tripping threshold of the inverter interfaces. With the limited fault current contribution, IBDGs should be modeled as constant current sources in fault analysis. A consequent need thus exists for fault analysis methods that can facilitate operational studies of power systems in presence of IBDGs.

In this chapter, two power flow based fault analysis methods are developed for radial and loop power systems containing IBDGs. For both cases, IBDGs are initially considered as PQ generators in fault analysis, and the voltage profile of the system is obtained. Having the system voltage profile and the power references of the IBDGs, the current contributions

of these units are calculated. If the current contribution of an IBDG is higher than its current threshold, the IBDG will be modeled as a constant current source in the fault analysis. Considering the IBDG as a constant current source, the fault analysis is repeated again and the new voltage profile of the system is obtained. This process is repeated until it is clear that there is no IBDG to be converted to constant current source.

The backward-forward sweep algorithm is used to solve the load flow problem for radial systems during fault conditions. This load flow method is more convenient for weakly meshed distribution systems. In such cases, the current of IBDGs is added to the nodal current equation in the backward sweep. The fault is treated as a load with a small resistance connected to the system, while its current is considered in the nodal current equation. On the other hand, the Newton-Raphson (NR) power flow algorithm is modified for fault analysis of loop systems with IBDGs. For this purpose, in addition to the conventional PQ and PV nodes, a new type of node called the constant current node (I node) has been defined in the Newton-Raphson algorithm. This novel modified Newton-Raphson power flow algorithm enables the inclusion of both power and current elements in one matrix, thus eliminating the need to represent the I nodes in terms of their equivalent powers. As a result, the proposed modified NR method is able to overcome the inadequacy of the conventional NR algorithm in considering constant current nodes in the formulation. In order to extend the modified NR algorithm to fault conditions, a 3-phase fault is considered as a phase-to-ground impedance at the faulty bus when calculating the Ybus matrix.

The rest of this chapter is organized as follows. Section 5.2 presents the backward-forward based fault analysis algorithm proposed for radial systems with IBDGs. Section 5.3 describes the new modified NR power flow algorithm employed for power flow analysis of loop systems with constant current nodes, and fault analysis of loop systems in presence of IBDGs. The algorithm is explained along with the development of the modified Jacobian matrix for both instances: constant current loads and constant current sources. Section 5.4 describes the validation of the proposed algorithms, using two test systems that enables an examination of both radial and loop systems. A summary is provided in section 5.6.

5.2 Backward-Forward Sweep Based Fault Analysis Model for Radial Systems with IBDGs

This section proposes a power flow based technique is for analyzing the fault response of radial systems in the presence of IBDGs. The backward-forward sweep algorithm is used to solve the load flow problem during fault conditions. This load flow method is more

convenient for weakly meshed distribution systems. The loads are modeled as constant impedances during fault conditions. The solution will help to determine which IBDG operates as a constant current source with the maximum allowable current threshold.

The majority of radial distribution system power flow algorithms use the backward-forward sweep method. In the backward sweep, the line current or the power flows from the extremities to the root are summed. The forward sweep is a voltage drop calculation, providing updates to the voltage profile, based on the current estimates of the backward sweep [94].

Backward Sweep: the nodal current in iteration k, at node i, normally is calculated as:

$$I_i^k = (\frac{S_i}{V_i^{k-1}})^* + Y_i V_i^{k-1} \quad \forall i = 1, 2, ..., n \tag{5.1}$$

where, Y_i is the shunt branch of the feeder (if any). In (5.1), the loads are modeled as constant PQ load type. However, in faulty conditions, the loads are modeled as constant impedances. The nodal current equation should be modified as follows:

$$I_i^k = (\frac{V_i^{k-1}}{Z_L}) + Y_i V_i^{k-1} \quad \forall i = 1, 2, ..., n \tag{5.2}$$

If there is an IBDG connected to the node, i, the IBDG current contribution is calculated from its P_{ref} and Q_{ref} as in:

$$I_{IBDG_i}^k = (\frac{S_{IBDG}}{V_i^{k-1}})^* \tag{5.3}$$

In the iterations, if the I_{IBDG} calculated from (5.3) exceeds the I_{IBDG} current threshold, the PQ model for IBDG is replaced with a constant current source. In both cases, the nodal current equation at busses that include IBDGs should have an added term for the contribution of IBDGs as follows:

$$I_i^k = (\frac{V_i^{k-1}}{Z_L})^* + Y_i V_i^{k-1} - I_{IBDG_i}^k \quad \forall i = 1, 2, ..., n \tag{5.4}$$

At the faulty bus, the nodal current equation must include the fault current (I_{fault}) which can be calculated as:

$$I_{flt}^k = \frac{V_i^{k-1}}{R_{f_i}} \tag{5.5}$$

where R_f is the fault resistance. In this case, at the fault bus, the nodal current equation is as follows:

$$I_i^k = (\frac{V_i^{k-1}}{Z_L})^* + Y_i V_i^{k-1} - I_{IBDG_i}^k + I_{flt} \quad \forall i = 1, 2, ..., n \tag{5.6}$$

In iteration k, starting from the branches that are connected to end nodes and moving towards the branches connected to the substation node, the current in branch L, given by I_L, is calculated as:

$$I_L^k = I_i^k + \sum_{m \in L} I_m \quad \forall L = n, n-1, ..., 1 \tag{5.7}$$

where I_m is the sum of the currents in all branches connected to bus i.

Forward Sweep: Nodal voltages are updated in a forward sweep from branches connected to substation nodes toward the end nodes. For each branch L, the voltage at node i is calculated using the updated voltage at the previous node and branch currents calculated in the preceding backward sweep, as follows:

$$V_i^k = V_h^k - Z_L I_L^k \quad \forall i = 1, 2, ..., n \tag{5.8}$$

where Z_L is the series impedance of branch L. All the backward and forward steps are repeated until convergence is achieved.

5.3 Modified Newton-Raphson Based Fault Analysis Model for Loop Systems with IBDGs

In this section, a novel power flow based method is proposed for the fault analysis of loop systems in the presence of IBDGs. For this purpose, first, the NR algorithm is modified to incorporate the model of constant current nodes, i.e., constant current sources and constant current loads, in terms of their current elements. In the next step, the modified NR power flow algorithm is used for the fault analysis of loop systems with IBDGs. The result identifies those IBDGs that are severely affected and have their current contribution limited by their interface inverters as a consequence.

5.3.1 Modified Newton Raphson Algorithm for Power Flow of Loop Systems with Constant Current Sources

The proposed power flow method entails the modification of the NR algorithm in order to establish a precise model of the I nodes while also incorporating consideration of PV and PQ nodes. This new formulation produces the same convergence characteristics as a conventional NR power flow solution for PQ and PV buses, however, the algorithm exhibits superior ability with respect to meeting convergence criteria for buses that have constant current loads/sources. For this purpose, the Jacobian matrix is changed so that it indicates the linearized relationship between small changes in the bus voltage magnitude and phase angle, on the one hand, and small changes in the real and imaginary part of the current, on the other, as well as their relationship with active and reactive power. For the derivation of the current formulations, constant current nodes are divided into two general groups: nodes with constant current loads and nodes with constant current sources. The Jacobian matrix is then altered according to the type of constant current node.

Basic Power Formulations for Typical PQ and PV Nodes

For a typical power system with n buses, the current injected into bus i of the system can be obtained from [95]:

$$I_i = \sum_{j=1}^{n} Y_{ij} V_j \tag{5.9}$$

where Y_{ij} is the bus admittance matrix of the system, which can be written as $|Y_{ij}|\angle\theta_{ij}$ in polar form. The expression for the bus-injected current can be written in polar form as follows:

$$I_i = \sum_{j=1}^{n} |Y_{ij}||V_j|\angle\theta_{ij} + \delta_j \tag{5.10}$$

where δ_j is the corresponding phase angle of the voltage at bus j.

The resulting complex power expression for typical PQ and PV nodes can then be obtained as:

$$P_i - jQ_i = |V_i|\angle\delta_i \sum_{j=1}^{n} |Y_{ij}||V_j|\angle\theta_{ij} + \delta_j \tag{5.11}$$

The active and reactive power expression for PQ nodes and the active power for PV nodes can thus be found respectively from:

$$P_i = \sum_{j=1}^{n} |V_i||V_j||Y_{ij}|cos(\theta_{ij} - \delta_i + \delta_j) \tag{5.12}$$

$$Q_i = -\sum_{j=1}^{n} |V_i||V_j||Y_{ij}|sin(\theta_{ij} - \delta_i + \delta_j) \tag{5.13}$$

Current Formulations for I Nodes

As with PV and PQ buses, for constant current nodes, the injected current is calculated from (5.10). However, for these types of nodes with constant current loads or sources, the load current or the source-generated current is the element of interest. For buses with constant current loads, the load current is represented by the negative of the injected current. For this case, the following relation exists between the current elements of the node:

$$I_{L_i} = -I_i \tag{5.14}$$

where I_{L_i} is the load current at bus i.

For system buses with constant current sources, if a load is connected to the bus with a constant current source, the following relation exists between the current elements of the bus:

$$I_{G_i} = I_i + I_{l_i} \tag{5.15}$$

where I_{G_i} is the current generated by the current source at bus i and I_{l_i} is the current absorbed by the PQ load at bus i.

It is clear that if no load is connected to the bus in this case, I_{l_i} is eliminated, and the current generated by the source will be equal to the injected current.

For the load current and source current, substituting the corresponding terms for I_i and I_{l_i}, enables the expressions obtained in (5.14) and (5.15), to be written respectively as:

$$I_{L_i} = -\sum_{j=1}^{n} |Y_{ij}||V_j|\angle(\theta_{ij} + \delta_j) \tag{5.16}$$

$$I_{G_i} = \sum_{j=1}^{n} |Y_{ij}||V_j|\angle(\theta_{ij} + \delta_j) + |\frac{S_{L_i}}{V_i}|\angle(\delta_i - \theta_L) \tag{5.17}$$

where S_{L_i} the load complex power at bus i and θ_L is the load phase angle.

Each of the expressions shown in (5.16) and (5.17) can be rearranged in the form of their real and imaginary components. Consequently, depending on whether the constant current node is a constant current load or a constant current source, two current equations result for each node.

For nodes with constant current loads, the respective real and imaginary current components can be determined as follows:

$$\begin{aligned} I_{LR_i} &= |I_{L_i}|cos(\gamma_i) \\ &= -\sum_{j=1}^{n} |Y_{ij}||V_j|cos(\theta_{ij} + \delta_j) \end{aligned} \tag{5.18}$$

$$\begin{aligned} I_{LI_i} &= |I_{L_i}|sin(\gamma_i) \\ &= -\sum_{j=1}^{n} |Y_{ij}||V_j|sin(\theta_{ij} + \delta_j) \end{aligned} \tag{5.19}$$

where I_{LR_i} and I_{LI_i} are the real and imaginary components of the constant load current at bus i, and γ_i is the corresponding phase angle of this current.

In a similar manner, two components are produced for each node that has a constant current source:

$$\begin{aligned} I_{GR_i} &= |I_{G_i}|cos(\gamma_i') \\ &= \sum_{j=1}^{n} |Y_{ij}||V_j|cos(\theta_{ij} + \delta_j) + |\frac{S_{L_i}}{V_i}|cos(\delta_i - \theta_L) \end{aligned} \tag{5.20}$$

$$\begin{aligned} I_{GI_i} &= |I_{G_i}|sin(\gamma_i') \\ &= \sum_{j=1}^{n} |Y_{ij}||V_j|sin(\theta_{ij} + \delta_j) + |\frac{S_{L_i}}{V_i}|sin(\delta_i - \theta_L) \end{aligned} \tag{5.21}$$

where I_{GR_i} and I_{GI_i} are the real and imaginary components of the current generated by the constant current source at bus i, and γ_i' is the corresponding phase angle of this current.

Bus power and current nonlinear expressions for the PQ, PV, and I nodes can thus be obtained in terms of voltage magnitudes and phase angles.

Modifications to the Newton-Raphson Power Flow Algorithm

The modified Jacobian matrix includes the real and imaginary components of the constant current at the current nodes in addition to the active and reactive components of the power at the PQ and PV nodes. This matrix is obtained by expanding the Taylor series of power and current equations around an initial estimate of the solution for the voltage magnitude and angle, with the higher-order terms of the series being neglected. The result is a system of linear relations that correlate the small changes in voltage magnitude and phase angle with the small changes in the active and reactive power of the PQ nodes, the active power of the PV nodes, and the real and imaginary components of the constant current at the I nodes.

The modified Jacobian matrix for a system with constant current nodes is shown in (5.22). This equation is written for the general case in which ΔI_{cnst_R} and ΔI_{cnst_I} are expressions that denote the small changes in the real and imaginary constant current components at the I nodes. In fact, I_{cnst} is either the current of the constant current load at the I nodes specified in (5.16) or the current of the constant current source shown in (5.17). In (5.22), J_1, J_2, J_3 and J_4 are the elements of the Jacobian matrix that are conventionally used to indicate the linear relationship between the small changes in active and reactive power and the small changes in voltage magnitude and phase angle. Four new components J_5, J_6, J_7 and J_8 have been added to the original Jacobian matrix to accommodate the existence of the constant I nodes. These four elements express the partial derivatives of the real and imaginary components of the generated current or the load current at the I buses with respect to voltage magnitude and phase angle.

$$\begin{bmatrix} \Delta P \\ \Delta Q \\ \Delta I_{cnst_R} \\ \Delta I_{cnst_I} \end{bmatrix} = \begin{bmatrix} J1 & J2 \\ J3 & J4 \\ J5 & J6 \\ J7 & J8 \end{bmatrix} \begin{bmatrix} \Delta\delta \\ \Delta|V| \end{bmatrix} \tag{5.22}$$

If bus 1 is considered the slack bus J_5, J_6, J_7 and J_8 are defined as follows:

$$J_5 = \begin{bmatrix} \frac{\partial I_{cnst_{R_2}}}{\partial \delta_2}^{(k)} & \cdots & \frac{\partial I_{cnst_{R_2}}}{\partial \delta_n}^{(k)} \\ \vdots & \ddots & \vdots \\ \frac{\partial I_{cnst_{R_n}}}{\partial \delta_2}^{(k)} & \cdots & \frac{\partial I_{cnst_{R_n}}}{\partial \delta_n}^{(k)} \end{bmatrix} \tag{5.23}$$

$$J_6 = \begin{bmatrix} \frac{\partial I_{cnst_{R_2}}}{\partial |V|_2}^{(k)} & \cdots & \frac{\partial I_{cnst_{R_2}}}{\partial |V|_n}^{(k)} \\ \vdots & \ddots & \vdots \\ \frac{\partial I_{cnst_{R_n}}}{\partial |V|_2}^{(k)} & \cdots & \frac{\partial I_{cnst_{R_n}}}{\partial |V|_n}^{(k)} \end{bmatrix} \tag{5.24}$$

$$J_7 = \begin{bmatrix} \frac{\partial I_{cnst_{I_2}}}{\partial \delta_2}^{(k)} & \cdots & \frac{\partial I_{cnst_{I_2}}}{\partial \delta_n}^{(k)} \\ \vdots & \ddots & \vdots \\ \frac{\partial I_{cnst_{I_n}}}{\partial \delta_2}^{(k)} & \cdots & \frac{\partial I_{cnst_{I_n}}}{\partial \delta_n}^{(k)} \end{bmatrix} \tag{5.25}$$

$$J_8 = \begin{bmatrix} \frac{\partial I_{cnst_{I_2}}}{\partial |V|_2}^{(k)} & \cdots & \frac{\partial I_{cnst_{I_2}}}{\partial |V|_n}^{(k)} \\ \vdots & \ddots & \vdots \\ \frac{\partial I_{cnst_{I_n}}}{\partial |V|_2}^{(k)} & \cdots & \frac{\partial I_{cnst_{I_n}}}{\partial |V|_n}^{(k)} \end{bmatrix} \tag{5.26}$$

The new elements of the Jacobian matrix can then be derived separately for constant current loads and constant current sources.

On the other hand, the power and current mismatches at PQ, PV, and I buses can be determined from the following expressions:

$$\begin{aligned} \Delta P_i^{(k)} &= P_i^{(sp)} - P_i^{(k)} \\ \Delta Q_i^{(k)} &= Q_i^{(sp)} - Q_i^{(k)} \\ \Delta I_{cnst_{R_i}}^{(k)} &= I_{cnst_{R_i}}^{(sp)} - I_{cnst_{R_i}}^{(k)} \\ \Delta I_{cnst_{I_i}}^{(k)} &= I_{cnst_{I_i}}^{(sp)} - I_{cnst_{I_i}}^{(k)} \end{aligned} \tag{5.27}$$

where, $P_i^{(sp)}$, $Q_i^{(sp)}$, are the specified active and reactive power values at bus i; $I_{cnst_{R_i}}^{(sp)}$ and $I_{cnst_{I_i}}^{(sp)}$ are the values of the real and imaginary constant current components specified at the I bus i; $P_i^{(k)}$, $Q_i^{(k)}$ are the active and reactive power values calculated at bus i; and $I_{cnst_{R_i}}^{(k)}$ and $I_{cnst_{I_i}}^{(k)}$ are the real and imaginary components of the current calculated at bus i. The superscript k denotes the number of the iteration.

A more detailed expression of the modified Jacobian matrix is shown in (5.28). Given the modified Jacobian matrix and the power and current mismatches, (5.28) can be used to find the voltage magnitude and phase angle mismatch for each iteration. It should noted that each bus can be modeled only as one of the three bus types: PV, PQ, or I.

$$
\begin{bmatrix}
\Delta P_2^{(k)} \\
\vdots \\
\Delta P_n^{(k)} \\
\Delta Q_2^{(k)} \\
\vdots \\
\Delta Q_n^{(k)} \\
\Delta I_{cnst_{R_2}}^{(k)} \\
\vdots \\
\Delta I_{cnst_{R_n}}^{(k)} \\
\Delta I_{cnst_{I_2}}^{(k)} \\
\vdots \\
\Delta I_{cnst_{I_n}}^{(k)}
\end{bmatrix}
=
\begin{bmatrix}
\frac{\partial P_2}{\partial \delta_2}^{(k)} & \cdots & \frac{\partial P_2}{\partial \delta_n}^{(k)} & \frac{\partial P_2}{\partial |V|_2}^{(k)} & \cdots & \frac{\partial P_2}{\partial |V|_n}^{(k)} \\
\vdots & \ddots & \vdots & \vdots & \ddots & \vdots \\
\frac{\partial P_n}{\partial \delta_2}^{(k)} & \cdots & \frac{\partial P_n}{\partial \delta_n}^{(k)} & \frac{\partial P_n}{\partial |V|_2}^{(k)} & \cdots & \frac{\partial P_n}{\partial |V|_n}^{(k)} \\
\frac{\partial Q_2}{\partial \delta_2}^{(k)} & \cdots & \frac{\partial Q_2}{\partial \delta_n}^{(k)} & \frac{\partial Q_2}{\partial |V|_2}^{(k)} & \cdots & \frac{\partial Q_2}{\partial |V|_n}^{(k)} \\
\vdots & \ddots & \vdots & \vdots & \ddots & \vdots \\
\frac{\partial Q_n}{\partial \delta_2}^{(k)} & \cdots & \frac{\partial Q_n}{\partial \delta_n}^{(k)} & \frac{\partial Q_n}{\partial |V|_2}^{(k)} & \cdots & \frac{\partial Q_n}{\partial |V|_n}^{(k)} \\
\frac{\partial I_{cnst_{R_2}}}{\partial \delta_2}^{(k)} & \cdots & \frac{\partial I_{cnst_{R_2}}}{\partial \delta_n}^{(k)} & \frac{\partial I_{cnst_{R_2}}}{\partial |V|_2}^{(k)} & \cdots & \frac{\partial I_{cnst_{R_2}}}{\partial |V|_n}^{(k)} \\
\vdots & \ddots & \vdots & \vdots & \ddots & \vdots \\
\frac{\partial I_{cnst_{R_n}}}{\partial \delta_2}^{(k)} & \cdots & \frac{\partial I_{cnst_{R_n}}}{\partial \delta_n}^{(k)} & \frac{\partial I_{cnst_{R_n}}}{\partial |V|_2}^{(k)} & \cdots & \frac{\partial I_{cnst_{R_n}}}{\partial |V|_n}^{(k)} \\
\frac{\partial I_{cnst_{I_2}}}{\partial \delta_2}^{(k)} & \cdots & \frac{\partial I_{cnst_{I_2}}}{\partial \delta_n}^{(k)} & \frac{\partial I_{cnst_{I_2}}}{\partial |V|_2}^{(k)} & \cdots & \frac{\partial I_{cnst_{I_2}}}{\partial |V|_n}^{(k)} \\
\vdots & \ddots & \vdots & \vdots & \ddots & \vdots \\
\frac{\partial I_{cnst_{I_n}}}{\partial \delta_2}^{(k)} & \cdots & \frac{\partial I_{cnst_{I_n}}}{\partial \delta_n}^{(k)} & \frac{\partial I_{cnst_{I_n}}}{\partial |V|_2}^{(k)} & \cdots & \frac{\partial I_{cnst_{I_n}}}{\partial |V|_n}^{(k)}
\end{bmatrix}
\begin{bmatrix}
\Delta \delta_2^{(k)} \\
\vdots \\
\Delta \delta_n^{(k)} \\
\Delta |V_2^{(k)}| \\
\vdots \\
\Delta |V_n^{(k)}|
\end{bmatrix}
\tag{5.28}
$$

Accordingly, in (5.28), the subscripts are modified so that each bus is represented only by one set of formulation in the algorithm. The new estimates for bus voltage magnitude and phase angle can consequently be calculated as follows:

$$\begin{aligned} \delta_i^{(k+1)} &= \delta_i^{(k)} + \Delta\delta_i^{(k)} \\ |V_i^{(k+1)}| &= |V_i^{(k)}| + \Delta|V_i^{(k)}| \end{aligned} \tag{5.29}$$

Calculation of the Jacobian Matrix Elements for Constant Current Loads

In the case of constant current loads, the elements J_5, J_6, J_7 and J_8 express the partial derivatives of the real and imaginary components of the load current at the I buses with respect to voltage magnitude and phase angle. For this case, the respective diagonal and off-diagonal elements of J_5, J_6, J_7 and J_8 can be calculated as follows:

$$\begin{aligned} \frac{\partial I_{LR_i}}{\partial \delta_i} &= |V_i||Y_{ii}|sin(\theta_{ii} + \delta_i) \\ \frac{\partial I_{LR_i}}{\partial \delta_j} &= |V_j||Y_{ij}|sin(\theta_{ij} + \delta_j) \qquad j \neq i \end{aligned} \tag{5.30}$$

$$\begin{aligned} \frac{\partial I_{LR_i}}{\partial |V_i|} &= -|Y_{ii}|cos(\theta_{ii} + \delta_i) \\ \frac{\partial I_{LR_i}}{\partial |V_j|} &= -|Y_{ij}|cos(\theta_{ij} + \delta_j) \qquad j \neq i \end{aligned} \tag{5.31}$$

$$\begin{aligned} \frac{\partial I_{LI_i}}{\partial \delta_i} &= -|V_i||Y_{ii}|cos(\theta_{ii} + \delta_i) \\ \frac{\partial I_{LI_i}}{\partial \delta_j} &= -|V_j||Y_{ij}|cos(\theta_{ij} + \delta_j) \qquad j \neq i \end{aligned} \tag{5.32}$$

$$\begin{aligned} \frac{\partial I_{LI_i}}{\partial |V_i|} &= -|Y_{ii}|sin(\theta_{ii} + \delta_i) \\ \frac{\partial I_{LI_i}}{\partial |V_j|} &= -|Y_{ij}|sin(\theta_{ij} + \delta_j) \qquad j \neq i \end{aligned} \tag{5.33}$$

respectively.

Calculation of the Jacobian Matrix Elements for Constant Current Sources

In the case of constant current sources, the elements J_5, J_6, J_7 and J_8 express the partial derivatives of the real and imaginary components of the source current at the I buses with respect to voltage magnitude and phase angle. For this case, the respective diagonal and off-diagonal elements of J_5, J_6, J_7 and J_8 can be found as follows:

$$\begin{aligned} \frac{\partial I_{GR_i}}{\partial \delta_i} &= -|V_i||Y_{ii}|sin(\theta_{ii}+\delta_i) - |\frac{S_{L_i}}{V_i}|sin(\delta_i-\theta_L) \\ \frac{\partial I_{GR_i}}{\partial \delta_j} &= -|V_j||Y_{ij}|sin(\theta_{ij}+\delta_j) \qquad j \neq i \end{aligned} \tag{5.34}$$

$$\begin{aligned} \frac{\partial I_{GR_i}}{\partial |V_i|} &= |Y_{ii}|cos(\theta_{ii}+\delta_i) - |\frac{S_{L_i}}{V_i^2}|cos(\delta_i-\theta_L) \\ \frac{\partial I_{GR_i}}{\partial |V_j|} &= |Y_{ij}|cos(\theta_{ij}+\delta_j) \qquad j \neq i \end{aligned} \tag{5.35}$$

$$\begin{aligned} \frac{\partial I_{GI_i}}{\partial \delta_i} &= |V_i||Y_{ii}|cos(\theta_{ii}+\delta_i) + |\frac{S_{L_i}}{V_i}|cos(\delta_i-\theta_{load}) \\ \frac{\partial I_{GI_i}}{\partial \delta_j} &= |V_j||Y_{ij}|cos(\theta_{ij}+\delta_j) \qquad j \neq i \end{aligned} \tag{5.36}$$

$$\begin{aligned} \frac{\partial I_{GI_i}}{\partial |V_i|} &= |Y_{ii}|sin(\theta_{ii}+\delta_i) - |\frac{S_{L_i}}{V_i^2}|sin(\delta_i-\theta_{load}) \\ \frac{\partial I_{GI_i}}{\partial |V_j|} &= |Y_{ij}|sin(\theta_{ij}+\delta_j) \qquad j \neq i \end{aligned} \tag{5.37}$$

5.3.2 Fault Analysis Using the Modified NR Algorithm

For fault analysis, fault impedance is considered as a phase to ground impedance at the faulty bus of the system when calculating the Ybus matrix. The IBDGs are initially modeled as PQ generators in the power flow analysis so as to obtain the primary voltage profile of the system. Having the system voltage profile and the power references of the IBDGs, the current contributions of these units are calculated. If the fault current contribution of an IBDG is less than the current threshold of its PE interface, the unit is modeled as a PQ generator. On the other hand, if the current contribution of the IBDG increases beyond the rating of the inverter interface, it is limited to a predefined value and the IBDG is modeled as a constant current source. The fault analysis algorithm is repeated if the

mode of operation of any of the IBDGs is changed to constant current source mode. The modified NR algorithm is used for fault analysis of the system in the presence of constant current IBDGs.

5.4 Simulation Results

5.4.1 Validation of Modified Newton-Raphson Power Flow Algorithm

Two test systems were used to verify the accuracy of the proposed modified NR algorithm in the presence of constant current loads and constant current sources. A 3-bus balanced system was used for the validation of the new algorithm for the case of constant current loads. The second test system, the IEEE 30-bus loop system, was used for the validation of the proposed algorithm on a more complicated system and with several constant current sources. The results produced by the proposed modified NR method were then compared with those obtained when the equivalent power references of the constant current nodes are used in the conventional NR power flow algorithm (power-based method). A comparison of the voltage, power, and current components resulting from the two methods demonstrates the superiority of the modified NR method with respect to meeting the convergence criteria for buses that have constant current loads/sources.

Power Flow Result for the 3-Bus System

The 3-bus test system shown in Figure 5.1 is a simple balanced system that served as a means of examining the accuracy of the proposed modified NR method for calculating constant current loads. Bus 1 of the system is considered the slack bus operating with a voltage magnitude of 1 pu and a phase angle of 0°. A constant current load is connected to bus 2. The real and imaginary components of the load current are rated at 0.1 pu and -0.02 pu, respectively. A 3-phase PQ load of 0.19 pu with a power factor of 0.96 is connected to bus 3. The line information for this system is provided in Table 5.1. |

The goal of calculating the power flow is to determine a voltage profile of the system that also complies with the values specified for the constant current and PQ loads. Equations (5.30), (5.31), (5.32) and (5.33) were used for calculating the current elements of the modified Jacobian matrix. Power and current mismatches were then found for each PQ and I constant load. The power flow solution converged after three iterations. The power

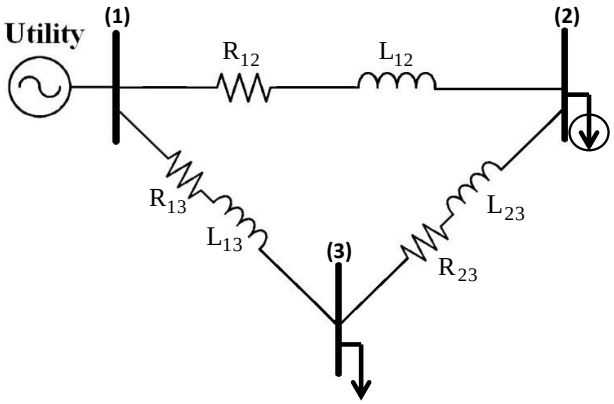

Figure 5.1: 3-bus test system.

Table 5.1: Line information for the 3-bus system

Line	R(pu)	L(pu)
L_{12}	0.03	0.035
L_{13}	0.02	0.03
L_{23}	0.015	0.02

flow results obtained using the modified NR method are shown in Table 5.2. It is clear that the real and imaginary components of the load current at bus 2 (constant current load bus) and the active and reactive powers of the load at bus 3 (PQ load bus) reach their specified values with an accuracy of 10^{-5}.

To demonstrate the accuracy of the modified Newton-Raphson method, the results obtained using this method were compared with those produced by the power-based method. For this purpose, bus 2 is assumed to operate at $1\angle 0^{\circ}$ pu. Employing this voltage and based on the specified value of the load current at bus 2, the corresponding active and reactive components of the load complex power are calculated to be 10 MW and 2 MVAr, respectively. The calculated power values are used in the conventional power flow algorithm as the values specified for the load power at bus 2. The results for this case are listed in Table 5.3. A comparison of the results shown in Table 5.2 and Table 5.3 reveals that not only can the proposed modified NR method provide a voltage profile identical to the one produced by the conventional power flow method, but it also guarantees the achievement of the levels specified for the current components at the constant current load bus (bus 2). As can be seen in Table 5.3, while the active and reactive power components of the PQ load at bus 3 reach their specified values, errors of 0.2% and 1% in the real and imaginary current components are evident with respect to the constant current load at bus

2. The reason for this discrepancy in the load current is that the value of the bus voltage chosen as the initial guess for this scenario ($V_2 = 1\angle 0^\circ$ pu) differs from the actual bus 2 voltage. In this case, because the test system is small, the initial voltage chosen for bus 2 is close to the actual bus voltage obtained from the power flow solution. As indicated in the following subsection, for larger systems, if the initial value diverges from the actual bus voltage, the final result for the load current will also differ from the desired value. It is clear that the power-based method that relies on a conventional power flow algorithm performs well only if the exact bus voltage value is used for the calculation of the active and reactive power components at the constant current node. However, since the voltages are calculated simultaneously, it is impossible for the exact value of the bus voltage to be available for use in the calculation of the corresponding power elements at the constant current bus. For this reason, the conventional power flow algorithm is incapable of providing accurate current information when constant current loads are connected to the system.

Table 5.2: Power flow results produced by the modified newton-raphson method for the 3-bus system

Bus	$\|V\|$(pu)	$\theta_v(^\circ)$	P_L(MW)	Q_L(MVAr)	I_{LR}(pu)	I_{LI}(pu)
1	1	0	0	0	0	0
2	0.9979	−0.1010	9.9829	1.9783	0.1000	−0.0200
3	0.9988	−0.0622	0.1824	0.0532	0.0018	−0.0005

Table 5.3: Power flow results produced by the power-based method for the 3-bus system

Bus	$\|V\|$(pu)	$\theta_v(^\circ)$	P_L(MW)	Q_L(MVAr)	I_{LR}(pu)	I_{LI}(pu)
1	1	0	0	0	0	0
2	0.9979	−0.1010	10	2	0.1002	−0.0202
3	0.9988	−0.0622	0.1824	0.0532	0.0018	−0.0005

Power Flow Result for the 30-Bus System

The IEEE 30-bus system illustrated in Figure 5.2 was used for the investigation of the effectiveness of the proposed modified power flow algorithm in a more complicated system with a variety of node types. The system is a balanced 3-phase system with two nominal bus voltages: 11 kV, 132 kV, and 33 kV. The load data and line information for this system

can be found in [96]. The system has 24 PQ buses, five PV buses, and one bus that is designated as the slack bus. Ten DGs are also connected to the system, four of which are considered to be constant current sources. Table 5.4 lists the details about the location and ratings of these four current sources. The other six DGs are connected to the system at buses 3, 10, 14, 15, 18 and 29, with each providing 10 MVA at unity PF. |

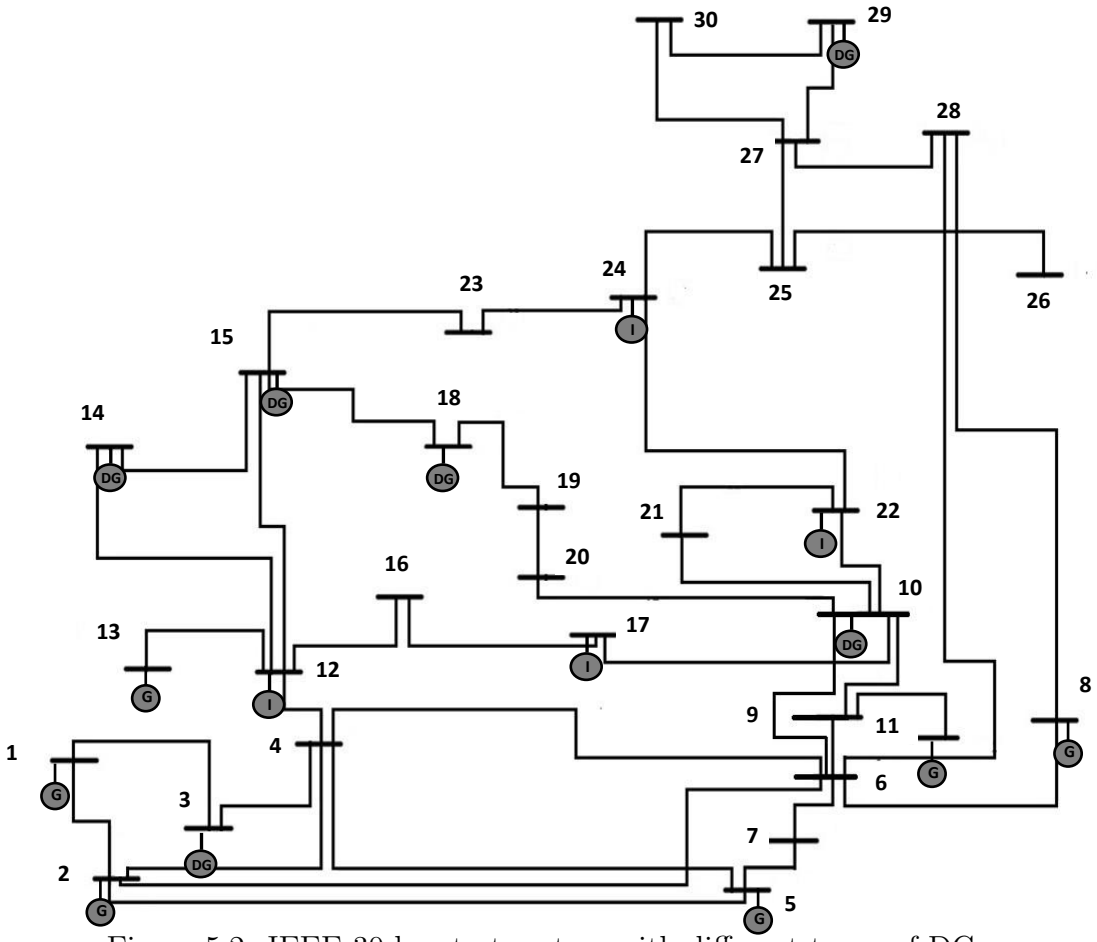

Figure 5.2: IEEE 30-bus test system with different types of DGs

The proposed modified NR power flow algorithm for the 30-bus system was developed using MATLAB, and the results obtained from its implementation are shown in Table 5.5. As can be seen, when the power flow solution converges, both the constant current generators and the PQ generators reach their desired values. These findings mean that the proposed modified power flow method guarantees identical convergence characteristics for

Table 5.4: Locations and current ratings of the constant current sources connected to the 30-bus system

Bus	$I_{GR}(pu)$	$I_{GI}(pu)$
12	0.09	0.007
17	0.06	0.007
22	0.11	−0.008
24	0.093	−0.03

PQ generators and constant current generators, the former in terms of power mismatches and the latter in terms of current mismatches. The results obtained show that the constant current generators connected at buses 12, 17, 22, and 24 achieve their specified current with an accuracy of 10^{-5}. Figure 5.3 and Figure 5.4 show the real and imaginary components of the current for the constant current generators; all of the current components reach their specified values within four iterations as the solution converges.

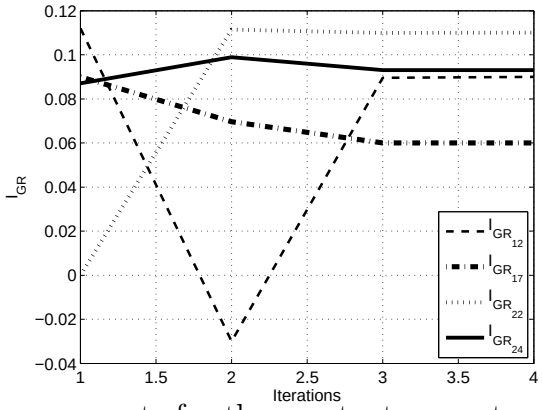

Figure 5.3: Real current components for the constant current generators at buses 12, 17, 22, and 24.

To demonstrate the superiority of the modified NR method, the power-based method introduced in subsection 5.4.1 was used to acquire the power flow solution for the 30-bus system. For this purpose, a voltage of $1\angle 0°$ is assumed for the buses that have constant current generators. Based on the desired current values for these generators, their corresponding active and reactive power components are determined. The nodes are then considered as normal PQ generators, and the calculated power components are used in the conventional NR analysis. The power flow results obtained for this scenario are shown in Table 5.6. To facilitate the evaluation of the current elements of the constant current nodes, the real and imaginary current components at the buses are in color in Table 5.5

Table 5.5: Power flow results produced by the modified Newton-Raphson method for the 30-bus system with PQ and I constant generators

Bus	$\|V\|$ (pu)	θ_v(angle) (°)	P_G (MW)	Q_G (MVAr)	I_{GR} (pu)	I_{GI} (pu)
1	1.0600	0.0000	155.436	1.021	1.466	−0.010
2	1.0430	−3.2425	40.000	28.367	0.368	−0.293
3	1.0298	−3.9107	10.000	0.000	0.097	−0.007
4	1.0209	−4.9813	0.000	−0.000	−0.000	−0.000
5	1.0100	−10.6928	−0.000	33.878	−0.062	−0.330
6	1.0169	−6.2758	−0.000	−0.000	0.000	−0.000
7	1.0063	−8.6087	0.000	−0.000	0.000	−0.000
8	1.0100	−6.8375	0.000	16.672	−0.020	−0.164
9	1.0458	−6.5566	0.000	0.000	0.000	−0.000
10	1.0299	−6.7066	10.000	−0.000	0.096	−0.011
11	1.0820	−6.5566	0.000	18.830	−0.020	−0.173
12	1.0547	−6.4317	9.350	−1.797	0.090	0.007
13	1.0710	−6.4317	0.000	12.491	−0.013	−0.116
14	1.0484	−6.1812	10.000	−0.000	0.095	−0.010
15	1.0392	−6.3822	10.000	0.000	0.096	−0.011
16	1.0374	−6.6932	−0.000	−0.000	−0.000	−0.000
17	1.0273	−6.7020	6.038	−1.434	0.060	0.007
18	1.0304	−6.4253	10.000	−0.000	0.096	−0.011
19	1.0221	−6.9597	−0.000	0.000	−0.000	−0.000
20	1.0232	−6.9519	−0.000	0.000	−0.000	−0.000
21	1.0197	−6.9728	0.000	0.000	−0.000	−0.000
22	1.0303	−6.0729	11.357	−0.379	0.110	−0.008
23	1.0211	−6.8985	−0.000	−0.000	−0.000	−0.000
24	1.0206	−6.3976	9.774	1.985	0.093	−0.030
25	1.0175	−7.0828	−0.000	−0.000	−0.000	−0.000
26	0.9998	−7.5023	−0.000	−0.000	−0.000	−0.000
27	1.0246	−7.2459	0.000	−0.000	0.000	−0.000
28	1.0159	−6.5119	−0.000	−0.000	0.000	−0.000
29	1.0205	−6.8170	10.000	−0.000	0.097	−0.012
30	1.0025	−8.3890	−0.000	−0.000	−0.000	−0.000

Table 5.6: Power flow results produced by the Power-Based method for the 30-bus system with PQ and I constant generators

Bus	$\|V\|$ (pu)	θ_v(angle) (°)	P_G (MW)	Q_G (MVAr)	I_{GR} (pu)	I_{GI} (pu)
1	1.0600	0.0000	156.691	0.545	1.478	−0.005
2	1.0430	−3.2677	40.000	28.096	0.368	−0.291
3	1.0301	−3.9578	10.000	0.000	0.097	−0.007
4	1.0212	−5.03970	0.000	0.000	0.000	−0.00
5	1.0100	−10.7331	−0.000	33.704	−0.062	−0.328
6	1.0172	−6.3410	0.000	0.000	0.000	−0.000
7	1.0065	−8.6635	0.000	0.000	−0.000	−0.000
8	1.0100	−6.8980	0.000	15.693	−0.019	−0.154
9	1.0473	−6.6657	0.000	0.000	−0.000	−0.000
10	1.0327	−6.8387	10.000	−0.000	0.096	−0.012
11	1.0820	−6.6657	0.000	18.071	−0.019	−0.166
12	1.0565	−6.5377	9.000	−0.700	0.085	−0.003
13	1.0710	−6.5377	−0.000	11.106	−0.012	−0.103
14	1.0504	−6.2936	10.000	−0.000	0.095	−0.010
15	1.0414	−6.5044	10.000	−0.000	0.095	−0.011
16	1.0399	−6.8166	−0.000	−0.000	−0.000	−0.000
17	1.0305	−6.8420	6.000	−0.700	0.059	−0.000
18	1.0329	−6.5514	10.000	0.000	0.096	−0.011
19	1.0247	−7.0856	−0.000	0.000	−0.000	−0.000
20	1.0259	−7.0792	−0.000	−0.000	−0.000	−0.000
21	1.0227	−7.1143	0.000	0.000	−0.000	−0.000
22	1.0345	−6.2911	11.000	0.800	0.105	−0.019
23	1.0241	−7.0440	0.000	−0.000	−0.000	−0.000
24	1.0248	−6.6217	9.300	3.000	0.087	−0.040
25	1.0206	−7.2284	0.000	0.000	−0.000	−0.000
26	1.0029	−7.6453	−0.000	−0.000	−0.000	−0.000
27	1.0268	−7.3465	0.000	0.000	0.000	−0.000
28	1.0164	−6.5834	0.000	0.000	0.000	−0.000
29	1.0228	−6.9195	10.000	0.000	0.097	−0.012
30	1.0048	−8.4844	0.000	0.000	−0.000	−0.000

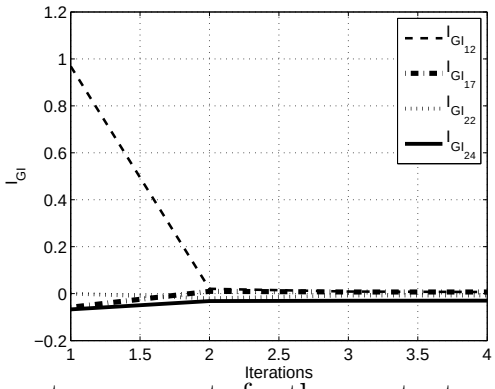

Figure 5.4: Imaginary current components for the constant current generators at buses 12, 17, 22, and 24.

and Table 5.6. When the current elements of buses 12, 17, 22, 24 are compared with their desirable values as listed in Table 5.4, the conventional power flow solution is clearly deficient with respect to achieving the target levels for the current components of the constant current generators. The errors are 5.5%, 1.7%, 4.5% and 6.4% in real components, and 142.8%, 100%, −137.5% and −33.3% in the imaginary components of the generator currents at buses 12, 17, 22, and 24, respectively. The inability of the conventional power flow algorithm to provide correct current information arises from the fact that the voltages assumed for the current generator buses are not good approximations of the actual bus voltages. In other words, a voltage of $1\angle 0^\circ$ is not close enough to a voltage that guarantees the desired currents at the constant current generator buses (e.g., $1.0537\angle -9.4841^\circ$ at bus 12).

5.5 Simulation Results for the Fault Analysis Based Power Flow Algorithms

Two test systems are used to verify the accuracy of the proposed power flow based fault analysis algorithms for radial and loop systems in the presence of constant current IBDGs. The Canadian Urban Benchmark Distribution System is used for validation of the backward-forward based fault analysis algorithm in radial systems. The PSCAD/EMTDC software is used to validate the results produced for this scenario. The second test system, the IEEE 30-bus loop system, is used for the validation of the NR based fault analysis algorithm with several IBDGs. The simulation results of this algorithm are compared with

those obtained from the OpenDSS software. For both of the algorithms, comparison of the fault current contribution of IBDGs demonstrate the accuracy of the proposed methods in exploring the behavior of IBDGs during fault conditions.

Simulation Results for the Backward-Forward Based Fault Analysis Method

The Canadian Urban Benchmark Distribution System [40] is used to investigate the effectiveness of the backward-forward based fault analysis technique. The test system is a 3-phase balanced system at the nominal voltage of 12.47 kV. As shown in Figure 5.5, four IBDGs are connected to the system at buses 4, 5, 6, 9. Inverter based DGs are connected through four 12.47kV/480 V transformers, and each provides 1 MVA at unity power factor.

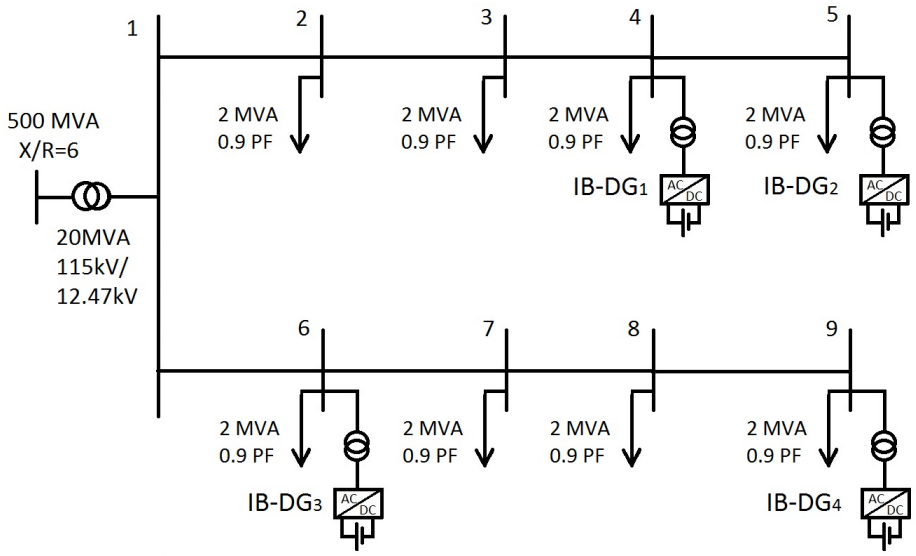

Figure 5.5: Canadian Urban Benchmark Distribution System

The backward-forward based fault analysis technique is used to investigate the current contribution of IBDGs for a balanced fault with $R_f = 0.48\Omega$ at bus 5. For accurate system modeling, all connected loads are considered as constant impedances in the proposed algorithm. A current threshold of 0.11 kA, which is slightly less than twice the rated current of IBDGs, is assigned to each unit so as to guarantee the safe operation of PE interfaces. Table 5.7 compares the current contribution of IBDGs obtained from the proposed load flow based technique with the ones obtained from the PSCAD software. As can be seen,

the backward-forward based technique is able to provide a very good approximation of the IBDG currents. It is also clear that the $IBDG_2$, which is located at bus 5, the faulty bus, has reached the defined current threshold and should consequently be considered as a constant current IBDG.

Table 5.7: Simulation results for the Canadian Urban Benchmark Distribution System

	Load Flow Based Technique	PSCAD
$IBDG_1$	0.094 kA	0.099 kA
$IBDG_2$	0.110 kA	0.115 kA
$IBDG_3$	0.063 kA	0.065 kA
$IBDG_4$	0.063 kA	0.065 kA

Simulation Results for the NR Based Fault Analysis Method

The IEEE 30-bus system illustrated in Figure 5.6 is used to investigate the effectiveness of the proposed modified NR based algorithm in performing fault analysis for loop systems with PQ, PV and I nodes. The system is a balanced 3-phase system with three nominal bus voltages: 132 kV, 33 kV, and 11 kV. The load data and line information for this system can be found in [96]. The system has 24 PQ buses, five PV buses, and one bus that is designated as the slack bus. Ten IBDGs are also connected to the system at buses 3, 10, 12, 14, 15, 17, 18, 22, 24 and 29. Table 5.8 shows the current threshold of the 10 IBDGs.

Table 5.8: Current threshold of IBDGs

Bus	IBDG	Current
3	$IBDG_1$	0.41 pu
10	$IBDG_2$	0.51 pu
12	$IBDG_3$	0.51 pu
14	$IBDG_4$	0.3 pu
15	$IBDG_5$	0.4 pu
17	$IBDG_6$	0.51 pu
18	$IBDG_7$	0.2 pu
22	$IBDG_8$	0.4 pu
24	$IBDG_9$	0.44 pu
29	$IBDG_{10}$	0.4 pu

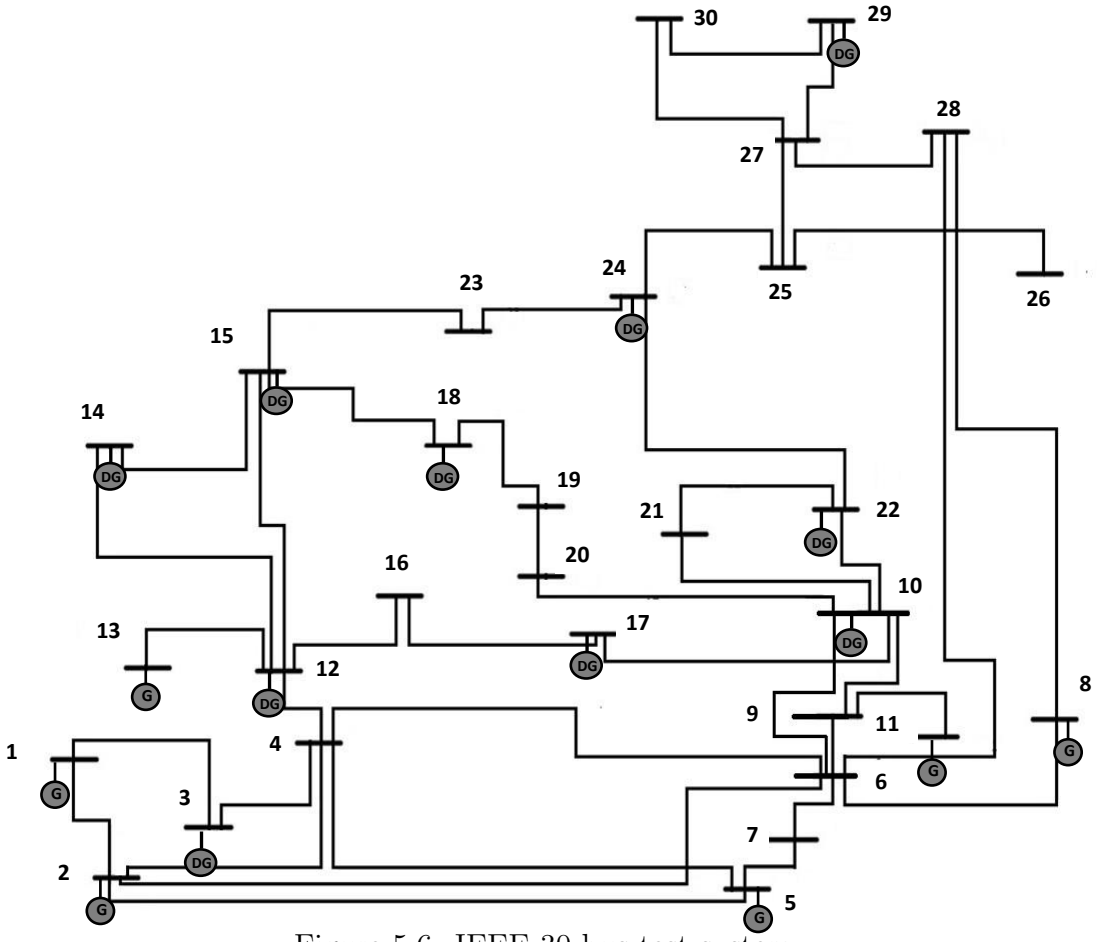

Figure 5.6: IEEE 30-bus test system.

The accuracy of the method is examined for a 3-phase fault at bus 15. The proposed modified NR based fault analysis algorithm was developed using MATLAB. The IBDGs are initially modeled as PQ generators and the primary voltage profile of the system is obtained. Table 5.9 provides the fault current contribution of the ten IBDGs obtained from the implementation of the NR based fault analysis algorithm when IBDGs operate as PQ generators. The results show that, of the 10 IBDGs connected to the system, the ones connected to buses 14, 15, 18, and 24 have fault current contributions higher than their assigned thresholds, and as a result, their buses are considered as I nodes in the modified NR algorithm. The algorithm is repeated with the new constant current nodes, and the results obtained for this scenario are shown in Table 5.10. As can be seen, the fault current contributions of $IBDG_{14}$, $IBDG_{15}$, $IBDG_{18}$, and $IBDG_{24}$ are controlled to their specified

threshold shown in Table 5.8. As the fault current contribution of none of the other IBDGs increases beyond its threshold there is no need to repeat the fault analysis algorithm and the results are considered to be the final values.

Table 5.9: Current contribution of IBDGs when operating as PQ generators - modified NR algorithm

Bus	IBDG	Current
3	$IBDG_1$	0.22 pu
10	$IBDG_2$	0.35 pu
12	$IBDG_3$	0.4 pu
14	$IBDG_4$	0.37 pu
15	$IBDG_5$	1.41 pu
17	$IBDG_6$	0.36 pu
18	$IBDG_7$	0.34 pu
22	$IBDG_8$	0.3 pu
24	$IBDG_9$	0.46 pu
29	$IBDG_{10}$	0.25 pu

Table 5.10: Current contribution of IBDGs when $IBDG_{14}$, $IBDG_{15}$, $IBDG_{18}$, and $IBDG_{24}$ operate as constant current sources - modified NR algorithm

Bus	IBDG	Current
3	$IBDG_1$	0.22 pu
10	$IBDG_2$	0.38 pu
12	$IBDG_3$	0.43 pu
14	$IBDG_4$	0.3 pu
15	$IBDG_5$	0.4 pu
17	$IBDG_6$	0.39 pu
18	$IBDG_7$	0.2 pu
22	$IBDG_8$	0.33 pu
24	$IBDG_9$	0.44 pu
29	$IBDG_{10}$	0.27 pu

To demonstrate the accuracy of the NR based fault analysis method, the same fault condition is simulated with OpenDSS on the 30-bus system with the connected IBDGs. Results of this implementation are shown in Table 5.11. The IBDGs are initially modeled

as PQ buses. The voltage profile of the systems and the fault current contribution of the IBDGs are obtained. As shown, $IBDG_{14}$, $IBDG_{15}$, $IBDG_{18}$, and $IBDG_{22}$ have fault current contributions higher then the specified thresholds. It is clear that the results obtained for the fault current contribution of IBDGs are in agreement with what is calculated by the modified NR algorithm. When IBDGs with high fault current contributions are detected, the models of these units are converted to the type with limited current contributions, and the short circuit analysis is repeated. Comparing the results shown in Table 5.10 with the ones obtained from the OpenDSS software, Table 5.11, show the effectiveness of the modified NR based algorithm in estimating the fault current contribution of IBDGs in loop systems

Table 5.11: Current contribution of IBDGs when IBDGs are modeled as PQ nodes and when $IBDG_{14}$, $IBDG_{15}$, $IBDG_{18}$, and $IBDG_{24}$ have limited current contributions - OpenDSS results

Bus	IBDG	IBDGs as PQ buses (pu)	IBDGs with limited current (pu)
3	$IBDG_1$	0.2174	0.22
10	$IBDG_2$	0.3469	0.36
12	$IBDG_3$	0.4013	0.42
14	$IBDG_4$	0.3695	0.3
15	$IBDG_5$	1.403	0.4
17	$IBDG_6$	0.3596	0.37
18	$IBDG_7$	0.3325	0.2
22	$IBDG_8$	0.2956	0.31
24	$IBDG_9$	0.4526	0.43
29	$IBDG_{10}$	0.2506	0.26

5.6 Summary

This chapter has presented two power flow based methods for analyzing the behavior of IBDGs during fault condition in radial and loop systems. In both, IBDGs are initially modeled as PQ generators during fault condition. If their current contribution exceeds the predefined threshold levels set for each IBDG, the currents will be limited to the level safe for IBDG protection and the models are converted to constant current sources. The fault is treated as a load with a small resistance connected to the system, while its current is

considered in the nodal current equation. The backward-forward sweep algorithm is used to solve the load flow problem for radial systems during fault conditions. In this case, the current of IBDGs is added to the nodal current equation in the backward sweep. On the other hand, the Newton-Raphson power flow algorithm is modified for fault analysis of loop systems with IBDGs. In the modified Newton-Raphson algorithm, buses with IBDGs are modeled as either PQ nodes or constant current (I) nodes. In the novel NR based fault analysis algorithm, current formulations rather than conventional power formulations are developed for constant current sources. This approach permits mismatches in the real and imaginary components of the current at the I nodes to be obtained in addition to the conventional active and reactive power mismatches. This novel modified Newton-Raphson power flow algorithm enables the inclusion of both models of IBDGs, PQ nodes or I nodes, in one matrix, thus eliminating the need to represent the I nodes in terms of their equivalent powers. Two case studies are developed to investigate the effectiveness of the developed algorithms for fault analysis of radial and loop systems in the presence of IBDGs. The Canadian Urban Benchmark Distribution System is used for validation of the backward-forward based fault analysis algorithm in radial systems. The algorithm is developed in MATLAB, and the results are compared with the ones obtained from the implementation of the system in PSCAD/EMTDC software. The second test system, the IEEE 30-bus loop system, is used to examine the modified NR power flow algorithm and the NR based fault analysis algorithm with several IBDGs. The algorithm is developed in MATLAB and the results are validated with the use of a power based method incase of power flow analysis, and with OpenDSS simulations results in case of fault analysis. The simulation results show the effectiveness of the algorithms in performing fault analysis in the presence of IBDGs for radial and loop systems.

Chapter 6

Construction of Protection Zones with Self-Healing Capability in Loop Systems

6.1 Introduction

This chapter presents an algorithm for constructing protection zones with fault current management capability for fault conditions in loop systems which have high penetrations of IBDGs and synchronous DGs. The idea of FCM operation defined for IBDGs and synchronous DGs in Chapters 3 and 4 is used as the basis of this operation. Having a large power system, the contribution of DGs in fault currents varies depending on their closeness to the fault location. Hence, there is no need to operate all IBDGs as FCM units. A more optimized operation is obtained if for each fault location, a zone called the protection zone is found, and only the IBDGs that are located in the zone are controlled to operate as FCM units. In other words, for each fault location, the proposed algorithm divides the system into two sectors: 1) the protection zone, which includes the faulty sector; The IBDGs inside this zone are the ones affected by the fault, and are the main elements of the fault current management algorithm; 2) the healthy sector, which can operate in islanded mode. The DGs in this sector can continue feeding their local loads in islanded mode. It should be noted that the focus of this work is to propose an algorithm that constructs protection zones with self fault current management capability. Any algorithm available for construction and operation of the islanded sectors can work in parallel with the proposed algorithm for the healthy sectors.

The proposed algorithm for constructing protection zones in loop systems consists of two main steps. First, all the paths from the grid points to the fault location are identified. This step is required because in the FCM operation, the grid current is considered to be the reference current based on which the fault current is controlled. In the second step, the IBDGs located on the fault current paths are selected as the potential FCM units. From these IBDG, the ones which are affected by the fault, and thus their fault currents are kept below the tripping threshold of their inverter interfaces, operate as FCM units. The current paths from the grid points to the fault location, and the IBDGs selected as FCM units, determine the boundaries of protection zones. All the IBDGs located outside the protection zone can continue their operation and feed their local loads if operated in islanded mode. One other factor to be considered when doing FCM operations in loop systems is the calculation of reference phase angle required for the FCM operation. As shown in (3.13), the reference phase angle calculated for the FCM in zone B, δ_B, is a function of the grid current phase angle, θ_s, and the fault current, θ_{flt}. However, in loop systems where there are multiple grid points, it is not possible to consider one single phase angle as the grid current phase angle. Hence, it is proposed that each IBDG manages the fault current locally at the bus it is connected to.

This chapter is organized as follows: Section 6.2 presents the algorithm proposed for constructing protection zones with FCM capability. Section 6.3 describes the modifications required for implementation of FCM operation on loop systems. Simulation results are presented in section 6.4. Section 6.5 presents possible reasons for errors in the results of FCM operation in loop systems. A summary is provided in section 6.6.

6.2 Construction of Protection Zones

The idea of the protection zone is proposed to gain more optimized FCM operation in large systems with numerous DGs. As mentioned, not all DGs contribute to the fault current equally, and hence it is not necessary to operate them all as FCM units. Many DGs located far from the fault point are not affected by the fault and their contribution to the fault does not cause a serious protection problem. Hence, the idea is to find an optimized algorithm to manage the fault current in large power systems with DGs. The steps that should be taken to construct the protection zones are shown in Figure 6.1. As shown, there are three important factors to be considered when constructing the protection zones with FCM capability: determination of the FCM current paths, selection of the FCM units, and the identification of FCM zone. These Steps are explained in detail in the next three subsections:

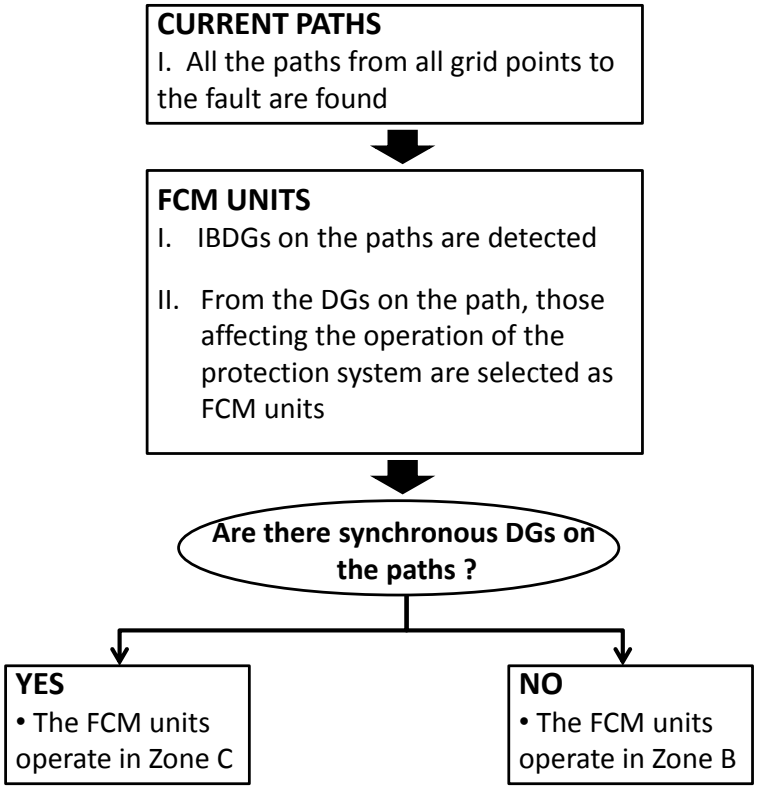

Figure 6.1: Construction of protection zones in loop systems

6.2.1 Paths of Protection

Inverter based DGs are able to manage their own fault current and the fault current contribution of synchronous DGs by operating as FCM units in zone B or zone C. For this operation, the phase angle of IBDGs is modified at the moment of fault detection. As shown in (3.13) and (4.1), the formulas used to calculate the reference phase angles for zone B and zone C operation are functions of the grid current phase angle and fault current phase angle. In radial systems, there is only one grid point for the system. Hence, for any fault location, there is only one current path from the grid to the fault. On the other hand, in loop systems, there is more than one grid point connection. Additionally, for each grid point, depending on the line impedances, there will be multiple fault current paths. Hence, in order to perform an effective FCM operation in loop systems, all the current paths from the grid points should be carefully examined for each fault location.

As can be seen in Figure 6.1, the first step in constructing protection zones is to find all the possible current paths from the grid points to the fault location. For this purpose the power system is considered as a network with N numbers of nodes (buses). Considering each line impedance as its weight, Dijkstra's algorithm is used to find the first M paths with the lowest total weight from the source node (grid) to the destination node (fault bus). Assuming a large value for M, the algorithm gives all the available paths from a grid point to the fault location. Depending on the system size, the system configuration and the line impedances, there will be several paths from each grid point to a fault location. This operation is repeated for each grid point to find all the current paths for a specific fault location. These current paths are the outputs of the first step of the protection zone construction algorithm.

6.2.2 Selection of FCM Units

The purpose of the second step is to select the IBDGs that should operate as FCM units. For a specific fault location, not all IBDGs are located on the current paths from the grid points to the fault. Since the FCM operation is performed based on the grid current phase angle, the IBDGs which are not on the current paths from the grids to the fault are not included in the protection zone. Hence, in the second step, first, the IBDGs which are on the current paths from the grids to the fault location are selected. Next, from these IBDGs, the ones affected by the fault current and having high fault current contributions, are chosen to operate as the FCM units. In other words, from the IBDGs which are on the current paths, the ones that have a fault current contribution higher than a predefined threshold and increase the current beyond the short circuit capacity of the system, are responsible to mitigate the problem they have caused by operating as FCM units. Hence, when the IBDGs on the paths are determined, the ones with a fault current contribution more than twice their current rating are selected. The current magnitude of these IBDGs is limited to 1.2 times their current rating to protect their interface, and their phase angle is modified according to the desired operation of the FCM units, either in zone B or zone C.

6.2.3 Zone of Operation for FCM Units

Depending on the location and number of synchronous DGs that exist in the system, the IBDGs selected as FCM units operate in zone B or zone C. As mentioned in Chapter 4, since the current contribution of IBDGs is limited by the protection system of their inverter

interfaces, these units contribute less than synchronous DGs in the fault current. Hence, FCM units should operate in zone C when synchronous DGs exist on their current paths. In addition, more than one IBDG is required to operate as an FCM unit for each synchronous DG. However, the number of FCM units required for the FCM of each synchronous DG, and the phase angle of Δ added to δ_B for each unit, depends on the location of synchronous DGs and IBDGs and the current ratings of those IBDGs. As an example, if the synchronous DGs are located far from the fault location, they are not affected by the fault severely, and hence, their contribution in the fault current might not much higher than that of the IBDGs. On the other hand, on a current path, if a synchronous DG is located closer to the fault location than an IBDG, its fault current contribution is significantly higher than the IBDGs', and consequently, multiple IBDGs are required to manage its fault current. Moreover, a larger phase angle Δ must be added to δ_B.

6.3 Calculation of FCM Phase Angle for Loop Systems

The reference phase angles required for FCM operation in zone B and C, calculated in Chapter 3 and 4, are presented as:

$$\delta_B = 180 - \frac{180 - |\theta_s - \theta_{flt}|}{2} - |\theta_s| \tag{6.1}$$

$$\delta_C = \delta_B + \Delta \tag{6.2}$$

As can be seen, the phase angle δ_B, and consequently δ_C, are functions of the grid current and the fault current phase angles. These phase angles are proposed based on the topology and configuration of radial systems. In radial systems, for any fault, there is one grid current path only, and as a result, the grid current phase angle, θ_s, can be simply measured. On the other hand, for loop systems, since there is more than one grid point, it is not possible to find the source of the current detected by a relay, and as a result, the grid current phase angle required for calculating the reference phase angle of FCM operation cannot be measured directly. Even if there is one grid point only, there are multiple current paths from the grid point to the fault, and the relays installed on a path see only a part of the fault current fed by the grid, based on the impedance of their path. To overcome this problem, it is purposed that IBDGs manage the fault current locally at the bus they are connected to.

6.3.1 Local Management of Fault Currents

For the purpose of FCM operation in loop systems, it is proposed that each IBDG manages its fault current contribution and the contribution from the synchronous DGs on the same path, locally. In order to clarify this operation, consider a single bus of the IEEE 30-bus loop system, as shown in Figure 6.2. Locally managing the fault current means that the IBDG installed on bus 3 manages the fault current seen by the relay $R_{3,4}$ to be equal to the fault current seen by $R_{1,3}$. When synchronous DGs exist on the path, the desired operation is to manage the fault current seen by $R_{3,4}$ so that it is less the one seen by $R_{1,3}$. The current gap generated in this case is used to compensate for the extra fault current contribution of synchronous DGs. This a simple operation, which can be applied by substituting the θ_s phase angle in (6.1) with the phase angle of the current injected to the bus with IBDG ($\theta_{1,3}$ in Figure 6.2), and θ_{flt} with the phase angle of the current going out of the bus with the IBDG ($\theta_{3,4}$ in Figure 6.2).

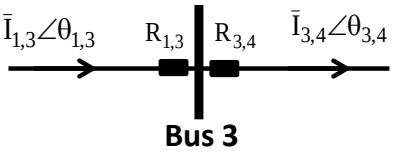

Figure 6.2: Example of a bus with one line going in and one coming out of

The operation becomes more complicated for the buses that have multiple lines connected to them. Bus 12 in Figure 6.3 shows an example of such buses. For this type of bus, the FCM operation can be performed on the total fault current going into the bus and the total fault current coming out of the bus. For a given bus, the line currents with positive real component are considered as the currents injected to the bus, and the ones with negative real components are the currents coming out of the bus. The total fault current injected into the bus and the total of the fault current coming out the bus are obtained by the vector summation of the individual currents.

For the bus 12 example shown in Figure 6.3, the injected currents are $I_{4,12}$, $I_{13,12}$, and the currents coming out the bus are $I_{12,15}$, $I_{12,16}$ and $I_{12,14}$. Hence, the total fault current going into the bus and the total fault current coming out of the bus 12 are obtained as:

$$\begin{aligned} \overline{I}_{in_{12}}\angle\theta_{in_{12}} &= \overline{I}_{4,12}\angle\theta_{4,12} + \overline{I}_{13,12}\angle\theta_{13,12} \\ \overline{I}_{out_{12}}\angle\theta_{out_{12}} &= \overline{I}_{12,15}\angle\theta_{12,15} + \overline{I}_{12,16}\angle\theta_{12,16} + \overline{I}_{12,14}\angle\theta_{12,14} \end{aligned} \tag{6.3}$$

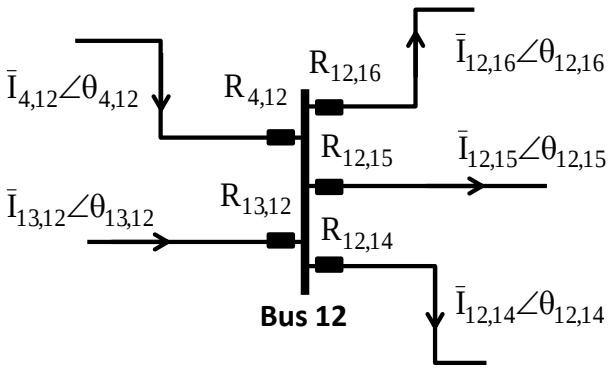

Figure 6.3: Example of a bus with multiple lines

In this case, the grid current phase angle, θ_s, in (6.1) is substituted with the phase angle of the total fault current injected into the bus with the IBDG (θ_{in_5} in (6.3)), and θ_{flt} is substituted with the phase angle of the total current coming out of the bus with the IBDG (θ_{out_5} in (6.3)).

Another point should be considered: since there are multiple lines connected to the bus in this case, the FCM operation is performed on the total fault current going into and coming out of the bus with the IBDG. Hence, it is expected that the magnitude of the total fault current going out of the bus with IBDG is managed to a value equal to the magnitude of the total fault current injected in to the bus. However, the fault current seen on each line might not be at the exact same level as it was when there was no DG connected to the system.

6.4 Simulation Results

The IEEE 30-bus system shown in Figure 6.4 is used for the validation of the proposed algorithm on a loop system with different types of DGs. The load data and line information can be found in [96]. Two case studies are proposed here to investigate the effectiveness of the proposed algorithm in constructing protection zones with fault current management capability. The first study is for the case where IBDGs and synchronous DGs exist in the system, and the second is for the case when only IBDGs exist in the system.

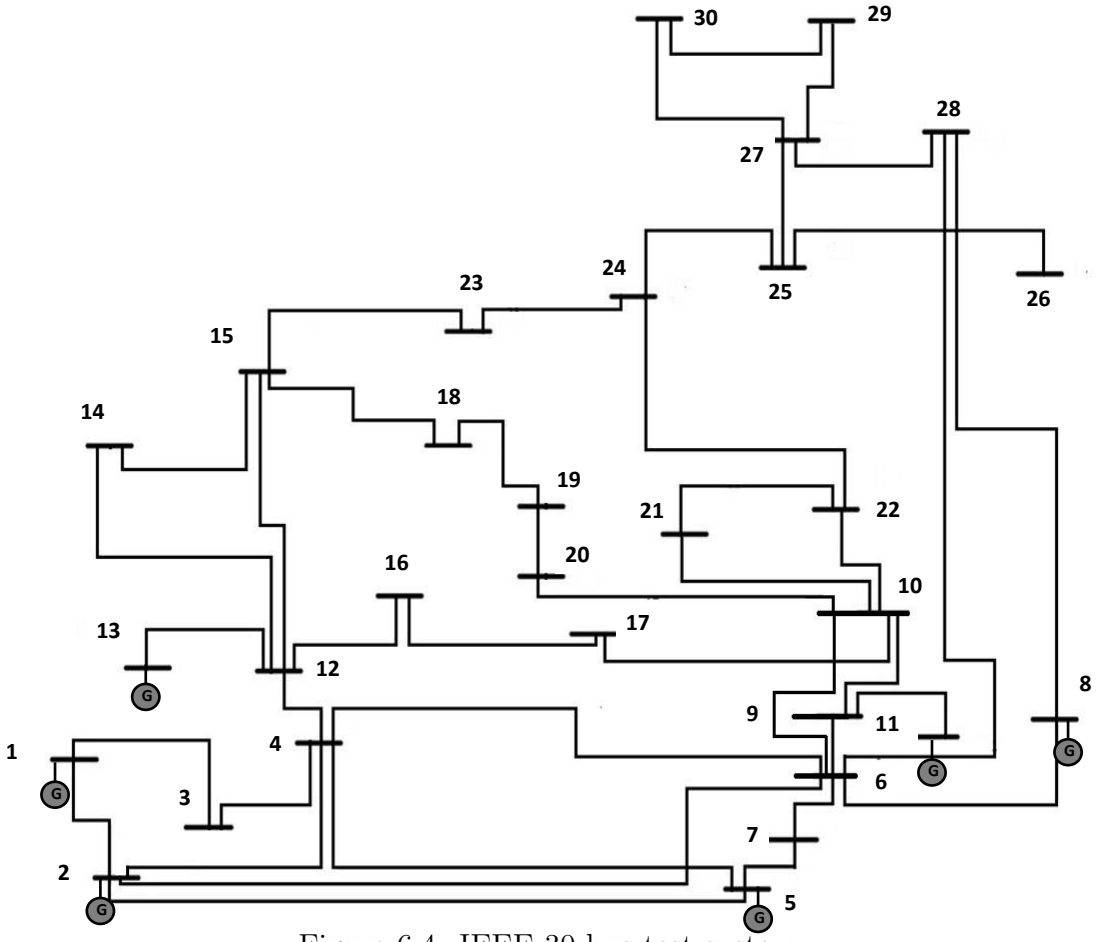

Figure 6.4: IEEE 30-bus test system

6.4.1 Validation Results for the IEEE 30-bus System with IBDGs and Synchronous DGs

It is assumed that 10 DGs are connected to the IEEE 30-bus system, of which two are synchronous DGs and eight others are IBDGs. The location and the power ratings of these 10 DGs are shown in Table 6.1. The system is connected to the grid from 6 points: buses 1, 2, 5, 8, 11 and 13.

For a three-phase balanced fault at bus 15, Table 6.2 compares the total fault current and the fault current seen on lines connected to buses 12, 14, 18, 23, and 15 for three scenarios: when there is no DG connected to the system, when DGs are connected to the system but there is no FCM operation, and when DGs are connected to the system and

Table 6.1: Location and power ratings of the IBDGs and synchronous DGs connected to the 30-bus system

DG	Type	Location	Power Ratings	Power Factor
DG_1	IBDG	Bus 3	15 MVA	1
DG_2	IBDG	Bus 7	15 MVA	1
DG_3	IBDG	Bus 12	20 MVA	1
DG_4	IBDG	Bus 14	20 MVA	1
DG_5	IBDG	Bus 19	20 MVA	1
DG_6	IBDG	Bus 22	25 MVA	1
DG_7	IBDG	Bus 23	20 MVA	1
DG_8	IBDG	Bus 29	20 MVA	1
DG_9	Synch DG	Bus 4	20 MVA	1
DG_{10}	Synch DG	Bus 24	35 MVA	1

the proposed algorithm is applied to construct the protection zone and manage the fault current. It should be noted that bus 15 is the fault bus, and buses 12, 14, 18, and 23 are chosen as examples of DG buses with two or multiple current lines connected to them.

As can be seen, for all the system buses shown in Table 6.2, when there is no DG connected to the system the fault current entering each bus is equal to the fault current going out of the bus. When DGs are connected to the system, the total fault current going out of the buses with DGs are higher than the total fault current injected into them. The difference between the currents injected into these buses and the currents going out of them is because of the current contribution of the DGs connected to them. As shown in Table 6.2, since bus 18 has no DG connected to it, the fault current injected into this bus is equal to the bus current going out of it. However, the total fault current seen by the protective devices connected to this bus, in the presence of DGs, is higher than the current seen when no DG is connected to the system. The fault current seen by protective devices installed on lines 23-15 and 24-23 increases when DGs are connected to the system. Not only that, but it is also shown in Table 6.2 that because of the current contribution of DG_7 the fault current going out of bus 23, I_{23-15}, is higher than the fault current injected into this bus, I_{24-23}. On the other hand, as seen in Table 6.2 when DGs are connected to the system, the total fault current injected into bus 14 is lower than that when DGs are not connected. This reduction in the fault current can be justified by the explanation in section 2.7. It is also shown that with the current contribution of DG_4 at bus 14, the fault current going out of this bus has a higher magnitude than that current injected into this bus.

Table 6.2: Fault currents seen on lines connected to buses 12, 14, 18, 23, and 15 for a 3-phase fault at bus 15

	Current (pu) no DG installed	Current (pu) with DG but no FCM operation	Current (pu) with DG and FCM operation
$I_{15,23}$	0.7418∠ 1.9623	1.162∠1.9469	0.9825∠1.8794
$I_{24,23}$	0.7418∠-1.1793	0.9212∠-1.2606	1.0166∠-1.4896
$I_{15,18}$	0.8094∠ 1.9171	0.9945∠ 2.105	0.8236∠2.0982
$I_{19,18}$	0.8094∠-1.2245	0.9945∠-1.0366	0.8236∠-1.0434
$I_{12,14}$	0.6606∠ -1.383	0.5745∠-1.142	0.6367∠ -1.3969
$I_{15,14}$	0.6606∠1.7586	0.7976∠2.0576	0.6131∠2.1074
$I_{4,12}$	2.3696∠ -0.8506	2.1535∠-0.8309	2.2482∠ -0.9111
$I_{13,12}$	1.9004∠-2.5691	1.1824∠-2.3773	1.4941∠ -2.4205
$I_{14,12}$	0.6606∠1.7586	0.5745∠ 1.9996	0.6367∠ 1.7447
$I_{15,12}$	2.5789∠1.5815	2.7043∠1.8253	2.4850∠1.7536
$I_{16,12}$	0.4738∠-0.6872	0.5042∠-0.7075	0.4558∠ -0.8189
$I_{In_{12}}$	2.8381∠-0.8234	2.6546∠-0.8075	2.7024∠ -0.8956
$I_{Out_{12}}$	2.8087∠2.2427	2.9212∠2.2231	2.6796∠ 2.2504
I_{flt}	4.7281	5.6217	4.8491

Column 3 of Table 6.2 shows the results when the algorithm explained in section 6.2 is used to construct the protection zone for the fault applied at bus 15. For this operation, first, all the paths from the grid points to the faulty bus, bus 15, are found. In the second step, the IBDGs located on the current paths from the grid points to the fault point are detected. For the applied fault at bus 15, all the IBDGs except from DG_8 at bus 29 are detected as the ones on the current paths. From these IBDGs, $IBDG_{12}$, $IBDG_{14}$, $IBDG_{19}$, $IBDG_{22}$, and $IBDG_{23}$ which have a fault current contribution more than 1.2 times of their rated current, are selected as FCM units. Since, synchronous DGs exist in the system, the FCM units are operated in zone C to manage the fault current contributed by the synchronous DGs in addition to their own fault current. For this purpose, a Δ value of 20° is added to the reference phase angle calculated for the FCM operation in zone B, δ_B.

The results show the capability of the proposed algorithm in constructing an effective protection zone and consequently managing the fault current contributed by the DGs. To better show the effectiveness of the proposed algorithm, the percentage error of the fault current seen by the protective devices located on the lines connected to the faulty bus are compared for three different fault locations: bus 15, bus 16, and bus 10. Table 6.3, Table 6.4 and Table 6.5 compare the percentage errors of the fault current seen by the

protective relays for the case when there is no FCM operation, and the case when the proposed algorithm is used to construct the protection zones, and the selected IBDGs operate as FCM units.

Table 6.3: Comparison of the fault current seen on the faulty lines for a fault at bus 15 ($IBDG_{12}$, $IBDG_{14}$, $IBDG_{19}$, $IBDG_{22}$ and $IBDG_{23}$ operate as FCM units)

	% error with DGs but no FCM operation	% error with DGs and FCM operation
$I_{12,15}$	4.8606	-2.9388
$I_{14,15}$	20.7435	-13.1481
$I_{18,15}$	22.8650	-1.5894
$I_{23,15}$	56.6444	27.0261

Table 6.4: Comparison of the fault current seen on the faulty lines for a fault at bus 16 ($IBDG_{12}$, $IBDG_{22}$ operate as FCM units)

	% error with DGs but no FCM operation	% error with DGs and FCM operation
$I_{12,16}$	7.8628	-1.5480
$I_{17,16}$	8.8153	1.9123

Table 6.5: Comparison of the fault current seen on the faulty lines for a fault at bus 10 ($IBDG_{19}$, $IBDG_{22}$, $IBDG_{23}$ operate as FCM units)

	% error with DGs but no FCM operation	% error with DGs and FCM operation
$I_{6,10}$	3.0577	4.6106
$I_{9,10}$	-3.3436	-1.9597
$I_{17,10}$	15.7773	11.0770
$I_{20,10}$	47.0377	21.9734
$I_{21,10}$	106.0192	57.0192
$I_{22,10}$	105.9793	56.9888

It is clear from the results shown in the above three tables that the proposed algorithm is capable of managing the fault current seen by the protective devices. For most of the cases, the percentage error, which is calculated based on the fault current seen by the protective devices in the original system without DGs, is improved noticeably when the

proposed algorithm is applied and the selected IBDGs operate as FCM units. However, errors still occur in some of the measurements. Possible reasons for errors in the results of FCM operation are explained in section 6.5.

6.4.2 Validation Results for the IEEE 30-bus System with IBDGs

In this case, it is assumed that only 10 IBDGs are connected to the IEEE 30-bus system and no synchronous DGs exist in the system. The location and ratings of IBDGs are shown in Table 6.6.

Table 6.6: Location and power ratings of the IBDGs connected to the 30-bus system

DG	Type	Location	Power Ratings	Power Factor
DG_1	IBDG	Bus 3	15 MVA	1
DG_2	IBDG	Bus 4	20 MVA	1
DG_3	IBDG	Bus 7	15 MVA	1
DG_4	IBDG	Bus 12	20 MVA	1
DG_5	IBDG	Bus 14	20 MVA	1
DG_6	IBDG	Bus 19	20 MVA	1
DG_7	IBDG	Bus 22	25 MVA	1
DG_8	IBDG	Bus 23	20 MVA	1
DG_9	IBDG	Bus 24	35 MVA	1
DG_{10}	IBDG	Bus 29	20 MVA	1

Table 6.7 compares the total fault current and the fault current seen on lines connected to buses 12, 14, 18, 23, and 15 for three scenarios when a three-phase balanced fault is applied at bus 15. When IBDGs are connected to the system, the fault current seen by some of the protective devices increases, while the current seen by some others decrease. The reason for the increased and decreased fault current in the presence of IBDGs is explained in section 2.7. The third column shows the results for the case when the proposed algorithm is used to construct the protection zone, and the selected IBDGs are operated as FCM units. The operation shows effective management of fault current for buses with two lines connected to them. As shown, in presence of IBDGs and without the proposed FCM operation, the total fault current injected to bus 12 is reduced to a value below the level observed without IBDGs. Hence, when the protection zone algorithm is applied, the FCM

unit connected to bus 12 is operated in zone C to increase the fault current to a higher value.

Table 6.7: Fault currents seen on lines connected to buses 12, 14, 18, 23, and 15 for a 3-phase fault at bus 15

	Current (pu) no DG installed	Current (pu) with DG but no FCM operation	Current (pu) with DG and FCM operation
$I_{15,23}$	0.7418∠ 1.9623	1.1183∠2.4581	0.8523∠2.6171
$I_{24,23}$	0.7418∠-1.1793	0.8926∠-0.7248	0.8422∠-0.7958
$I_{15,18}$	0.8094∠ 1.9171	0.9146∠2.3361	0.7243∠2.3786
$I_{19,18}$	0.8094∠-1.2245	0.9146∠-0.8055	0.7243∠-0.7630
$I_{12,14}$	0.6606∠ -1.383	0.5336∠-1.0585	0.6202∠ -1.2732
$I_{15,14}$	0.6606∠1.7586	0.7516∠2.1810	0.6022∠2.2401
$I_{4,12}$	2.3696∠ -0.8506	1.9035∠-0.6504	1.8946∠ -0.7276
$I_{13,12}$	1.9004∠-2.5691	1.4524∠-2.2016	1.6007∠-2.1989
$I_{14,12}$	0.6606∠1.7586	0.5336∠ 2.0831	0.6298∠ 1.8707
$I_{15,12}$	2.5789∠1.5815	2.5411∠1.9316	2.4690∠1.8812
$I_{16,12}$	0.4738∠-0.6872	0.5058∠-0.3264	0.4116∠ -0.2507
$I_{In_{12}}$	2.8381∠-0.8234	2.3885∠-0.5829	2.2682∠-0.6442
$I_{Out_{12}}$	2.8087∠2.2427	2.6170∠2.4497	2.5069∠2.4192
I_{flt}	4.7281	5.1963	4.4104

Table 6.8, Table 6.9, and Table 6.10 compare the percentage error in the fault current seen by protective devices installed on the faulty lines for three fault locations: bus 15, bus 16 and bus 10. With the proposed operation, the errors decrease, and the fault currents seen by protective devices on the faulty lines get closer to the values they were originally designed for. However, as observed in the first case study, the proposed algorithm for loop systems in the presence of IBDGs is not capable of reducing the fault current error to zero. Possible reasons for the errors in FCM operation are explained in the next subsection.

6.5 Problems associated with FCM operation in loop systems

It is clear from the results of the above two case studies that for the loop systems, the proposed FCM operation manages the fault current seen by the protective devices with a

Table 6.8: Comparison of the fault current seen on the faulty lines for a fault at bus 15 ($IBDG_{12}$, $IBDG_{14}$, $IBDG_{19}$, $IBDG_{22}$, $IBDG_{23}$ and $IBDG_{24}$ operate as FCM units)

	% error with DGs but no FCM operation	% error with DGs and FCM operation
$I_{12,15}$	-1.4667	-4.2630
$I_{14,15}$	13.7702	-7.3875
$I_{18,15}$	12.9952	-10.3882
$I_{23,15}$	50.7513	15.0606

Table 6.9: Comparison of the fault current seen on the faulty lines for a fault at bus 16 ($IBDG_{12}$, $IBDG_{14}$ and $IBDG_{22}$ operate as FCM units)

	% error with DGs but no FCM operation	% error with DGs and FCM operation
$I_{12,16}$	4.9068	-1.5450
$I_{17,16}$	5.3348	-2.0322

Table 6.10: Comparison of the fault current seen on the faulty lines for a fault at bus 10 ($IBDG_{19}$, $IBDG_{22}$, $IBDG_{23}$ and $IBDG_{24}$ operate as FCM units)

	% error with DGs but no FCM operation	% error with DGs and FCM operation
$I_{6,10}$	-11.2766	-15.2272
$I_{9,10}$	-10.7777	-11.7134
$I_{17,10}$	6.8064	0.0426
$I_{20,10}$	44.4493	27.2093
$I_{21,10}$	121.7794	75.1750
$I_{22,10}$	121.7364	75.1411

higher percentage of error, compared to the case of radial systems. The following points make the FCM operation more complicated in loop systems in presence of IBDGs and synchronous DGs.

- Depending on the location and rating of IBDGs, their connection to power systems can decrease the fault current seen by some of the protective devices. This effect is observed more commonly in loop systems than in radial ones.
- Loop systems, have multiple grid connection points, making FCM operation more

complicated as there is more than one path from each grid connection to the fault.

- Unlike radial systems, loop systems have many system buses with more than two lines connected to them. As a result, the modified method proposed in subsection 6.3.1 should be used to calculate the reference current phase angle required for the FCM operation. Hence, for these system buses, the FCM operation is in fact performed on the total fault current entering and existing the bus, and not on each line current individually. Using this approximate method increases the error of the proposed operation.

- Because of the structure of loop systems, there are multiple current paths from the grid points to the fault location. The current paths with smaller impedances are selected to carry the largest portion of the grid currents contribution. When DGs are connected to the system, they also contribute to the fault current. Moreover, depending on the type of DG, their connection may change the total impedance seen from each grid point. Hence, when DGs are connected to the system, the currents entering or existing each bus may have different directions from the case where DGs are not connected to the system. This point should be considered when performing the FCM operation in loop systems.

6.6 Summary

This chapter has developed a novel algorithm for constructing protection zones with FCM capability in loop systems. The algorithm is developed in two steps: 1) all the current paths from the grid points to the fault bus are obtained; 2) the IBDGs located on the fault current paths are selected, and the ones containing a fault current higher than a predefined threshold level are chosen as FCM. The method used for calculating the reference phase angle that enables the FCM operation is modified for the case of system buses with multiple lines connected to them. The algorithm and the proposed operation are tested on the IEEE 30-bus system for two scenarios: one with both IBDGs and synchronous DGs in the system, and one with only IBDGs connected to the system. The results of the algorithm show that connection of IBDGs and synchronous DGs to the loop systems can cause the current seen by protective devices to deviate from the level they are designed for. By implementing the proposed protection zone algorithm and operating IBDGs as FCM units, the fault current seen by the protective devices are improved by getting closer to the level they were originally designed for. The percentage errors of the currents seen by protective devices are calculated based on the original currents they were designed to accommodate with no

DG connected to the system. The calculated percentage errors improve considerably when the proposed algorithm is applied and the selected IBDGs operate as FCM units. On the other hand, the results also show that the proposed FCM operation in loop systems is not capable of reducing the fault current error to zero as it does in radial systems. Possible reasons for errors in the results of FCM operation in loop systems are discussed in detail.

Chapter 7

Conclusions

7.1 Summary and Conclusions

The main objective of the research presented in this thesis is to manage the fault current flows through systems using IBDGs. To achieve this objective, a novel technique is developed to utilize IBDGs as FCM units during fault condition. Accordingly, when a fault is detected in the system, the function of IBDGs is modified from that of PQ generators to that of FCM units, by changing the current injected by IBDGs into the system.

For the purposes of FCM using IBDGs, it is assumed that IBDGs are kept connected to the system during a fault and that their contribution to the fault current is limited to a value below the tripping level of the connected PE interfaces. Of the two controllable parameters of the IBDG output current, current magnitude and current phase angle, the current phase angle is chosen as the means of controlling the fault current magnitude. This reference current phase angle is calculated based on the relation between the fault current elements and their phase angles. The phase angle is calculated for the case of one IBDG existing in the system, and extended for the situation where multiple IBDGs are installed in the system. The results of the case study simulations prove the effectiveness of the FCM units in radial systems and in the presence of multiple IBDGs. In order to evaluate the reliability of the FCM operation, the sensitivity of fault current magnitude is examined for a typical error of 10% in the calculated fault current phase angle for the 3-bus test system. The results of this study show that even with an error of 10% in the fault current phase angle, the FCM unit is able to effectively reduce the total fault current magnitude.

The idea of FCM is extended, and IBDGs are employed to manage the fault current contribution of synchronous DGs. It is shown that keeping the magnitude of the IBDG's

current constant and changing its phase angle permits the introduction of three zones of FCM operation: zones A, B, and C. Zone B gives the boundary condition which separates the other two regions. When only IBDGs are connected to the system, working in zone B results in a fault current that has the same magnitude as the original fault current. If the phase angle of IBDG current is set to follow a value less than the boundary condition, zone B, the total fault current would be more than the original fault current meaning an operation in region A. On the other hand, when the reference phase angle is larger than the boundary condition, the system operates in zone C, which results in a fault current that is less than the initial current without DGs. Depending on the amount of fault current reduction in zone C, the current gap generated between the reduced fault current and the original current can be used to manage the synchronous DG contribution to the current. Three factors that affect the operation of FCM units in zone C are discussed in detail. The simulation results of this operation, show the capability of IBDGs in managing their own fault current as well as the fault current contribution of directly connected DGs.

To explore the implementation of the FCM technique in large loop systems, two models, backward-forward based fault analysis method and modified NR based algorithm, are developed to perform short circuit analysis in the presence of IBDGs. For both, the buses with IBDGs connected to them are modeled as either PQ nodes or I nodes, depending on their fault current contribution. The backward-forward sweep algorithm is developed for the fault analysis of radial systems in the the presence of DGs. The NR algorithm is also modified to accommodate the model of IBDGs as constant current sources in terms of their current elements. The novel modified NR based fault analysis algorithm enables the inclusion of both power and current elements in one matrix, thus eliminating the need to represent the constant current IBDGs in terms of their equivalent powers. The test results show the effectiveness of both the algorithms in modeling of IBDGs during fault analysis.

Using the developed power flow based fault analysis algorithms, the proposed FCM operation is examined on loop systems as well. The structures of loop systems are more complicated than those of radial systems. Loop systems are connected to the grid from more than one point and, depending on the location of DGs and the fault, the fault currents flow in different paths in the system. Moreover, in the presence of DGs, the fault currents injected by the grids will be different from those injected when DGs are not connected to the system. These complexities are considered when the FCM operation is implemented for loop systems. In large systems, not all IBDGs contribute equally to the fault current. Hence, by selecting the units that have contribution higher than a specified value, a more optimized FCM operation can be performed in large systems. The last part of this thesis introduces a novel algorithm for constructing protection zones with FCM capability in loop systems. For this case, the IBDGs inside this zone are the ones affected by the fault, and

are the main elements of the FCM algorithm. The algorithm is constructed in two steps and deals with both IBDGs and synchronous DGs. The method used for calculating the reference current phase angle for FCM operation in radial systems is extended for the case of system buses with multiple lines connected to them. Further calculations and illustrations are developed to show how the FCM operation can be applied for loop systems. The simulation results demonstrate the capability of the proposed algorithm in constructing protection zones with FCM capability in loop systems.

7.2 Contributions

The main contributions of this thesis are as follows:

1. A novel FCM technique is successfully developed to manage the fault current flows through the system using IBDGs. In this work, for the first time, IBDGs, the assets of power systems which are normally left idle during fault condition, are utilized as FCM units to manage the fault current in local and remote locations. As an important result of this novel operation, the distribution and protection system constraints on new IBDG connections are eased. From a short circuit point of view, IBDGs with larger capacity can be connected to any location in the system without affecting the fault current magnitude. Another outcome of this operation is the elimination of the need to disconnect IBDGs for each temporary fault. Moreover, the need to upgrade protective devices in the presence of IBDGs is reduced.

2. A fault current control scheme is created to address the incorporation of directly connected DGs, i.e., synchronous DGs, in conjunction with IBDGs. A new zone of operation is identified, and a control strategy is developed to use existing IBDGs to enable the current management of synchronous DGs. The factors affect the FCM operation of synchronous DGs are studied in detail and the following conclusions are drown:
   a) IBDGs with higher current capacity are more effective units in managing the fault current of synchronous DGs.
   b) Higher current contribution from synchronous DGs can be managed as the reference current phase angle of zone C IBDGs increases.
   c) As opposed to current practice, this novel method encourages connection of more and more IBDGs in order to enhance the current management of synchronous DGs in fault current.

3. Comprehensive power flow based fault analysis techniques are developed to model the behavior of IBDGs as constant current sources during fault condition for radial and loop systems. These techniques are the backward-forward based fault analysis method and the modified NR based algorithm. While the backward-forward power flow is able to accommodate the model of constant current sources easily, the NR algorithm is modified to accommodate constant current sources in terms of their current elements as apposed to power elements. For the modified NR based fault analysis algorithm, current formulations rather than conventional power formulations are developed for constant current IBDGs. This task permits mismatches in the real and imaginary components of the current at I nodes to be obtained as well as conventional active and reactive power mismatches. Hence, the method enables the inclusion of both power and current elements in one matrix, thus eliminating the need to represent the constant current IBDGs in terms of their equivalent powers.

4. A novel technique is developed to construct protection zones with FCM capability. Using this technique only the IBDGs that disturb the short circuit capacity condition of the system are responsible to mitigate the problem they have caused. This action will enhance the self-healing characteristic of the system.

5. A modified version of FCM operation is developed to manage the fault current contribution of DGs in loop systems using IBDGs. The application of FCM on loop systems requires more calculations and considerations. Unlike radial systems, loop systems have system buses with more than two lines connected to them. Hence, the FCM is modified to be applicable for cases where multiple lines connected to a bus.

7.3 Future Work

Based on the research presented in this thesis, the following subjects are suggested for future studies:

1. The analysis presented in this thesis is for balanced conditions. However, the proposed scheme can be extended for unbalanced faults, either by managing each phase independently in *abc* frame, or by regulating the positive and negative sequence current separately in d-q frame.

2. The contribution of DGs in the fault current varies depending on their type and location. Simulation results show that if only IBDGs exist in loop systems there are

short comings in the application of the FCM operation. Future studies shold address the deficiencies of this operation.

3. The FCM operation manages the fault current seen by protective devices to a level close to that of the original fault current they were designed for. More detailed studies can be performed to investigate the effect of the proposed algorithm on the coordination of protective devices in radial and loop systems.

References

[1] G. Pepermans, J. Driesen, D. Haeseldonckx, R. Belmans, W. D'Haeseleer, "Distributed generation: definition, benefits and issues," Energy Policy - Elsevier, Vol. 33, Issue 6, pp. 787-798, April 2005.

[2] T. Ackermann, G. Andersson, L. Soder, "Distributed generation: a definition," Electric Power Systems Research - Elsevier, Vol. 57, Issue 3, pp. 195204, April 2001.

[3] P. Dondi, D. Bayoumi, C. Haederli, D. Julian, M. Suter, "Network integration of distributed power generation," Journal of Power Sources - Elsevier, Vol. 106, Issues 1-2, pp. 1-9, April 2002.

[4] W. El-Khattam, M.M.A. Salama, C. Haederli, D. Julian, M. Suter, "Distributed generation technologies, definitions and benefits," Electric Power Systems Research - Elsevier, Vol. 71, Issues 2, pp. 119-128, October 2004.

[5] P. Barker and R. W. de Mello, "Determining the impact of distributed generation on power systems: Part 1 Radial power systems," in Proc. IEEE Power Eng. Soc. Summer Power Meeting, Vol. 3, pp. 1645-1656, 2000.

[6] W. El-Khattam, M.M.A. Salama, "Impact of distributed generation on voltage profile in deregulated distribution system," presented at Power System Conference, Impact of Distributed Generation, Sc, USA, March 2002.

[7] N. Hadjsaid, J.-F. Canard, and F. Dumas, "Dispersed generation impact on distribution networks," IEEE Computer Applications in Power, Vol. 12, Issue. 2, pp. 2228, April 1999.

[8] H.B. Puttgen, P.R. MacGregor, ; F.C. Lambert,"Distributed generation: Semantic hype or the dawn of a new era?," IEEE Power and Energy Magazine, Vol. 1, Issue. 1, pp. 22-29, January-February 2003.

[9] M.M.A. Salama, H. Temraz, A.Y. Chikhani, M.A. Bayoumi, "Fault-current limiter with thyristor-controlled impedance," IEEE Transaction on Power Delivery, Vol. 8, Issue. 3, pp. 1518- 1528 , July 1993.

[10] E.F. King, A.Y. Chikhani, R. Hackam, M.M.A. Salama, "A microprocessor-controlled variable impedance adaptive fault current limiter," IEEE Transaction on Power Delivery, Vol. 5, Issue. 4, pp. 1830-1838, October 1990.

[11] F. Blaabjerg, Z. Chen, and S. B. Kjaer, "Power electronics as ecient interface in dispersed power generation systems," IEEE Transaction on Power Electronics, Vol. 19, Issue. 5, pp. 1184-1194, September 2004.

[12] IEEE Std. 15472003 "IEEE standard for interconnecting distributed resources with electric power systems," 2003.

[13] B. Kroposki, C. Pink, .R. DeBlasio, H. Thomas, M. Simoes, P.K. Sen "Benefits of power electronic interfaces for distributed energy systems," IEEE Power Engineering Society General Meeting, 2006.

[14] N. Jenkins, R. Allan, P. Crossley, D. Kirschen , G. Strbac, "Embedded Generation," The Institution of Engineering and Technology (IET), London, 2000.

[15] T.K. Abdel-Galil, A.E.B. Abu-Elanien, E.F. El-Saadany, A. Girgis, Y.A.R.I. Mohamed, M.M.A. Salama, H.H.M. Zeineldin, Qualsys Engco. Inc, "Protection Coordination Planning with Distributed Generation," June 2007.

[16] A. Girgis and S. Brahma, "Effect of distributed generation on protective device coordination in distribution system," in Large Engineering Systems Conference on Power Engineering. LESCOPE 01: Power Engineering, pp. 115-119, July 2001.

[17] R.C. Dugan and T.E. McDermott, "Operating conflicts for distributed generation on distribution system," in Rural Electric Power Conference, pp. A3/1 - A3/6, 2001.

[18] G. Tang, M. R. Iravani "Application of a Fault Current Limiter To Minimize Distributed Generation Impact on Coordinated Relay Protection," presented at the Int. Conf. Power Systems Transients, Montreal, QC, Canada, Jun. 2005.

[19] M. Noe, M. Steurer "High-temperature superconductor fault current limiters: concepts, applications, and development status, Superconducting Science Technology," Superconductor Science and Technology, R15R29, 2007.

[20] M. Chen, W. Paul, M. Lakner, L. Donzel,M. Hoidis, P. Unternaehrer, R. Weder,M. Mendik "6.4 mva resistive fault current limiter based on bi-2212 superconductor," Physica C: Superconductivity, vol. 372, no. 3, pp. 16571663, August 2002.

[21] L. Ye, A. M. Campbell "Case study of HTS resistive superconducting fault current limiter in electrical distribution systems," Journal of Electric Power Systems Research, Elsevier, Vol. 77, Issue. 5-6, pp. 534-539, April 2007.

[22] G. G. Karady, "Principles of fault current limitation by a resonant LC circuit," IEE Proceedings on Generation, Transmission and Distribution, Vol. 139, Issue. 1, pp. 1-6, January 1992.

[23] E.F. King, A.Y. Chikhani, R. Hackam, M.M.A. Salama "A microprocessor - controlled variable impedance adaptive fault current limiter," IEEE Transactions in Power Delivery, Vol. 5, Issue. 4, pp. 1830-1838, November 1990.

[24] R.K. Smith, P.G. Slade, M. Sarkozi, B.J. Stacey "Solid state distribution current limiter and circuit breaker: Application requirements and control strategies," IEEE Transactions on Power Delivery, vol. 8, Issue. 3, pp. 11551164, July 1993.

[25] S.A.A. Shahriari, M. Abapour, A. Yazdian, M. R. Haghifam "Cost reduction of distribution network protection in presence of distributed generation using optimized fault current limiter allocation,"International Journal of Electrical Power and Energy Systems Elsevier, Vol. 43, Issue. 1, pp. 1453-1459, June 2012.

[26] P.K.C. Meyer, R.W. DeDoncker, "Design of a novel low loss fault current limiter for medium-voltage systems," in Applied Power Electronics Conference and Exposition, vol. 3. IEEE APEC, 2004, pp. 18251831.

[27] R.M. Chabanloo, H.A. Abyaneh, A. Agheli, H. Rastegar "Overcurrent relays coordination considering transient behaviour of fault current limiter and distributed generation in distribution power network," Generation, Transmission and Distribution, IET, Vol. 5, Issue. 9, pp. 903-911, September 2011.

[28] IEEE Std. C37.112, "IEEE standard inverse-time characteristic equations for overcurrent relays", 1996.

[29] S.A.A. Shahriari, M. Abapour, A. Yazdian, M. R. Haghifam "Minimizing the impact of distributed generation on distribution protection system by solid state fault current limiter," in IEEE PES Transmission and Distribution Conference and Exposition, pp. 1-7, April 2010.

[30] S.A.A. Shahriari, M. Abapour, A. Yazdian, M. R. Haghifam "Cost reduction of distribution network protection in presence of distributed generation using optimized fault current limiter allocation,"International Journal of Electrical Power and Energy Systems Elsevier, Vol. 43, Issue. 1, pp. 1453-1459, June 2012.

[31] S.A.A. Shahriari, A. Yazdian "Fault current limiter allocation and sizing in distribution system in presence of distributed generation," Power and Energy Society General Meeting,pp. 1-6, July 2009.

[32] T. Sato, M. Yamaguchi, T. Terashima, S. Fukui, J. Ogawa, H. Shimizu, T. Sato "Study on the Effect of Fault Current Limiter in Power System With Dispersed Generators," IEEE Transactions on IEEE Applied Superconductivity, Vol. 17, Issue. 2, pp. 2331-2334, June 2007.

[33] L. Ye, L. Z. Lin "Study of SuperconductingFault Current Limiters for System Integration of Wind Farms," IEEE Transactions on IEEE Applied Superconductivity, Vol. 20, Issue. 3, pp. 1233-1237, June 2010.

[34] H.J. Lee, G. Son, J.W. Park "A Study on Wind-Turbine Generator System Sizing Considering Overcurrent Relay Coordination With SFCL," IEEE Transactions on IEEE Applied Superconductivity, Vol. 21, Issue. 3, pp. 2140-2143, June 2011.

[35] W.J. Park, B.C. Sung, J.W. Park "The Effect of SFCL on Electric Power Grid With Wind-Turbine Generation System," IEEE Transactions on IEEE Applied Superconductivity, Vol. 20, Issue. 3, pp. 1177-1181, June 2010.

[36] W. El-Khattam, T. S. Sidhu "Restoration of Directional Overcurrent Relay Coordination in Distributed Generation Systems Utilizing Fault Current Limiter," IEEE Transactions on Applied Superconductivity, Vol. 23, Issue. 2, pp. 576-585, April 2008.

[37] J.R.S.S. Kumara, A. Atputharajah,J.B. Ekanayake, F.J. Mumford "Over Current Protection Coordination of Distribution Networks with Fault Current Limiters," Power Engineering Society General Meeting IEEE, 2006.

[38] S. Torii, H. Kameda, T. Kumano, H. Sakaki, H. Kubota, K. Yasuda "Operation Tests for SN Transition Superconducting Fault Current Limiter in the Power System Simulator," IEEE Transactions on Applied Superconductivity, Vol. 15, Issue. 2, pp. 2134-2137, June 2005.

[39] Y. Zhang, R. A. Dougal "Novel Dual-FCL Connection for Adding Distributed Generation to a Power Distribution Utility," IEEE Transactions on Applied Superconductivity, Vol. 21, Issue. 3, pp. 2179-2183, June 2011.

[40] W. Najy, H. Zeineldin, W. Woon "Optimal Protection Coordination for Microgrids with Grid-Connected and Islanded Capability," IEEE Transactions on Industrial Electronics, Vol. 60, Issue. 4, pp. 1668-1677, April 2013.

[41] S.M. Brahma and A.A. Girgis "Microprocessor-Based Reclosing to Coordinate Fuse and Recloser in a System with High Penetration of Distributed Generation," IEEE Power Engineering Society Winter Meeting, Vol. 13, pp. 453-458, 2002.

[42] M.A. Zamani,T.S. Sidhu, A. Yazdani "A Protection Strategy and Microprocessor-Based Relay for Low-Voltage Microgrids," IEEE Transactions on Power Delivery, Vol. 26, Issue. 3, pp. 1873-1883, July 2011.

[43] M. Dewadasa, A. Ghosh, G. Ledwich, M. Wishart "Fault isolation in distributed generation connected distribution networks," IET Generation, Transmission and Distribution, Vol. 5, Issue. 10, pp. 1053-1061, 2011.

[44] M. Dewadasa, A. Ghosh, G. Ledwich "Fold back current control and admittance protection scheme for a distribution network containing distributed generators," IET Generation, Transmission and Distribution, Vol. 4, Issue. 8, pp. 952-962, 2010.

[45] M. Dewadasa, A. Ghosh, G. Ledwich "An Inverse Time Admittance Relay for Fault Detection in Distribution Networks Containing DGs," IEEE Asia-Pacific Region-10 Conference TENCON09 Singapore, January 2009.

[46] M. Baran, I. El-Markabi "Adaptive Over Current Protection for Distribution Feeders with Distributed Generators," IEEE Power Systems Conference and Exposition, Vol. 2, pp. 715-719, October 2004.

[47] T. Loix, T. Wijnhoven, G. Deconinck "Protection of Microgrids with a High Penetration of Inverter-Coupled Energy Sources," CIGRE/IEEE Symposium, pp. 1-6, July 2009.

[48] M. A. Zamani, T. S. Sidhu, and A. Yazdani, "A strategy for protection coordination in radial distribution networks with distributed generators," Power Engineering Society General Meeting IEEE, Jul. 2010, pp. 18.

[49] R.C. Christie, H. Zadehgol, M.M. Habib, "High impedance fault detection in low voltage netwoks," IEEE Transaction on Power Delivery, Vol. 8, Issue. 4, pp. 18291836, October 1993.

[50] S.M. Brahma and A.A. Girgis "Development of Adaptive Protection Scheme for Distribution Systems With High Penetration of Distributed Generation," IEEE Transactions on Power Delivery, Vol. 19, No. 1, January 2004.

[51] T.S. Ustun, C. Ozansoy, A. Zayegh "Modeling of a Centralized Microgrid Protection System and Distributed Energy Resources According to IEC 61850-7-420," IEEE Transactions on Power Systems, Vol. 27, Issue. 3, pp. 1560-1567, August 2012.

[52] T.S. Ustun, A. Zayegh "A Central Microgrid Protection System for Networks with Fault Current Limiters," 10th International Conference on Environment and Electrical Engineering (EEEIC), May 2011.

[53] H. Yazdanpanahi, Y. Li, W. Xu, "A New Control Strategy to Mitigate the Impact of Inverter-Based DGs on Protection System," IEEE Transactions on Smart Grid, Vol. 3, Issue. 3, September 2012.

[54] H. Yazdanpanahi, W. Xu, and Y. W. Li "A Novel fault current control scheme to reduce synchronous DGs impact on protection coordination," IEEE Transactions on Power Deivery, Vol. 29, Issue. 2, pp. 542-551, April 2014.

[55] H. Wan, K.K. Li, K.P. Wong "An Adaptive Multiagent Approach to Protection Relay Coordination With Distributed Generators in Industrial Power Distribution System," IEEE Transactions on Industry Applications, Vol. 46, Issue. 5, pp. 2118-2124, October 2010.

[56] P. Mahat, Z. Chen, B. Bak-Jensen, C.L. Bak "A Simple Adaptive Overcurrent Protection of Distribution Systems With Distributed Generation," IEEE Transactions on Smart Grid , Vol. 2, Issue. 3, pp. 428-437, September 2011.

[57] X. Zeng, K.K. Li, W.L. Chan, S. Su "Multi-Agents Based Protection for Distributed Generation Systems," IEEE Intemational Conference on Electric Utility Deregulation, Restructuring and Power Technologies, Vol. 1, pp. 393-397, April 2004.

[58] E. Sortomme, S.S. Venkata, J. Mitra "Microgrid Protection Using Communication-Assisted Digital Relays," IEEE Transactions on Power Delivery, Vol. 25, Issue. 4, pp. 2789-2796, October 2010.

[59] N. Perera, A.D. Rajapakse, T.E. Buchholzer "Isolation of Faults in Distribution Networks With Distributed Generators," IEEE Transactions on Power Delivery, Vol. 23, Issue. 4, pp. 2347-2355, October 2008.

[60] N. Nimpitiwan, G.T. Heydt, R. Ayyanar, S. Suryanarayanan "Fault Current Contribution From Synchronous Machine and Inverter Based Distributed Generators," IEEE Transaction on Power Delivery, Vol. 22, Issue. 1, PP. 634-641, January 2007.

[61] Th. Ackermann, V. Knyazkin "Interaction between distributed generation and the distribution network: operation aspects," in IEEE/PES Transmission and Distribution Conference and Exhibition Conference, Vol. 2, pp. 1357-1362, 2002.

[62] M.E. Baran, I. El-Markaby, "Fault Analysis on Distribution Feeders With Distributed Generators," IEEE Transactions on Power Systems, Vol. 20, Issue. 4, pp. 1575-1764, November 2005.

[63] S.R. Wall, "Performance of inverter interfaced distributed generation," IEEE/PES Transmission and Distribution Conference and Exposition, Vol. 2, pp. 945-950, 2001.

[64] S.J. Chapman "Electric machinery and power system fundamentals," McGraw Hill Higher Education, ISBN-10: 0071226206, 2001.

[65] IEEE Recommended Practice for Calculating Short-Circuit Currents in Industrial and Commercial Power Systems, IEEE Standard 551-2006.

[66] F. Blaabjerg, R. Teodorescu, M. Liserre, A.V. Timbus "Overview of Control and Grid Synchronization for Distributed Power Generation Systems," IEEE Transaction on Energy Conversion, Vol. 53, Issue. 5, PP. 1398-1409, October 2006.

[67] E. Twining, D. G. Holmes "Grid current regulation of a three-phase voltage source inverter with an LCL input filter," IEEE Transaction on Power Electronics, Vol. 18, Issue. 3, pp. 888-895, May 2003.

[68] S.H. Ko, S.R. Lee, H. Dehbonei, C.V. Nayar "Application of voltage- and current-controlled voltage source inverters for distributed generation systems," IEEE Transaction on Energy Conversion, Vol. 21, Issue. 3, PP. 782-792, September 2006.

[69] M. Prodanovic, T.C. Green "Control and Filter Design of Three-Phase Inverters for High Power Quality Grid Connection," IEEE Transaction on Power Electronics, Vol. 18, Issue. 1, PP. 373-380, January 2003.

[70] N. Mohan, T. M. Undeland, W. P. Robbins "Power Electronics: Converters, Applications, and Design", Third edition, New York: Wiley, 2002.

[71] J. Morren, S. De Haan, and J. Ferreira, "Model reduction and control of electronic interfaces of voltage dip proof DG units," IEEE Power Engineering Society General Meeting, pp. 2168-2173, 2004.

[72] A. Darwish, A. Abdel-Khalik, A. Elserougi, S. Ahmed, and A. Massoud, "Fault current contribution scenarios for grid-connected voltage source inverter-based distributed generation with an LCL filter," Electric Power Systems Research, Vol. 104, pp. 93-103, 2013.

[73] M. Brucoli, T.C. Green, J.D.F. McDonald "Modelling and Analysis of Fault Behaviour of Inverter Microgrids to Aid Future Fault Detection," IEEE International Conference on System of Systems Engineering, SoSE, PP. 1-6, April 2007.

[74] C. A. Plet, M. Graovac, T.C. Green, R. Iravani "Fault response of grid-connected inverter dominated networks," IEEE Power and Energy Society General Meeting, PP. 1-8, July 2010.

[75] C. A. Plet, M. Brucoli, J.D.F. McDonald, T.C. Green "Fault Models of Inverter-Interfaced Distributed Generators: Experimental Verification and Application to Fault Analysis," IEEE Power and Energy Society General Meeting, PP. 1-8, July 2011.

[76] M. P. Kazmierkowski, L. Malesani "Current Control Techniques for Three-Phase Voltage-Source PWM Converters: A Survey," IEEE Transaction on Industrial Electronics, Vol. 45, Issue. 5, pp. 691-703, October 1998.

[77] C. D. Schauder, R. Caddy "Current Control of Voltage-Source Inverters for Fast Four-Quadrant Drive Performance," IEEE Transaction on Industry Applcations, Vol. IA-18, Issue. 2, pp. 163-171, March 1982.

[78] T. M. Rowan, R. J. Kerkman "A New Synchronous Current Regulator and an Analysis of Current-Regulated PWM Inverters," IEEE Transaction on Industry Applcations, Vol. IA-22, Issue. 4, pp. 678-690, July/August 1986.

[79] D. N. Zmood, D. G. Holmes, G. H. Bode "Frequency-Domain Analysis of Three-Phase Linear Current Regulators," IEEE Transaction on Industry Applcations, Vol. 37, Issue. 2, pp. 601-610, March/April 2001.

[80] D. N. Zmood, D. G. Holmes "Stationary Frame Current Regulation of PWM Inverters With Zero Steady-State Error," IEEE Transaction on Power Electronics, Vol. 18, Issue. 3, pp. 814-822, May 2003.

[81] B. Adkins, R. G. Harley "The General Theory of Alternating Current Machines: Application to Practical Problems", First edition, Chapman and Hall, 1975.

[82] X.Q. Guo, W.Y. Wu "Improved current regulation of three-phase grid-connected voltage-source inverters for distributed generation systems," IET Renewable Power Generation, Vol. 4, Issue. 2, pp. 101-115, 2010.

[83] Y. A. R. I. Mohamed, E. F. El-Saadany, "A Control Scheme for PWM Voltage-Source Distributed-Generation Inverters for Fast Load-Voltage Regulation and Effective Mitigation of Unbalanced Voltage Disturbances," IEEE Transactions on Industrial Electronics, Vol. 55, Issue. 5, May 2008.

[84] J. W. Choi, and S. K. Sul, "Fast Current Controller in Three-Phase AC/DC Boost Converter Using - Axis Crosscoupling," IEEE Transactions on Power Eelectronics, Vol. 13, Issue. 1, January 1998

[85] Y. A. I. Mohamed, and E. F. El-Saadany, "Adaptive Decentralized Droop Controller to Preserve Power Sharing Stability of Paralleled Inverters in Distributed Generation Microgrids," IEEE Transactions ON Power Electronics, Vol. 23, Issues. 6, November 2008.

[86] "IEEE standard for interconnecting distributed resources with electric power systems," IEEE Std 1547-2003, pp. 1-28, July 2003.

[87] W. Libo, Z. Zhengming, L. Jianzheng "A single-stage three-phase grid-connected photovoltaic system with modified MPPT method and reactive power compensation," IEEE Transactions on Energy Conversion, Vol. 22, Issue. 4, pp. 881-886, December 2007.

[88] T. Ackermann, V. Knyazkin "Interaction between distributed generation and the distribution network: operation aspects," Asia Pacific. IEEE/PES Transmission and Distribution Conference and Exhibition, Vol. 2, pp. 1357-1362, October 2002.

[89] F. Z. Peng, Y. W. Li, L. M. Tolbert, "Control and protection of power electronics interfaced distributed generation systems in a customer-driven microgrid," IEEE Power and Energy Society General Meeting, pp. 1-8, July 2009.

[90] H. Nikkhajoei, R. Lasseter "Microgrid protection" IEEE Power Engineering Society General Meeting, pp. 1-6, June 2007.

[91] A.G. Phadke "Synchronized phasor measurements in power systems," IEEE Computer Applications in Power, Vol. 6, Issue. 2, pp. 10-15, April 1993.

[92] J. De La Ree, V. Centeno, J.S. Thorp, A.G. Phadke "Synchronized Phasor Measurement Applications in Power Systems," IEEE Transactions on Smart Grid, Vol. 1, Issue. 1, pp. 20-27, June 2010.

[93] B. Venkatesh, R. Ranjan, H.B. Gooi "Optimal Reconfiguration of Radial Distribution Systems to Maximize Loadability," IEEE Transactions on Power Systems, Vol. 19, Issue. 1, pp. 260-266, February 2004.

[94] E. Bompard, E. Carpaneto, G. Chicco, and R. Napoli, "Convergence of the backward/forward sweep method for the load-flow analysis of radial distribution systems," International journal of electrical power and energy systems, Vol. 22, pp. 521-530, 2000.

[95] H. Saadat. Power System Analysis. PSA Publishing; Third Edition, Dec. 2010.

[96] IEEE 30 Bus Test Case, "Power Systems Test Case Archive," [Online]. Available: http://www.ee.washington.edu/research/pstca/